Kobe University Repository : Kernel

PDF issue: 2024-06-01

Estimation of avian body characters and ecology from avian track morphology; application to theropods and Cretaceous avian

田中, 郁子

(Degree)
博士（理学）

(Date of Degree)
2016-03-25

(Date of Publication)
2018-03-25

(Resource Type)
doctoral thesis

(Report Number)
甲第6612号

(URL)
https://hdl.handle.net/20.500.14094/D1006612

※ 当コンテンツは神戸大学の学術成果です。無断複製・不正使用等を禁じます。著作権法で認められている範囲内で、適切にご利用ください。

博　士　論　文

現生鳥類足印形態に基づく身体形態と生態の推定; 獣脚類と白亜紀鳥類への適用

平成 28 年 1 月

神戸大学大学院理学研究科

田中郁子

Acknowledgements

First of all, special thanks go to my supervisors Professor Masayuki Hyodo and Dr. Kazuhito Yamasaki. I met Professor Masayuki Hyodo in Taiwan for the first time when I was a master's course student. I believe it was a fateful meeting that changed my life. During my doctoral studies, Professor Hyodo provided me with many precious occasions, valuable experiences, great support and suggestions. Professor Hyodo always reminded me of my responsibility as a researcher and an educator. I have learnt so much from him and all these experiences have become my life's greatest treasures. I would also like to express my sincere gratitude to Dr. Kazuhito Yamasaki for his continuous support and for all our helpful discussions. Dr. Yamasaki allowed me to have total freedom to conduct independent research.

I would like to express my very special gratitude to Dr. Takao Ubukata. Dr. Ubukata always provided me with useful comments on my research and brought to my attention the importance of demonstrating commitment to integrity and ethical values as a researcher. His advice has been instrumental in doing my research and proud to follow his guidance. I also owe a debt of gratitude to Dr. Tai Kubo for his many helpful comments on track research.

I would like to extend my thanks to Professor Yasuo Ezaki for his helpful, constructive and suitable suggestions. Professor Ezaki provided the occasions for me to study about *Ciconia boyciana*. I also thank Mr. Minoru Funakoshi for his assistance on sampling.

I am particularly grateful to the following people for discussions, challenging questions and support throughout my research life: Professor Akihisa Kitamura,

Professor Michio Kato, Dr. Ikuko Kitaba and Dr. Sunao Mochizuki.

I wish to acknowledge all members of the Laboratory of Geology at Kobe University. I am also grateful to the following people for discussions and support: Dr. Yusuke Seto, Dr. Kotaro Hirose, Dr. Balázs Bradák and Ms. Kumiko Okumura.

I would like to acknowledge that I was supported by JSPS Research Fellowships for Young Scientists for one year, Kobe University foundation and academic foundation for supporting the reintroduction of oriental storks, Toyooka city, Hyogo prefecture.

Last but not the least, I would like to thank my family who has always supported me through the difficult times. I send them all my love and best wishes.

Abstract

The main goal of paleontology is to reveal the evolution of life. Fossils are the only evidence of extinct organisms. They greatly contribute to the studies of evolution. Animals have diversified morphology and surface pattern of their bodies as they have spread their habitat regions in the process of evolution. Therefore, their bodies are related with habitat as well as their physiology and ecology. Size and shape are the main elements of animal body structure. Size can constrain shape, and shape can constrain locomotion. To prove these relationships, it is important to make a research on living animals. It is because a fossil shows only a part of information for animal's body, but living animals can complement information for fossilized animals. Fossilized animals are often extinct. But if the relative animals are survived, we can research them and reveal fossilized animals' characters and ecology. This kind of research named neopaleontology has recently become active accompanied by technological innovations, and its degree of importance becomes high in paleontology. We carried out a study of neopaleontology. Ichnological experiments were conducted using modern birds. We also carried out a computer simulation experiment of theoretical morphometrics.

In the history of vertebrates' evolution, avian evolved in vertebrate lineages, having highly developed flight ability. Avian is a survivor of theropods that had flight ability in the later Jurassic period. Avians have two completely different styles of locomotion, flight and bipedal walking, and use them properly depending on situation. Their body bones and muscles are adapted to flight and bipedal walking. Light body weight is a special feature of avian which is a result of adaptation. Light bodies are profitable for flight against gravity and for supporting bodyweight with two legs. Avians have a

unique breezing system with air sac that was completed when they were primitive theropods. The air sac system is also closely related to lighter bones. Feather is light and strong material enables to have flight ability without losing locomotion of walking. In this study, we focus on avian. We measured avian body morphology and structure for avian taxa covering almost all avian orders, and collected avian track data based on ichnological experiments using living avians. From the analyses of the modern avian and track data, relationships between track morphological parameters, body weight, wing span, wing aspect ratio, and habitat. Applying the relationships, body parameters and habitats were estimated for extinct avians and theropods.

The relationship between body weight and footprint area of modern avians was derived and used to estimate the body weights of non-avian theropods taxa from the Triassic to Cretaceous and extinct avian taxa from the Cretaceous periods. Geometric information, such as the area and shape of fossil tracks of extinct avians and non-avian theropods, was used to estimate body weight and habitat type. The percentage prediction and standard error of estimates indicated that the body weight estimated from track area is comparable with body weight estimated from body fossils bones. Therefore, this approach is useful when the fossilized track record is richer than the fossilized skeletal record. The data sets for avians and reptiles were combined and used to derive a body weight–area relationship that may be applicable to a broader range of organisms, such as plantigrade quadrupeds and digitigrade bipeds. Additionally, scatter plots of the relationship between habitat type and footprint shape of modern avians were used to infer the habitat type of extinct avians. This finding suggests that the pes of animals, living in areas characterized by fluctuating water levels, and under conditions facilitating the preservation of footprints, were similar in form to those of extant

semi-aquatic avians

Avian wings designed for flying may be related to tracks made by walking, another form of locomotion. Modern avian wing area and span and bodyweight data were collected and analyzed to examine how the wings might be related to tracks. A discriminant analysis showed that avian wings can be divided into three groups, similar to tracks, which are divided morphologically into three groups corresponding to habitat type. Multiple regression analyses revealed that the avian wing loading and aspect ratio were closely correlated to the parameters of track shape, expressed by a simple equation. These results may reflect the adaptation of avian locomotion to habitat. The regression analyses revealed that wing area and span were related to track area. The relationship provides a method for estimating the wing area and wingspan from the fossil track area. Using this method, the wingspan and area were estimated from three tracks of extinct Cretaceous avian taxa. The estimated values suggest that *Archaeornithipus meijidei*, *Hwangsanipes choughi* and *Yacoraitichnus avis* had bodies similar to herons (or grus), large sandpipers (or small sea birds) and medium-sized gulls, respectively. The ecology of avian flight based on aerodynamics suggests that birds are divided by their wing aspect ratio into the two groups of "transport aircraft" and "fighter aircraft". The former includes sea birds and wading birds. The latter includes song birds, birds of prey and pheasants.

An ichnological experiment using *Ciconia boyciana* was carried out to reveal morphological variability of tracks left on a potter sediment. We obtained a total of 56 tracks, from which their areas, lengths, widths, depths, and volumes were measured. An average of track areas almost equals to the median. *Ciconia boyciana* generally left morphologically uniform tracks, suggesting that it controls digits-substrate interaction

to keep balance. A unique anatomical feature is that *Ciconia boyciana* does not leave metatarsal impression, unlike other wading birds, most of which leave it. This feature will be useful to identify *Ciconia boyciana* from other trackmakers having similar body weights and habitats. Track widths have a large range of variability up to 40 %, which would be reflected by how attached muscles on leg and foot of birds. The correlation analysis of track geometry revels that the width and depth of a track have a trade-off relationship as to keep a same volume. Application of the theoretical morphology analysis to the track data reveals *Ciconia boyciana* pressures the outside of its digits during walking.

To examine the development of pattern formation from the viewpoint of symmetry, we applied a two-dimensional discrete Walsh analysis to a one-dimensional cellular automata model under two types of regular initial conditions. The amount of symmetropy of cellular automata (CA) models under regular and random initial conditions corresponds to three Wolfram's classes of CAs, identified as Classes II, III, and IV. Regular initial conditions occur in two groups. One group that makes a broken, regular pattern formation has four types of symmetry, whereas the other group that makes a higher hierarchy pattern formation has only two types. Additionally, both final pattern formations show an increased amount of symmetropy as time passes. Moreover, the final pattern formations are affected by iterations of base rules of CA models of chaos dynamical systems. The growth design formations limit possibilities: the ratio of developing final pattern formations under a regular initial condition decreases in the order of Classes III, II, and IV. This might be related to the difference in degree in reference to surrounding conditions. These findings suggest that calculations of symmetries of the structures of one-dimensional cellular automata models are useful for

revealing rules of pattern generation for animal bodies.

Contents

Chapter 1

Introduction

The main goal of paleontology is to reveal the evolution of life. Fossils, the major target of paleontological studies, are the only proof of evolution through the past several hundred million years. For vertebrates, bone fossils provide direct evidence for their body structure and size, and locomotion. These lines of evidence are important to reveal the evolution. Vertebrates often remain track fossils. Track fossils also provide a lot of information about trackmakers. They show direct evidence for inhabitation at the place where a fossil was found, mainly fluvial deposits. They also show evidence for anatomy of feet and posture of limb, and further various kinds of ecological and biological information. Thus, track fossils provide many kinds of information, but they lack information on animal's body except feet, which are provided by bone fossils. Bone fossils are usually allochthonous, so that they do not have habitat information, which is provided by track fossils. Thus, track fossils and body fossils are complement. Combining both fossils information greatly contributes to a study of evolution.

Fossil tracks were first interpreted using recent animals' anatomy and lifestyle in the pioneering work by Sollas (1879), who used casts of footprints from emus, rheas and cassowaries to compare with the theropod footprints. At that time, he identified the trackmaker as the ancestor of ostrich, because dinosaurs fossils are poorly found out. This is still the principal method in experimental ichnology. Morphology of tetrapod footprints is dependent on both pes anatomy and pes-substrate interaction including kinematic and substrate condition (Baird 1957; Brown 1999; Padian 2003). Therefore,

anatomical signals are difficult to isolate, because of being overprinted by substrate-related (extramorphological) features (Lockley et al. 1995). However, ichnoloical experiments with living animals can solve it, because abundant numbers of track fossils produced by a same trackmaker enable to isolate anatomical components from morphology (Kubo 2008). The problem about the relationship between trackmaker's behavior and sediment has been understood in the ichnoloical experiment with emu by Brown (1999). Tracks do not always reflect the anatomy of a trackmaker, as kinematic and substrate conditions may alter it (Padian 2003). Track morphology can vary with kinematic or substrate conditions (Kubo 2008). These problems can also be solved by experimental ichnology using living animals, that can reveal how faithfully record the anatomy and the range of variability. Identification of an animal of a fossil is important as the first step for studies of track fossils as well as bone fossils. For track fossils, the trackmakers are often extinct, so that living animals' characters and ecology become important to identify them.

The experimental ichnology deals with many kinds of subject. Some are associated with the development of study methods. A big technological innovation was brought by Ishigaki & Fujisaki (1989). They introduced three dimensional (3D) documentation technique that consists of moiré photogrametry. Now, the technique is composed of laser distance measurement and stereo imaging (Gatesy et al. 2005). Therefore, foot movements can be reconstructed even from low quality fossil tracks by the detailed documentation with photogrammetry (e.g Thulborn 1990; Matthews & Breithaupt 2006), or 3D simulation techniques with laser (e.g. Falkingham 2014; Gatesy et al. 2005; Falkingham & Gatesy 2014). Foot movements of theropod were estimated by comparing theropod footprints with those of turkey (Gatesy et al. 1999) and guineafowl

(Falkingham & Gatesy 2014). There are papers focusing on sediments as well as trackmaker. Some studies have revealed the relationship between track morphology and physical features of sediments, based on ichnological experiments, and clarified the relationship between track morphology and limb motion (Milàn 2006; Milàn & Bromley 2006; Milàn & Bromley 2008). The body sizes of animals are influenced by their physiology and ecology, and therefore estimation of body weight is important in paleontology. Body weights of fossil animals can be estimated from fossil tracks as well as from body fossils. Fossil track data become valuable when skeletal fossils are rare like a period from Middle Triassic to Early Jurassic (e.g. Kubo 2011; Martinez et al. 2011). From Middle Permian to Early Triassic, skeletal records are concentrated only in South Africa (e.g. Kubo & Ozaki 2011), so that in such a period fossil track records become valuable in other regions.

In geological times with poor body fossils of animals, researches with abundant track fossils are more reliable than those with few body fossils. Triassic Archosaur trackways demonstrated that several ichnogenera gradually erected through the Triassic time (Klein & Lucas 2010), the same as Permian vertebrates (McKeewer & Haubold 1996) and Permian amphibians (McKee 1947). Theropods are sparsely remained as fossils from the Triassic to the Early Jurassic (Heckert & Lucas 1998; Martinez et al. 2011), because they have thin and delicate bones that are rarely preserved as fossils. Cretaceous avian fossil records are also poor, because of the same reason (Fountaine et al. 2005; Martinez et al. 2011). To the study of these animals having flight capability (e.g. pterosaurs and extinct birds and their ancestors), ichnological approaches have been applied. Some track analysis studies are focused on track morphology. Based on measurments of tracks' morphology, methods to estimate trackmaker's ecology and

physiology are invented. Different kinds of relationship between track morhpology and body character provide methods to estimate various features of a trackmaker: rotation of limb posture (Kubo & Ozaki 2009), bodyweight (Kubo 2011; Tanaka 2015) and habitat type (Tanaka 2015).

There was a controversy on identification of a trackmaker. *Pteraichnus* was described by Stokes (1957) as the trackway from a pterosaur. However, Padian & Olsen (1989) investigated modern crocodilians' walking on a clay, and interpreted the trackmaker of *Pteraichnus* was crocodilian according to the comparison of walking styles between pterosaur and crocodilian. Lockley et al (1995) re-interpreted as pterosaur from morphological similarity of *Pteraichnus*, and Kubo (2008) also interpreted as pterosaur, based on the difference between crocodilian and *Pteraichnus* of manus' digits number, tailmark and the ratio of manus width/pes width. In these researches, it is important to find strong track features left on every sediment. The ancestor of avian originally had a lighter bodyweight as synapomorphy, so that its body is rarely remained as a fossil. Therefore tracks are useful to estimate body characters and behaviors of theropods. Wilson (2005) invented a method to combine data of body fossils and ichnofossils using stratocladistics. Ichnofossils identified by synapomorphies can act as an independent source of distributional data that can modify spatial, temporal, and character distributions, which in turn may influence hypotheses of locomotor evolution. Based on the conservative synapomorphy-based approach analysis of the footprints, the origin of the dinosaur stem lineage could shift back approximately 5-9 Myr, compared to the time indicated by body fossils (Brusatte et al. 2011).

The shape of the track is not affected by substrate but reflects the anatomy of trackmaker (e.g. Kubo 2008). This is an important principle of ichnology. Standard

morphological elements for measurement about tracks and trackway are stride and pace angulations from trackways, track length, track width and all divarication from tracks (Thulborn 1990). Items of track area (Michilsen et al. 2009; Kubo 2011; Tanaka 2015) and track outline (Tanaka 2015) are recently added. In the track shape research, the vertical section of the depression of track has been considered as more important than the horizontal section (Loope 1986), but recently both sections are considered as important equally (Difley & Exdale 2002).

Animals have changed their body surface patterns in the process of evolution, beside their body structures, ecology, and habitat. Animals possibly have their body patterns according to their survival strategy. Thus, the body pattern is an important study subject for evolution of life. However, body patterns are not remained as fossils. Therefore, theoretical approach is an important method for the study at present. The theoretical approach can show diversity of body pattern formation and evolution, and evaluate real appearance of pattern variations on the earth against all of ideal pattern variations. This method is applied to the body pattern formation as well as the track morphology.

The studies of track fossils aim to reconstruct trackmaker's information about behavior and living habitat because tracks provide information of all tetrapod's gates, foot dynamics, behavior and anatomical details such as phalangeal pads and skin impression. The previous researches are focused on (1) trackmaker's behavior, (2) trackmaker's ecology, (3) dynamics between sediments and trackmaker's behavior and life style, (4) evolution of trackmaker's behavior, (5) reconstruction of trackmaker's habitat. These studies reveal that track morphology shows not only morphology of trackmaker but also trackmaker's behavior and life style.

The purposes of this study are to estimate avian body characters and ecology from tracks, and to reveal the rules of animals' pattern generation. This work deals with four topics. The first and second topics are focused on examinations of the living avian body characters and tracks for the purpose of application to the studies of non-avian theropods and extinct avians. The first topic includes derivation of relationships between track areas and bodyweights, and between track shapes and habitat types. The second topic includes derivation of relationships between track area and wing span, and between tracks area and wing area. The third topic is focused on an ichnological experiment using *Ciconia Boycianas* for the purpose of distinguishing *Ciconia Boyciana*'s tracks from wading birds'. This topic deals with a key character of classification and the relationship between track morphology and walking style. The forth topic is focused on the geological theoretical method to reveal animals' surface pattern to use for estimation with extinct animals. This topic includes derivation of the relationship between surface pattern and lifestyle.

Chapter 2

Estimating body weight and habitat type from extinct avian and avian-like theropod footprints

2. 1. Introduction

Body weight is an important aspect of an organism's biology, because it influences development, reproduction, evolution, physiology and ecology (e.g. Schmidt-Nielsen 1984; Hone & Benton 2005). To obtain such biological information for extinct animals, we estimated body weight based on fossil records. Previous studies have used skeletal measurements to estimate the body weights of extinct animals (Anderson & Hall Martin 1985; Damuth & MacFadden 1990; Ericson et al. 2009). This kind of approach has been successfully applied to animals with well-preserved fossils, but it is difficult to apply to animals evolving the capability of flight (e.g. pterosaurs, extinct avians and ancestors of avians, i.e. avian-like theropods). Because these animals had thin and delicate bones that did not preserve well, their fossil record is poor compared with other animals. Various alternatives have been proposed, such as a 3D mathematical slicing method that uses partial information from bones (Henderson 1999, 2010) and statistical methods that use information from non-skeletal remains, such as tracks (e.g. Kubo 2011).

Well-preserved skeletons of theropods from the Triassic to Early Jurassic periods have been found, but track records are much richer than skeletal records (e.g. Kubo 2011; Martinez et al. 2011). Track records likely reflect the body weight of the

track-maker, but few data are available to demonstrate the relationship between body weight and foot contact area, except for mammals (Michilsens et al. 2009). Kubo (2011) used the tracks of modern reptiles and amphibians to derive this relationship in order to estimate the body weights of extinct animals, such as pterosaurs. Although this method, derived from plantigrade quadrupeds, appears to be widely applicable, the validity of its use for digitigrade bipeds, such as avian-like theropods and avians, remains unclear. Surface area has been the primary geometric information extracted from tracks in previous studies because it is closely related to body weight (Michilsens et al. 2009; Kubo 2011). Additionally, avian foot shape is known to be related to habitat type (Feduccia1996; Gill 2007), but quantitative data describing this relationship are lacking.

The purpose of this study was to derive the relationship between foot area and body weight based on modern avians and to apply it to estimate the body weights of avian-like theropods and extinct avians from fossilized tracks. The derived relationship along with morphology is expected to be useful also for estimating the palaeoecology of avian-like theropods and extinct avians.

2.2. Materials and methods

2.2.1. Track area and body weight

Modern avian track data were collected at Ishikawa Zoo, Ishikawa Prefecture. Avians were classified according to Hackett et al. (2008) and the studied taxa span diverse avian orders including Struthioniformes, Anseriformes, Charadriiformes, Sphenisciformes, Ciconiiformes, Gruiformes, Columbiformes and Passeriformes (Table

1).

Body weights and track areas (one-pes) of adult avians were measured on the same day. Substrate has a strong influence on the size and shape of the track (e.g. Milàn & Bromley 2006); therefore, only clay substrates were used to standardize this factor. The error for body weight was <1 g. Track areas were measured from trackway photographs using the method by Ubukata (2004).

Data were also collected from previous studies involving the fossilized tracks of theropods and theropods with avian-like feet from the Late Triassic to Middle Cretaceous periods and extinct avians from the Cretaceous Period (Table 2; Mehl 1931; Avnimelech 1966; Ellenberger 1970; Currie 1981; Alonso & Marquillas 1986; Ishigaki 1986; Lockley et al. 1992; Gierliński & Ahlberg 1994; Leonardi 1994; Zhen et al. 1994; Yang et al. 1995; Fuentes Vidarte 1996; Azuma et al. 2002; Lockley & Rainforth 2002; Milàn & Gierliński 2004; Lockley & Gierliński 2009; Lü et al. 2010; Xing et al. 2013). *Prototrisauropus* and *Seakatrisauropus* are synonyms of Eubrontes and Grallator (Klein & Haubold 2007). The substrate of extinct avian is almost mud-siltstone, and that of theropod and avian-like theropod is almost sandstone deposit in humid environment.

2.2.2. Track shape and habitat

Track shape was quantified by principal component analysis using the tpsRelw software (Bookstein 1996; Zelditch et al. 2004). This geometric morphometric method cannot be applied to tracks with discrete topologies. Thus, only continuous topology data from a total of 19 avian species were used (Table 1, asterisks). While Hackett et al.'s (2008) classification is used in this paper, I modified the definition of habitat types

as follows: 'Semi-aquatic bird' refer to birds that live mainly on or around water such as ponds, seas and rivers; 'ground bird' refers to birds that live mainly on the ground rather than in air or water; and 'arboreal birds' refers to birds that live mainly in trees and air.

Table 1. Track areas and body weights of living bipeds used in this study.

Order	Taxa	Track number *n*	Weight (g)	Area of footprint (mm2)	General ecological divisions after Hackett et al (2008)
1 Struthioniformes	*Dromaius novaehol**	1	23300	21999	Ground birds†
2 Galliformes	*Coturnix japonica**	8	124±2	287±26	Ground birds†
2 Galliformes	*Coturnix chinensis**	9	58±4	170±29	Ground birds†
2 Galliformes	*Phasianus versicolor**	2	867	947±89	Ground birds†
2 Galliformes	*Pavo cristatus*	1	3780	2637	Ground birds†
3 Columbiformes	*Streptopelia orientalis**	9	147±2	238±39	Ground birds
3 Columbiformes	*Columba livia*	1	300	532	Ground birds
4 Anseriformes	*Anas platyrhynchos*	2	907±89	1855±297	Semi-aquatic birds
4 Anseriformes	*Anas poecilorhyncha*	7	989	2166±483	Semi-aquatic birds
5 Gruiformes	*Balearica regulorum**	2	3100±500	3480±251	Semi-aquatic birds
5 Gruiformes	*Grus vipio*	1	5186	5023	Semi-aquatic birds
6 Sphenisciformes	*Spheniscus magellanicus*	2	3800	4396±356	Semi-aquatic birds
7 Pelecaniformes	*Nycticorax nycticorax**	1	800	973	Semi-aquatic birds
7 Pelecaniformes	*Egretta garzetta**	8	541±68	1654±159	Semi-aquatic birds
7 Pelecaniformes	*Ardea cinerea**	1	1500	1260	Semi-aquatic birds
8 Charadriiformes	*Cnaradrius dubius**	1	40	40	Semi-aquatic birds
8 Charadriiformes	*Larus crassirostris*	1	538	1341	Semi-aquatic birds
8 Charadriiformes	*Larus ridibundus**	2	321	601±15	Semi-aquatic birds
8 Charadriiformes	*Actitis hypoleucos**	24	61±5	229±25	Semi-aquatic birds
8 Charadriiformes	*Tringa brevipes**	6	100	142±28	Semi-aquatic birds
9 Accipitridae	*Pandion haliaetus**	1	1500	1932	Arboreal birds
10 Falconidae	*Milvus migrans**	2	880	1955±268	Arboreal birds
11 Passeriformes	*Motacilla cinerea**	4	21	1052±147	Arboreal birds
11 Passeriformes	*Motacilla alba leucopsis**	3	23	1039±48	Arboreal birds
11 Passeriformes	*Motacilla grandis**	7	35	703±119	Arboreal birds
11 Passeriformes	*Passer montanus**	11	24±1	25±10	Arboreal birds
11 Passeriformes	*Corvus corone**	14	964±139	1201±241	Arboreal birds

Data are reported as mean±standard deviation. *Species used in the geometric morphometric analysis. Number of tracks measured. †Species estimated from general ecological division of Hackett et al. (2008).

Table 2. List of outline of footprint. Nine are theropods and theropods with avian-like feet, and 11 are avian.

Paper	Species	D/B	Era	Area
Xing et al., 2013 p188 Fig 3	*Pengxianpus cifengensis*	Dinosaur	Late Triassic	China
Ellenberger, 1970 p358 Planche I 22	*Seakatrisauropus divergens*	Dinosaur	Late Triassic	South Africa
Milan&Gierlinski, 2004 p71 Fig 1 (Gierlinski&Ahlberg, 1994)	*Eubrontes giganteus*	Dinosaur	Late Triassic	Sweden
Lockley&Gierlinski, 2009 p436 Fig 3 T12	Grallator	Dinosaur	Late Triassic	United states
Lockley et al., 1992 p120 Fig 14	*Trisauropodiscus moabensis*	Dinosaur	Lower Jurassic	United states
Lockley et al., 2002 p408 Fig 17-3D (Avnimelech, 1966 PLATE IV)	Un-named	Dinosaur	Middle Cretaceous (Cenomanian)	Israel
Azuma et al. 2002 p4 Fig 3 Track3	*Aquatilavipes izumiensis*	Avian	Early Cretaceous (Valanginian)	Japan
Lockley et al., 1992 p116 Fig6 (Zhen and Chen, 1994)	*Aquatilavipes sinensis*	Avian	Early Cretaceous (Aptian)	China
Lockley et al., 2002 p408 Fig 17-4A (Fuentes Vidarte, C.F. 1996 p67 Fig 6,8)	*Archaeornithipus meijidei*	Avian	Early Cretaceous (Aptian-Albian)	Spain
Lockley et al., 2002 p408 Fig 17-4B (Fuentes Vidarte, C.F. 1996 p67 Fig 6)	*Archaeornithipus meijidei*	Avian	Early Cretaceous (Aptian-Albian)	Spain
Lockley et al., 1992 p118 Fig 10	*Jindongornipes kimi*	Avian	Early Cretaceous (Aptian-Albian)	South korea
Currie, 1981 p258 Fig 1	*Aquatilavipes swiboldae*	Avian	Early Cretaceous (Aptian-Albian)	Canada
Lü et al., 2010 p48 fig.4	Un-named	Avian	Lower Cretaceous	China
Lockley et al., 2002 p410 Fig 17-8A (Mehl 1931 p446 Fig 1)	*Ignotornis mcconnelli*	Avian	Middle Cretaceous (Cenomanian)	United states
Lockley et al., 2002 p413 Fig 17-12A (Yang et al. 1995)	*Hwangsanipes choughi*	Avian	Late Cretaceous (Campanian)	South Korea
Lockley et al.,2002 p414 Fig 17-13c (Leonardi 1994)	*Patagonichornis venetiorum*	Avian	Late Cretaceous (Maastrichtian)	Argentina
Lockley et al., 1992 p116 Fig 5 (Alonso&Marquillas, 1986)	*Yacoraitichnus avis*	Avian	Late Cretaceous (Maastrichtian)	Argentina

References in parentheses give original footprint data.

The geometric morphometric method has been described in detail elsewhere (e.g. Ubukata, 2004) and is only briefly summarized here. A total of 42 semilandmarks were digitized on the outline of the left track and the reversed right track (seven semilandmarks on each of six sections: bottom of Fig. 3). The scatter at each landmark for each individual was averaged to obtain a mean value of the error due to the orientation of the outline. Individual outlines recovered as semilandmark confirmations were compared with the mean or consensus shape of the analysed sample by mean (Bookstein 1996; Zelditch et al. 2004) and were simulated using the method by Ubukata (2004) to be subjected to the relative warp analysis with a thin plate spline method.

2.3. Results

2.3.1. Track area and body weight

Allometries between body weight (W) and track area (A) were evaluated. Figure 1

shows body weight plotted against track area. The grey line in Figure 1 shows the regression line of the reduced major axis given by:

$$\log W = 1.35 \log A - 1.37 \quad (1)$$

where $R^2 = 0.671$ and $P < 0.001$. The Smirnov–Grubbs test (significant difference: 5%) was performed, and three passeriform species were outliers. The regression line for the sample after exclusion of these three species is shown by the black line in Figure 1 and is expressed by:

$$\log W = 1.15 \log A - 0.63 \quad (2)$$

where $R^2 = 0.941$ and $P < 0.001$. The 95% confidence interval of the slope was 1.09–1.21. Using eqn (2), the body weights of theropods, some with widely divaricated avian-like feet, from the Late Triassic (theropod tracks) are estimated to range from 880 g to 103 kg (Fig. 2A), and those of extinct Cretaceous avians are estimated to range from 93 g to 2.48 kg (Fig. 2B).

2.3.2. Track shape and habitat

I determined a relationship for extant avians between track morphlogy and habitat types of 'semiaquatic bird', 'ground bird' and 'arboreal birds'. Figure 3 shows the results of the track geometric morphometric analysis. The relative warp analysis revealed that the two-first principal components (PC1 and PC2) explain 99.6% of the total variability of the sample (84.6% and 15.1%, respectively; Table 3). The distribution of semi-aquatic avians (black symbols) is separate from that of ground avians (white symbols). Moreover, arboreal birds tracks are also separate from those of other birds. Canonical discriminate analysis indicated that the misclassification rate was

4.7% (each of the ratios for ground birds, semi-aquatic birds and arboreal birds are 90.0%, 97.7% and 97.7%, respectively).

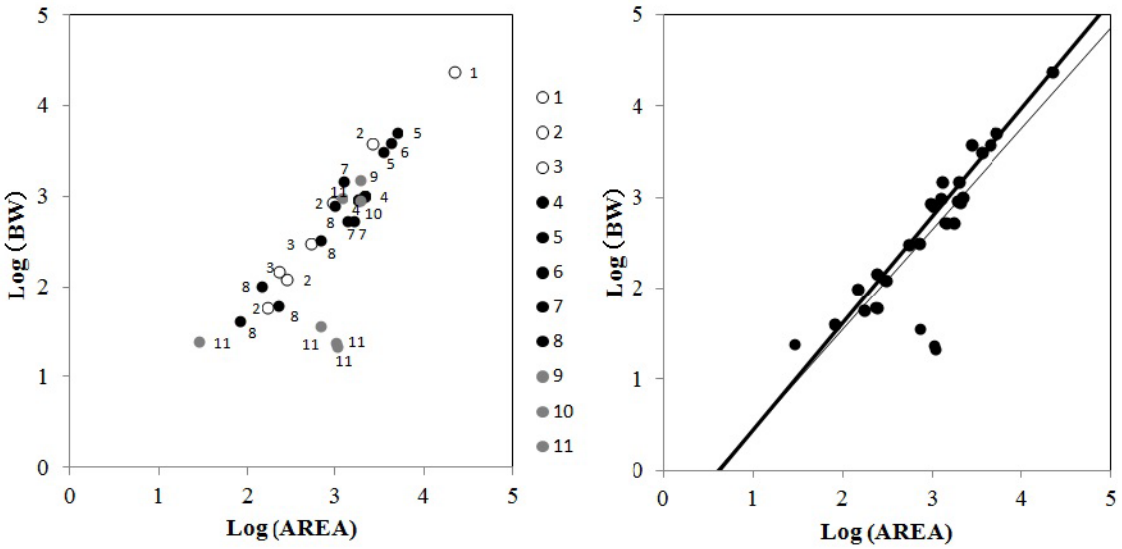

Fig. 1. The relationship between track area and body weight. A, classification (after Table 1). Numbers represent the avian order, and symbols represent habitat type. Open circles indicate ground birds, closed circles semi-aquatic birds, and grey circles arboreal birds. B, reduced major axis regression of body weight (g) on track area (m2) for living avians. The thin line shows regression line for all data point, and the heavy line shows that after the exclusion of Passeriformes outliers (circled).

2.4. Discussion

2.4.1. Comparison with body weight estimations from the skeletal record

Because trackway and skeletal records from the same individual do not exist for fossil vertebrate, it is not possible to directly compare weights estimated from these records. Therefore, the accuracy of predictive equations, such as eqn (2), was assessed based on the percentage prediction error (%PE) and the percentage standard error (%SEE) of the estimate, based on the method set out by Smith (1984). These values

were 8.4 and 28.8, respectively. Comparison with previous weight estimates for fragmentary skeletal specimens of mammals, avians, reptiles and amphibians (Anderson & Hall Martin 1985; Damuth & MacFadden 1990; Witton 2008; Michilsens et al. 2009; Kubo 2011) revealed that the body weights estimated from track areas (PE; 8–29%, SEE; 29–55%) were similar to body weights estimated from fragmentary bone fossils (PE; 15–88%, SEE; 15–57%). Therefore, this approach provides a powerful means of estimating weights when the trackway record is richer than the skeletal record.

The fossil record of theropods, some with avianlike feet, from the Triassic to the Early Jurassic is sparse (Heckert & Lucas 1998; Martinez et al. 2011), and the avian fossil record of the Cretaceous is poor (Fountaine et al. 2005; Martinez et al. 2011), making weight estimation difficult. The maximum body weight of theropod estimated from body fossils in Triassic is *Herrerasaurus*: 210–350 kg (Paul 1988; Nesbitt 2011). On the other hand in this study, the maximum body weight of theropod from track area in Triassic is *Prototrisauropus crassidigitus*: 103 kg. Regarding the mismatch between the largest estimated body weight value from track and that of from body fossil, further discussion is required. *Aquatilavipes izumiensis* from the Tetori Group of Japan is the oldest (Valanginian) known avian track in the world, with a body weight estimated in this study of 154 g (Fig. 2B). Estimates of body weight of the oldest avian *Archaeopteryx* based on skeletal records have ranged from 135 to 330 g (Henderson 1999; Hone et al. 2008; Yalden 2008; Nudds & Dyke 2010). Thus, the bodyweight of the *A. izumiensis* trackmaker is similar to that of *Archaeopteryx*.

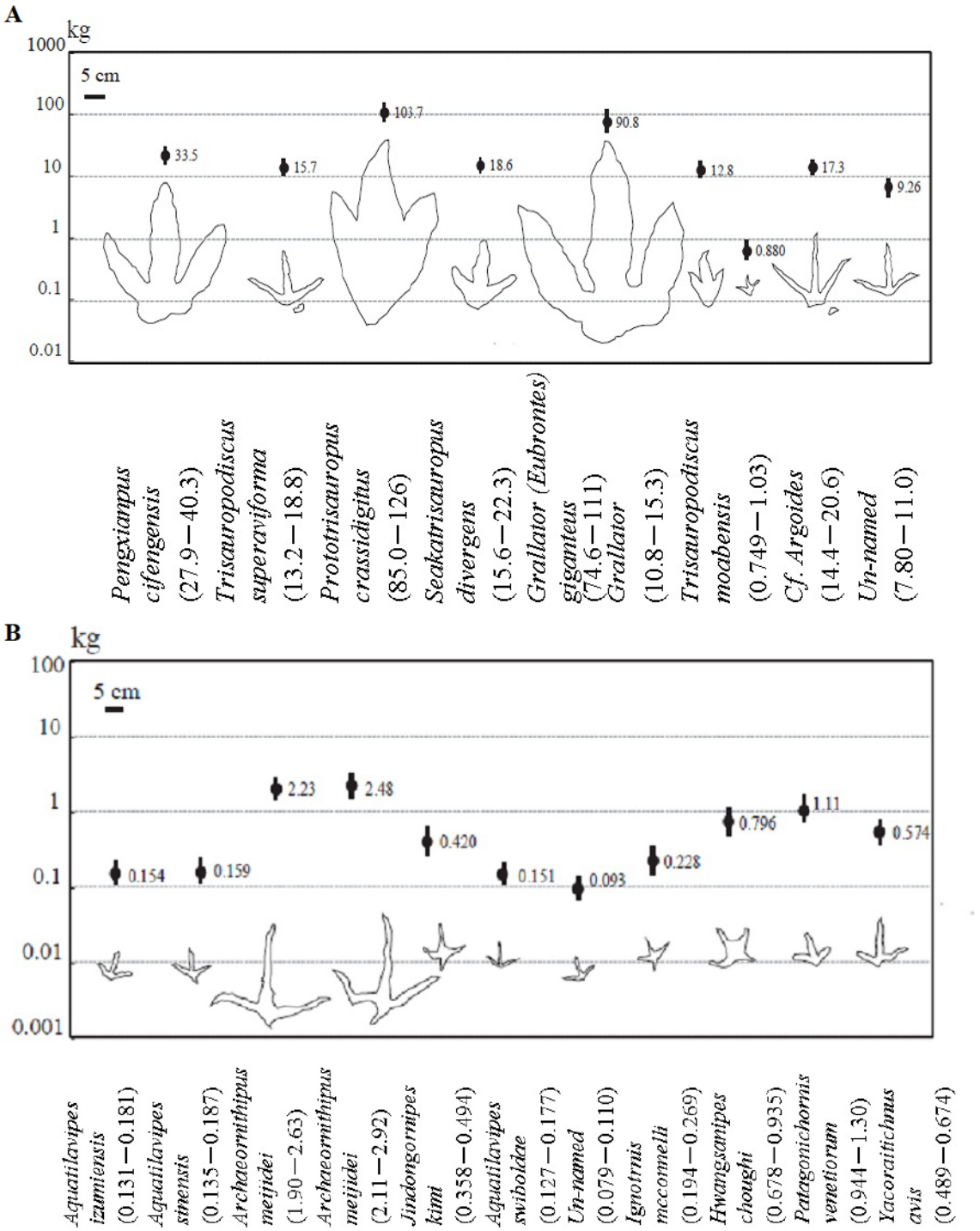

Fig. 2. Schematic diagrams of ichnospecies tracks and estimated body weights. Vertical black lines represent ranges, and solid black circles represent estimated mean body weight (in kilograms). See Table 2 for citations of papers. A, nine ichnotaxa attributed to theropods, avians and theropods and theropods with avian-like feet: the six tracks on the left are Late Triassic, the middle two tracks are Early Jurassic and the track on the right is Middle Cretaceous. B, eleven Cretaceous avian ichnospecies.

2.4.2. Comparison with other area–weight relationships

The relationship between body weight and track area based on modern avians was derived as eqn (2). This correlation is applicable to extinct avians and theropods with avian-like feet because there are digitigrade bipeds. In contrast, Kubo (2011) developed an equation to represent the correlation between track area (both manus and pes) and body weight based on modern plantigrade quadrupeds. Appling the reduced major axis regression method to Kubo's reptile data (Fig. 4) yields:

$$\log W = 1.39 \log A - 1.29 \quad (3)$$

where $R^2 = 0.958$ and $P < 0.001$. Because the body weight of reptiles is supported by four legs, the area in eqn (3) is the area of one-manus and one-pes. In contrast, the area of the avian tracks used in this paper is the area of one-pes, because avian weight is supported by two legs. Figure 4 shows very similar trends in the avian (black circle) and reptile data, despite two differences in the type of foot use (i.e. digitigrade vs. plantigrade, bipedal vs. quadrupedal). This finding is in accordance with the results obtained by Michilsens et al. (2009), who showed that the type of foot used on contact surfaces during walking had no significant effect on body weight.

A t-test (significant difference: 5%) with weight as a covariate and foot use as a factor identified no significant difference between groups. The avian (this paper) and reptile (after Kubo 2011) data sets were then combined to derive the following regression equation (Fig. 4, black line):

$$\log W = 1.25 \log A - 0.91 \quad (4)$$

where $R^2 = 0.939$ and $P < 0.001$. The 95% confidence interval of the slope was 1.20–1.29. Equation (4) may be applicable to a broader range of organisms (i.e.

plantigrade quadrupeds and digitigrade bipeds).

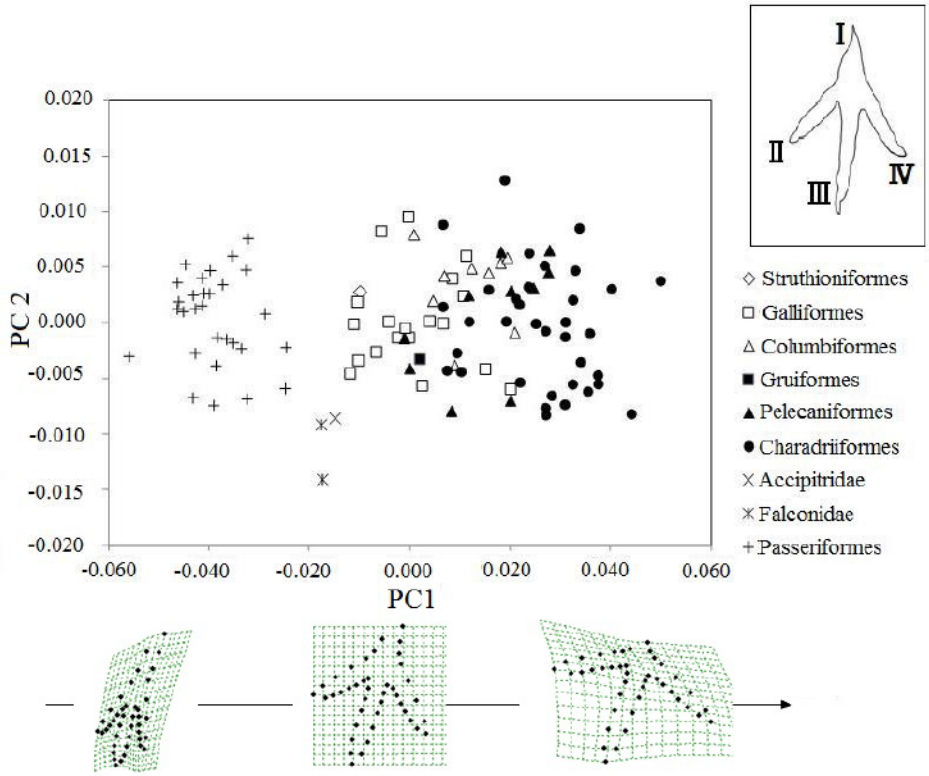

Fig. 3. Results of the geometric morphometric analysis of bird tracks (n = 107). Open symbols indicate ground avian and closed symbols indicate semi-aquatic birds. Note that arboreal birds' tracks are separate from those of other birds.

Table 3. Relative warp analysis results for the first ten principal components.

No.	Eigenvalue	% Explained variance	% Cumulative variance
1	0.02792	84.59	84.59
2	0.00497	15.06	99.64
3	0.00002	0.05	99.70
4	0.00002	0.05	99.75
5	0.00002	0.05	99.79
6	0.00001	0.04	99.83
7	0.00001	0.04	99.87
8	0.00001	0.02	99.89
9	0.00001	0.02	99.91
10	0.00001	0.02	99.93

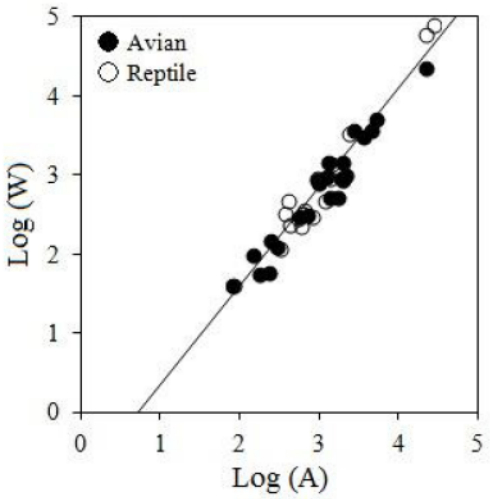

Fig. 4. The reduced major axis regression of body weight (g) on track area (mm2) for living avians and reptiles.

2.4.3. Track shape and habitat

The primary geometric information extracted from tracks in previous studies was the outline and measured area, which is closely related to body weight, as discussed above. Figure 3 also shows that track shape is related to avian habitat type. Specifically, the angle between digits II and IV is larger, and digit I is shorter in semi-aquatic birds compared with ground birds. A t-test showed that track area (i.e. avian weight) was independent of track shape (i.e. avian habitat type). In addition to track area, foot shape thus contains important ecological information.

The habitats of Triassic theropods and theropods with avian-like feet and Cretaceous avians were assessed based on the results of this analysis. The relative warp analysis revealed that the two-first principal components (PC1 and PC2) explained 99.26% of the total variability of the sample (82.89% and 16.37%, respectively; Table 4). Figure 5 shows that the extinct animals are distributed within the semi-aquatic bird type. This finding lends support to inferences made in previous studies that track sites were

floodplain and wetland environments (Lockley & Rainforth 2002). This implies that the pes of animals living in areas characterized by fluctuating water levels and under conditions facilitating the preservation of footprints is similar to that of extant emi-aquatic avian. It should be noted that Figure 5 should not be interpreted to mean that most Triassic and Jurassic theropods were semi-aquatic: because tracks do not preserve well under dry conditions, it simply means that most tracks of non-semi-aquatic theropods were not preserved.

Table 4. Relative warp analysis results for the first 10 principal components including fossil tracks.

No.	Eigenvalue	% Explained variance	% Cumulative variance
1	0.02635	82.89	82.89
2	0.00520	16.37	99.26
3	0.00005	0.17	99.42
4	0.00003	0.10	99.53
5	0.00002	0.07	99.60
6	0.00002	0.05	99.65
7	0.00001	0.05	99.70
8	0.00001	0.05	99.74
9	0.00001	0.04	99.78
10	0.00001	0.03	99.82

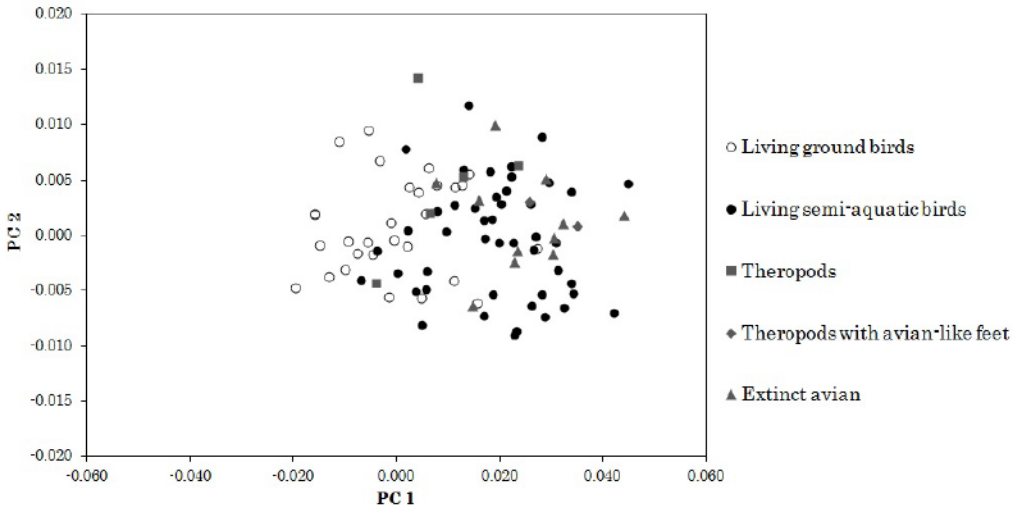

Fig. 5. The resulting geometric morphometric track distribution. PC1 explains that the divarication angle between digits II and IV increases and digit I shortens from left to right. The extinct avians, theropods and theropods with avian-like feet plotted within the distribution of living birds. PC2 explains the left or right warping of the track outline.

2.5. Conclusions

The relationship between body weight and footprint area of modern avians was derived and used to estimate the body weights of extinct theropod ichnotaxa from the Triassic to Early Cretaceous periods and avian ichnotaxa from the latter period. Body weights estimated from track area are similar to body weights estimated from fragmentary bone fossils, so this approach is useful when the fossilized track record is richer than the fossilized skeletal record.

Additionally, the data sets from avians were combined with those from other reptiles from Kubo (2011) and could derive the weight–area relation such as eqn (3). This generalized equation implies that the animals have a footprint area suitable for their weight and is applicable to a broader range of organisms, such as plantigrade-digitigrade quadrupeds and digitigrade bipeds.

Finally, the relationship between habitat type and footprint shape of modern avians was assessed based on scatter plots. The principal component analysis revealed that the angle between digits II and IV and the length of digit I in the track record are related to habitat type: semi-aquatic, ground or arboreal bird. In addition to track area, foot shape thus contains important ecological information. The shape–habitat relation was applied to extinct avians and demonstrated that the pes of extinct animals living in a semi-aquatic environment is similar to that of the present semi-aquatic avians.

Chapter 3

Avian wing loading, aspect ratio, area and span correlate with track

3. 1. Introduction

Animals move using structures such as legs or wings. The size and morphology of an animal's structure are related to its habitat, and the morphology is constrained by size (McMahon & Bonner 1983; Damuth & MacFadden 1990). In the process of evolution, habitat has constrained the morphology of animal structures, which has constrained locomotion (Schmidt-Nielsen 1984; Alexander 2002). The feet have the closest fit to habitat (Feduccia 1996; Gill 2007) and tracks are determined by the feet. Tracks reveal the form of walking movement and contain a significant amount of biological information. The area of the track can be used to estimate the bodyweights of reptiles and amphibians (Kubo 2011). For birds, even the habitat type can be deduced from the shape of the tracks, as well as the bodyweight from the track area (Tanaka 2015). The relationship between track area and bodyweight has been studied among mammals (Michilsens et al. 2009). This approach has been successfully applied to animals

having flight capability (e.g., pterosaurs and extinct birds and their ancestors; i.e., avian-like theropods). Because these animals have thin and delicate bones that are rarely preserved, their fossil records are poor compared with other animals. Therefore, records of their tracks become valuable for estimating the form of their bodies. Avian legs consist of two parts: forelegs, which are wings used for flight, and hind legs, which are used for bipedal walking. Birds use their legs effectively for the purpose of locomotion. Their tracks reflect their bipedal walking mode. Provided that the track morphology is constrained by habitat, the morphology of the wings, used for another type of locomotion, may also be similarly constrained.

Tanaka (2015) quantified track morphology using thin-plate spline relative warp analysis (e.g., Ubukata 2003; Zelditch et al. 2004) and classified the angle between digits II and IV and the length of digit I in avian track records based on the shape of the track into three groups in a global standard phylogeny of birds (Hackett et al. 2008), which he called “arboreal birds”, “ground birds” and “semi-aquatic birds”. The avian ecomorphological classification is often based on wing shape and bodyweight, represented by wing aspect ratio and loading. These two factors and their relationship have been used for aerodynamic studies of extant birds (e.g., Rayner 1988; Hazlehurst & Rayner 1992; Witton & Habib 2010) and bats (e.g., Norberg & Rayner 1987;

Neuweiler 2000), resulting in their grouping into five or six habitat types.

When considering body design concepts, it is plausible that avian wings are related to tracks. This relationship may provide a method to estimate wing shape and size from tracks. Avian hind legs, the most sensitive part of the body, have evolved to adapt to the surrounding environment (e.g. Gill 2007) and thus may have been affected by habitat. The purpose of this study was to examine if avian wings are constrained by habitat in a similar manner to track shape. We collected wing and bodyweight data from modern birds. Then, we calculated a quantitative relationship between the track and wing parameters. Finally, we tested if the relationship could be used to estimate the size and shape of wings of extinct birds.

3.2. Collection of modern avian data

Data sets of adult bodyweight, wing area and wingspan for 18 species (23 specimens) were collected from the Aicho Center in Niigata Prefecture, Yamashina Institute for Ornithology and Kobe University. For 11 species, data were obtained from live specimens. Bodyweights were measured within an error <1 g. The wingspans were measured within an error <1 cm, stretching the wings as widely as possible with the blade angle pressed down. The wing area and wingspan of 7 species were measured

using stuffed specimens kept in the Yamashina Institute for Ornithology, whose wings were stretched almost at maximum, with the blade angle pressed down as for the live specimens. For the 7 species of stuffed specimens we referred to Tanaka (2015) for wing measurement and bodyweight data. For both live and stuffed specimens, the wing areas were measured within an error <1 cm^2 by taking photographs of the wingspans on a meshed board and taking measurements from computer images using the method of Ubukata (2004).

Data were also collected from previous studies using the fossilized tracks of extinct birds from the Cretaceous and Cenozoic Periods (Table 4; Yang et al. 1995; Fuentes Vidarte 1996; Lockley & Rainforth 2002; Alonso & Marquillas 2009).

3.3. Method

To examine the relationship between tracks and wings, we defined the wing aspect ratio (P) and wing loading (Q) as follows:

$$P = \frac{b^2}{a} \quad , \tag{1}$$

$$Q = \frac{Mg}{a} \quad , \tag{2}$$

where a is wing area, b is wingspan, M is bodyweight and g is the acceleration due to gravity (9.81 m/s^2). We plotted P versus Q (N/m^2) for 18 species, with the track

group indicated for each data point, to directly examine the relationship between the wing parameters and tracks. We used the three groups defined by track shape (Tanaka 2015), denoted A, B and C (Fig. 1). Group A includes species whose angle between digits II and IV is smaller and digit I is longer than group B. Group C includes species whose angle between digits II and IV is larger and digit I is shorter than group B. Group B includes species whose track data lie between groups A and C.

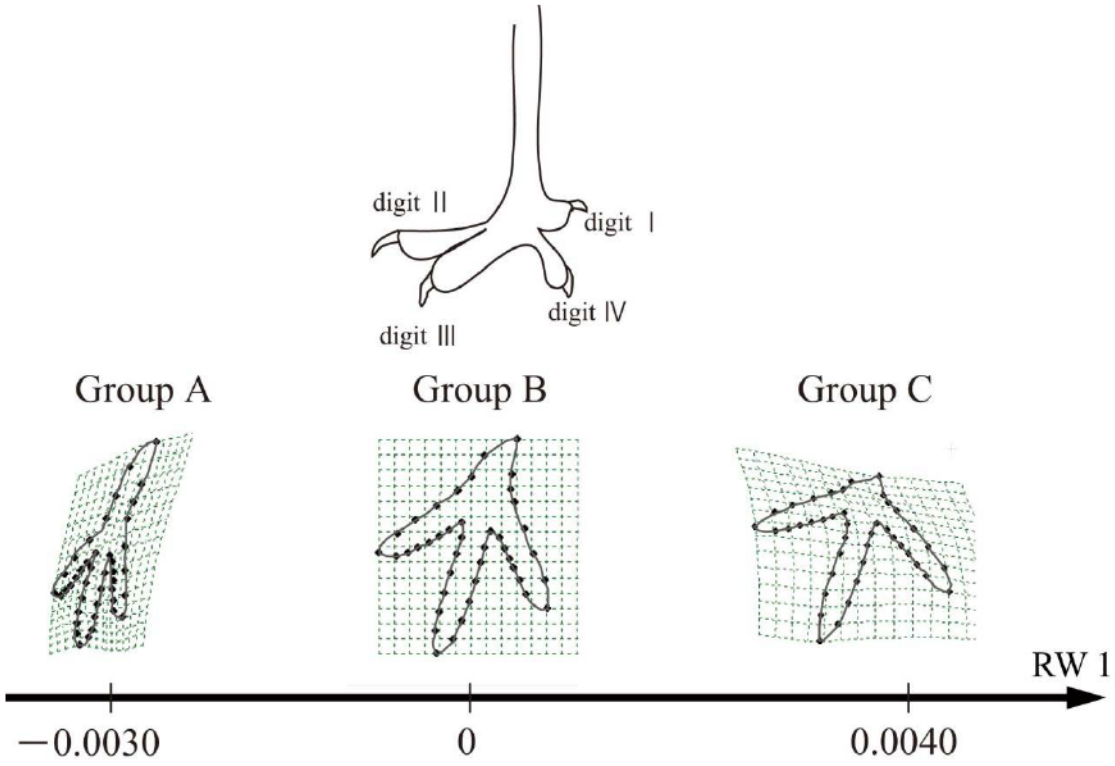

Fig. 1. Avian groups defined by track shape. The top diagram shows an avian left leg with digit numbers. The bottom diagrams shows typical track shapes for each group defined based on geometric morphometric analyses of avian tracks conducted on 107 specimens (Tanaka, 2014). RW1 is the primary principal component (contribution ratio 84.6%) of the relative warp analysis. Group A (RW1 from –0.0030 to –0.0086) includes species whose tracks have a smaller angle between digits II and IV and a longer digit I. Group C (RW1 from –0.0030 to 0.0040) includes species whose tracks have a larger angle between digits II and IV and a shorter

digit I. Group B (RW1 from –0.0045 to –0.0008) includes species whose angle between digits II and IV and length of digit I are between those of groups A and C.

To quantitatively evaluate the relationship between wing data and track shape for 18 species, we performed multiple regression analysis on the mean values for each species. We used the primary principal component, RW1, obtained from relative warp analysis of avian track shape data for 107 specimens (Tanaka 2015) as a proxy for track shape. Because of its high contribution ratio (84.6%), the value of RW1 closely represented track shape. RW1 was set as the objective variable Y, and Q and A as the explanation variables, X_1 and X_2, respectively.

We determined the ranges of the wing aspect ratio and wing loading for each group. Groups A, B and C were correlated with the habitat types of arboreal birds, ground birds, and semi-aquatic birds, respectively (Tanaka 2015). Birds that lack track data can be divided into the three groups using this correlation. The ranges of the wing parameters were determined using combined data sets of bodyweight, wing area and wingspan, combined with those for 60 modern bird species (110 specimens) published by Greenewalt (1962) and Witton & Habib (2010). In addition, we added new data for 4 species obtained from live specimens from the Aicho Center and for one species from a specimen from the Yamashina Institute for Ornithology. Because we could only measure

wing area and wingspan for the latter, its bodyweight was taken from Tanaka (2015). The published data for 110 modern birds are mainly from relatively large birds. Therefore, the data from small avian species obtained in this study will considerably improve the data set to enable more efficient extraction of the effects of size and shape. The birds were classified following Hackett et al. (2008) and the studied taxa spanned diverse avian orders, including Galliformes, Columbiformes, Anseriformes, Otididae, Procellariiformes, Ciconiiformes, Charadriiformes, Accipitridae, Strigiformes, Falconidae and Passeriformes (Tables 1 and 2). We performed canonical discriminant analysis for 133 data points to examine if avian wings can be grouped.

Table 1. List of avian body data (n=23, 18species). General ecological devisions are after Tanaka (2015). Reference # 1: Bodyweight, wing area and wing span of a living bird were measured in Kobe University and Niigata Prefectural Aicho Center. Reference # 2: Wing area and wing span were measured of spread wing specimens kept in Yamashina Institute for Ornithology (*Streptopelia orientalis YIO-63530, Nycticorax nyctiorax YIO-63264, Egretta garzetta YIO-62693, Charadrius dubius* YIO-20712, *Larus ridibundus* YIO-63773, *Actitis hypoleucos* YIO-64057/YIO-04057, *Pandion haliaetus* YIO-63207/YIO-08813),and their bodyweight data were referred to Tanaka (2014).

Order	Taxa	Weight (kg)	Wing area (m^2)	Wing span (m)	Aspect ratio	Wing loading (N/m^2)	General ecological division	Reference
Galliformes	*Coturnix japonica*	0.159	0.0234	0.38	6.2	66.7	Ground	1
Galliformes	*Coturnix chinensis*	0.057	0.0081	0.24	6.8	69.1	Ground	1
Galliformes	*Phasianus versicolor*	0.867	0.0809	0.72	6.4	105.1	Ground	1
Columbiformes	*Streptopelia orientalis*	0.147	0.0326	0.44	5.9	44.3	Ground	2
Columbiformes	*Columba livia*	0.300	0.0567	0.56	5.5	51.9	Ground	1
Pelecaniformes	*Nycticorax nyctiorax*	0.800	0.1236	0.98	7.8	63.5	Semi-aquatic	2
Pelecaniformes	*Egretta garzetta*	0.541	0.1011	0.92	8.3	52.5	Semi-aquatic	2
Pelecaniformes	*Ardea cinerea*	1.260	0.3300	1.62	8.0	37.5	Semi-aquatic	1
Charadriiformes	*Charadrius dubius*	0.040	0.0119	0.35	10.0	33.0	Semi-aquatic	2
Charadriiformes	*Larus ridibundus*	0.321	0.0859	0.86	8.6	36.7	Semi-aquatic	2
Charadriiformes	*Actitis hypoleucos*	0.061	0.0105	0.34	10.8	56.7	Semi-aquatic	2
Accipitridae	*Pandion haliaetus*	1.500	0.4016	1.61	6.5	36.6	Arboreal	2
Falconidae	*Milvus migrans*	1.010	0.6751	1.85	5.1	14.7	Arboreal	1
Falconidae	*Milvus migrans*	1.035	0.6900	1.96	5.6	14.7	Arboreal	1
Falconidae	*Milvus migrans*	0.940	0.6580	1.88	5.4	14.0	Arboreal	1
Passeriformes	*Motacilla cinerea*	0.026	0.0140	0.33	7.5	18.2	Arboreal	1
Passeriformes	*Motacilla cinerea*	0.023	0.0129	0.31	7.4	17.5	Arboreal	1
Passeriformes	*Motacilla alba leucopsis*	0.022	0.0144	0.30	6.3	15.0	Arboreal	1
Passeriformes	*Motacilla grandis*	0.024	0.0153	0.33	7.1	15.4	Arboreal	1
Passeriformes	*Passser montanus*	0.024	0.0135	0.23	3.8	17.4	Arboreal	1
Passeriformes	*Passser montanus*	0.022	0.0134	0.21	3.1	16.1	Arboreal	1
Passeriformes	*Corvus corone*	0.990	0.3207	1.18	4.3	30.3	Arboreal	1
Passeriformes	*Corvus corone*	1.013	0.3650	1.23	4.1	27.2	Arboreal	1

Table 2. List of avian body data (n=110, 60 species). General ecological divisions are after Hackett et al. (2012). Reference # 1: Greenwalt (1962); 2: Witton and Habib (2010); 3: Living bodies were measured in Niigata Prefectural Aicho Center;4: Wing area and wing span were measured of a spread wing specimen (*Larus crassirostris* YIO-63199) kept in Yamashina Institute for Ornithology, and its bodyweight was referred to Tanaka (2015).

Order	Taxa	Weight (kg)	Wing area (m^2)	Wing span (m)	Aspect ratio	Wing loading (N/m^2)	General ecological division	Reference
Galliformes	*Tetrao urogallus*	2.700	0.1785	1.160	7.5	148.4	Ground	1
Galliformes	*Tetrao tetrix*	2.600	0.1800	1.130	7.1	141.7	Ground	1
Galliformes	*Tetrao tetrix*	1.450	0.1380	1.020	7.5	103.1	Ground	1
Galliformes	*Tetrao tetrix*	1.350	0.0995	0.820	6.8	133.1	Ground	1
Galliformes	*Tetrao tetrix*	1.030	0.0850	0.800	7.5	118.9	Ground	1
Galliformes	*Tetrao tetrix*	1.200	0.0880	0.870	8.6	133.8	Ground	1
Galliformes	*Tetrao tetrix*	0.730	0.0530	0.625	7.4	135.1	Ground	1
Galliformes	*Tetrao tetrix*	1.000	0.0775	0.750	7.3	126.6	Ground	1
Galliformes	*Tetrao bonasia*	0.370	0.0340	0.520	8.0	106.8	Ground	1
Galliformes	*Tetrao bonasia*	0.375	0.0375	0.510	6.9	98.1	Ground	1
Galliformes	*Lagopus alpinus*	0.530	0.0640	0.660	6.8	81.2	Ground	1
Galliformes	*Lagopus alpinus*	0.650	0.0452	0.600	8.0	141.1	Ground	1
Galliformes	*Perdix rufa*	0.380	0.0400	0.510	6.5	93.2	Ground	1
Galliformes	*Perdix cinerea*	0.450	0.0365	0.600	9.9	120.9	Ground	1
Galliformes	*Perdix cinerea*	0.320	0.0336	0.510	7.7	93.4	Ground	1
Galliformes	*Perdix cinerea*	0.372	0.0382	0.490	6.3	95.5	Ground	1
Galliformes	*Perdix cinerea*	0.375	0.0366	0.530	7.7	100.5	Ground	1
Galliformes	*Pavo crist*	3.100	0.3480	1.280	4.7	87.4	Ground	1
Galliformes	*Phasianus colchicus*	0.950	0.0755	0.640	5.4	123.4	Ground	1
Galliformes	*Phasianus colchicus*	1.100	0.0855	0.720	6.1	126.2	Ground	1
Galliformes	*Phasianus colchicus*	1.000	0.0880	0.760	6.6	111.5	Ground	1
Galliformes	*Phasianus colchicus*	1.570	0.0895	0.720	5.8	172.1	Ground	1
Galliformes	*Phasianus colchicus*	1.250	0.0896	0.720	5.8	136.9	Ground	1
Galliformes	*Phasianus colchicus*	1.125	0.0900	0.730	5.9	122.6	Ground	1
Columbiformes	*Columba livia*	0.232	0.0598	0.700	8.2	38.1	Ground	1
Columbiformes	*Columba livia*	0.242	0.0541	0.640	7.6	43.9	Ground	1
Columbiformes	*Columba livia*	0.335	0.0650	0.640	6.3	50.6	Ground	1
Otididae	*Otis tarda*	8.900	0.5729	2.070	7.5	152.4	Ground	1
Otididae	*Otis tarda*	9.600	0.5937	2.080	7.3	158.6	Ground	1
Anseriformes	*Anas*	0.606	0.0642	0.780	9.5	92.6	Semi-aquatic	1
Anseriformes	*Anas boschas*	0.880	0.0685	0.830	10.1	126.0	Semi-aquatic	1
Anseriformes	*Anas boschas*	1.100	0.0900	0.940	9.8	119.9	Semi-aquatic	1
Anseriformes	*Anas boschas*	0.900	0.0710	0.835	9.8	124.4	Semi-aquatic	1
Anseriformes	*Anas boschas*	0.900	0.0735	0.890	10.8	120.1	Semi-aquatic	1
Anseriformes	*Anas boschas*	0.950	0.0838	0.875	9.1	111.2	Semi-aquatic	1
Anseriformes	*Anas boschas*	0.900	0.0813	0.880	9.5	108.6	Semi-aquatic	1
Anseriformes	*Anas boschas*	1.000	0.0687	0.850	10.5	142.8	Semi-aquatic	1
Anseriformes	*Cygnus columbianus*	3.070	0.4365	1.830	7.7	69.0	Semi-aquatic	3
Anseriformes	*Fuligula cristata*	1.116	0.0895	1.040	12.1	122.3	Semi-aquatic	1
Anseriformes	*Fuligula clangula*	0.827	0.0480	0.690	9.9	169.0	Semi-aquatic	1
Anseriformes	*Fuligula glacialis*	0.922	0.0550	0.740	10.0	164.5	Semi-aquatic	1
Procellariiformes	*Diomedea exulans*	8.160	0.6600	3.460	18.1	121.3	Semi-aquatic	2
Procellariiformes	*Diomedea exulans*	8.730	0.6100	3.030	15.1	140.4	Semi-aquatic	2
Procellariiformes	*Diomedea irrorata*	2.040	0.3600	2.310	14.8	55.6	Semi-aquatic	2
Procellariiformes	*Thalassarche melanophrys*	3.790	0.3600	2.160	13.0	103.3	Semi-aquatic	2
Procellariiformes	*Thalassarche chrysostoma*	3.790	0.3500	2.180	13.6	106.2	Semi-aquatic	2
Procellariiformes	*Phoebetria sp.*	2.840	0.3400	2.180	14.0	81.9	Semi-aquatic	2
Procellariiformes	*Macronectes sp.*	5.190	0.3300	1.990	12.0	154.3	Semi-aquatic	2
Procellariiformes	*Procellaria aequinoctialis*	1.370	0.1700	1.400	11.5	79.1	Semi-aquatic	2
Procellariiformes	*Fulmarus sp.*	0.820	0.1200	1.130	10.6	67.0	Semi-aquatic	2
Procellariiformes	*Puffinus pacificus*	0.380	0.1000	1.010	10.2	37.3	Semi-aquatic	2
Procellariiformes	*Puffinus nativitatis*	0.340	0.0700	0.820	9.6	47.6	Semi-aquatic	2

Table 2. (continued)

Order	Taxa	Weight (kg)	Wing area (m^2)	Wing span (m)	Aspect ratio	Wing loading (N/m^2)	General ecological division	Reference
Ciconiiformes	*Ciconia*	3.300	0.4880	1.700	5.9	66.3	Semi-aquatic	1
Ciconiiformes	*Botaurus stellaris*	1.500	0.1915	1.200	7.5	76.8	Semi-aquatic	1
Ciconiiformes	*Ardea alba*	1.280	0.3313	1.730	9.0	37.9	Semi-aquatic	3
Charadriiformes	*Haematopus ostralegus*	0.555	0.0722	0.810	9.1	75.4	Semi-aquatic	1
Charadriiformes	*Numenius arquatus*	0.695	0.0936	0.935	9.3	72.8	Semi-aquatic	1
Charadriiformes	*Numenius arquatus*	0.762	0.0924	0.980	10.4	80.9	Semi-aquatic	1
Charadriiformes	*Larus canus*	0.355	0.1118	1.080	10.4	31.1	Semi-aquatic	1
Charadriiformes	*Larus crassirostris*	0.538	0.0781	0.945	11.4	67.6	Semi-aquatic	4
Charadriiformes	*Sterna cantiaca*	0.174	0.0660	0.936	13.3	25.9	Semi-aquatic	1
Charadriiformes	*Sterna hirundo*	0.116	0.0427	0.790	14.6	26.7	Semi-aquatic	1
Charadriiformes	*Sterna minuta*	0.053	0.0185	0.500	13.5	28.0	Semi-aquatic	1
Charadriiformes	*Vanellus cristatus*	0.232	0.0730	0.660	6.0	31.2	Semi-aquatic	1
Charadriiformes	*Scolopax rusticola*	0.300	0.0500	0.630	7.9	58.9	Semi-aquatic	1
Charadriiformes	*Scolopax rusticola*	0.320	0.0500	0.640	8.2	62.8	Semi-aquatic	1
Charadriiformes	*Scolopax rusticola*	0.300	0.0505	0.630	7.9	58.3	Semi-aquatic	1
Charadriiformes	*Scolopax gallinago*	0.300	0.0440	0.590	7.9	66.9	Semi-aquatic	1
Charadriiformes	*Scolopax gallinago*	0.270	0.0490	0.620	7.8	54.1	Semi-aquatic	1
Charadriiformes	*Scolopax gallinago*	0.300	0.0505	0.600	7.1	58.3	Semi-aquatic	1
Accipitridae	*Haliaetus albicilla*	5.000	0.7973	2.260	6.4	61.5	Arboreal	1
Accipitridae	*Haliaetus albicilla*	4.500	0.7000	2.170	6.7	63.1	Arboreal	1
Accipitridae	*Haliaetus albicilla*	4.700	0.6200	2.090	7.0	74.4	Arboreal	1
Accipitridae	*Astur palumbarius*	0.800	0.1520	1.030	7.0	51.6	Arboreal	1
Accipitridae	*Accipiter nisus*	0.260	0.0800	0.750	7.0	31.9	Arboreal	1
Accipitridae	*Accipiter nisus*	0.275	0.0690	0.680	6.7	39.1	Arboreal	1
Accipitridae	*Accipiter nisus*	0.150	0.0496	0.555	6.2	29.7	Arboreal	1
Accipitridae	*Accipiter nisus*	0.250	0.0710	0.690	6.7	34.5	Arboreal	1
Accipitridae	*Buteo vulgaris*	0.900	0.2610	1.300	6.5	33.8	Arboreal	1
Accipitridae	*Buteo vulgaris*	0.900	0.2590	1.260	6.1	34.1	Arboreal	1
Accipitridae	*Buteo vulgaris*	0.800	0.2210	1.250	7.1	35.5	Arboreal	1
Accipitridae	*Buteo vulgaris*	0.600	0.2170	1.170	6.3	27.1	Arboreal	1
Accipitridae	*Buteo vulgaris*	1.217	0.2350	1.230	6.4	50.8	Arboreal	1
Accipitridae	*Archibuteo lagopus*	0.862	0.2280	1.200	6.3	37.1	Arboreal	1
Accipitridae	*Archibuteo lagopus*	1.000	0.2359	1.400	8.3	41.6	Arboreal	1
Accipitridae	*Archibuteo lagopus*	0.890	0.2020	1.290	8.2	43.2	Arboreal	1
Accipitridae	*Archibuteo lagopus*	1.000	0.2445	1.350	7.5	40.1	Arboreal	1
Accipitridae	*Archibuteo lagopus*	1.000	0.2510	1.440	8.3	39.1	Arboreal	1
Accipitridae	*Archibuteo lagopus*	0.900	0.2220	1.320	7.8	39.8	Arboreal	1
Accipitridae	*Archibuteo lagopus*	1.125	0.2880	1.430	7.1	38.3	Arboreal	1
Accipitridae	*Archibuteo lagopus*	0.750	0.2420	1.370	7.8	30.4	Arboreal	1
Accipitridae	*Butastur indicus*	0.410	0.0907	0.800	7.1	44.3	Arboreal	3
Strigiformes	*Strix flammea*	0.400	0.1190	0.970	7.9	33.0	Arboreal	1
Strigiformes	*Strix flammea*	0.250	0.1440	0.970	6.5	17.0	Arboreal	1
Strigiformes	*Strix uralensis*	0.680	0.2207	0.870	3.4	30.2	Arboreal	3
Strigiformes	*Asio otus*	0.275	0.1010	0.920	8.4	26.7	Arboreal	1
Strigiformes	*Asio otus*	0.232	0.1102	0.920	7.7	20.7	Arboreal	1
Strigiformes	*Asyo brachyotus*	0.370	0.1230	1.030	8.6	29.5	Arboreal	1
Strigiformes	*Smyrnium aluco*	1.777	0.3020	0.945	3.0	57.7	Arboreal	1
Falconidae	*Falco tinnunculus*	0.260	0.0680	0.650	6.2	37.5	Arboreal	1

Table 2. (continued)

Order	Taxa	Weight (kg)	Wing area (m^2)	Wing span (m)	Aspect ratio	Wing loading (N/m^2)	General ecological division	Reference
Passeriformes	*Psittacus erithacus*	0.200	0.0710	0.710	7.1	27.6	Arboreal	1
Passeriformes	*Turdus pilaris*	0.100	0.0186	0.390	8.2	52.7	Arboreal	1
Passeriformes	*Corvus cornix*	0.557	0.1260	0.780	4.8	43.4	Arboreal	1
Passeriformes	*Corvus frugilegus*	0.575	0.1285	0.920	6.6	43.9	Arboreal	1
Passeriformes	*Corvus monedula*	0.225	0.0601	0.600	6.0	36.7	Arboreal	1
Passeriformes	*Corvus monedula*	0.204	0.0610	0.640	6.7	32.8	Arboreal	1
Passeriformes	*Corvus pica*	0.202	0.0560	0.555	5.5	35.4	Arboreal	1
Passeriformes	*Corvus pica*	0.179	0.0482	0.510	5.4	36.4	Arboreal	1
Passeriformes	*Garrulus glandarius*	0.180	0.0565	0.560	5.6	31.3	Arboreal	1
Passeriformes	*Chrysotis amazonica*	0.300	0.0895	0.730	6.0	32.9	Arboreal	1

3.4. Results

3.4.1. Relationship between flight ecology and track shape

Figure 2 shows that each track group exhibits a specific distribution of wing loading and wing aspect ratio. The data points of group C shown by solid diamonds are clearly grouped and clearly separated from those of group B, shown by open circles.

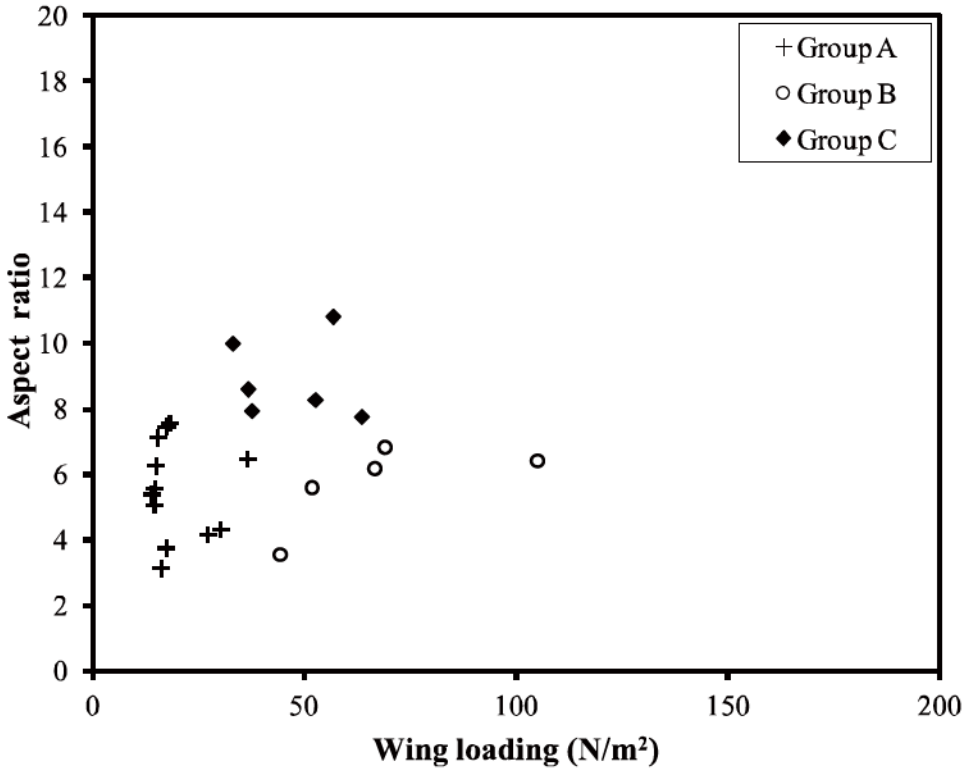

Fig. 2. Wing loading versus wing aspect ratio for 22 avian specimens (17 species). Groups A (crosses), B (open circles) and C (solid diamonds) are defined by track shape, as shown in Fig. 1. The data are from Table 1.

Furthermore, the data points of group A, shown by crosses, are clustered and clearly separated from other groups. These results suggest that bird wing evolution may have been constrained by habitat, similar to tracks. Multiple regression analysis for 17 species provided the following equation:

$$Y = (4.7 \times 10^{-4})Q + (7.8 \times 10^{-3})P - 0.079 \ (R^2 = 0.64) \ . \qquad (3)$$

The equation indicates a simple correspondence of track shape (Y; the primary principal component of the relative warp analysis of track shape (Tanaka 2015) to both wing loading (Q) and aspect ratio (P). Namely, avian wing loading and aspect ratio are closely related to track shape. The close relation can be interpreted as the habitat probably affecting the evolution of both avian wings and legs.

The 133 wing data points also showed separate clusters corresponding to habitat (Fig. 3). The 95% confidence interval ranges (mean$\pm 2\sigma$) of wing loading and wing aspect ratio were (Q: 34.3$\pm$27.0 N/m^2, P: 6.4$\pm$2.8) for group A (arboreal), (Q: 108.0 $\pm$70.6 N/m^2, P: 6.9$\pm$2.3) for group B (ground) and (Q: 78.3$\pm$79.0 N/m^2, P: 10.3$\pm$ 5.2) for group C (semi-aquatic; Table 3). Canonical discriminant analysis showed that the misclassification rate was only 18.2% (the identification ratios for groups A, B and C were 73.9%, 83.9% and 96.9%, respectively). This supports the validity of using the wing parameters to define avian groups. The aspect ratios for birds in group C had a wide range, from 5.9 to 18.0, whereas the aspect ratios for birds in groups A and B were smaller than those for group C, with narrow ranges, from 3.6 to 9.2 for A and from 4.6 to 9.2 for group B (Tables 1 and 2, Fig. 3). Thus, birds in group C have narrow wing shapes and birds in groups A and B have broad wing shapes. Birds in group A have a

narrow range of wing loading, whereas birds in groups B and C have broad ranges of wing loading (Fig. 3).

Table 3. 95% confidence interval ranges(2σ) of avian body data. for each group divided from track shape Group A: Arboreal birds; Group B: Ground birds; Group C: Semi-aquatic birds.

	Group A	Group B	Group C
Wing loading (N/m²)	34.3 ± 27.0	108.0 ± 70.6	78.3 ± 79.0
Aspect ratio	6.4 ± 2.8	6.9 ± 2.3	10.3 ± 5.2

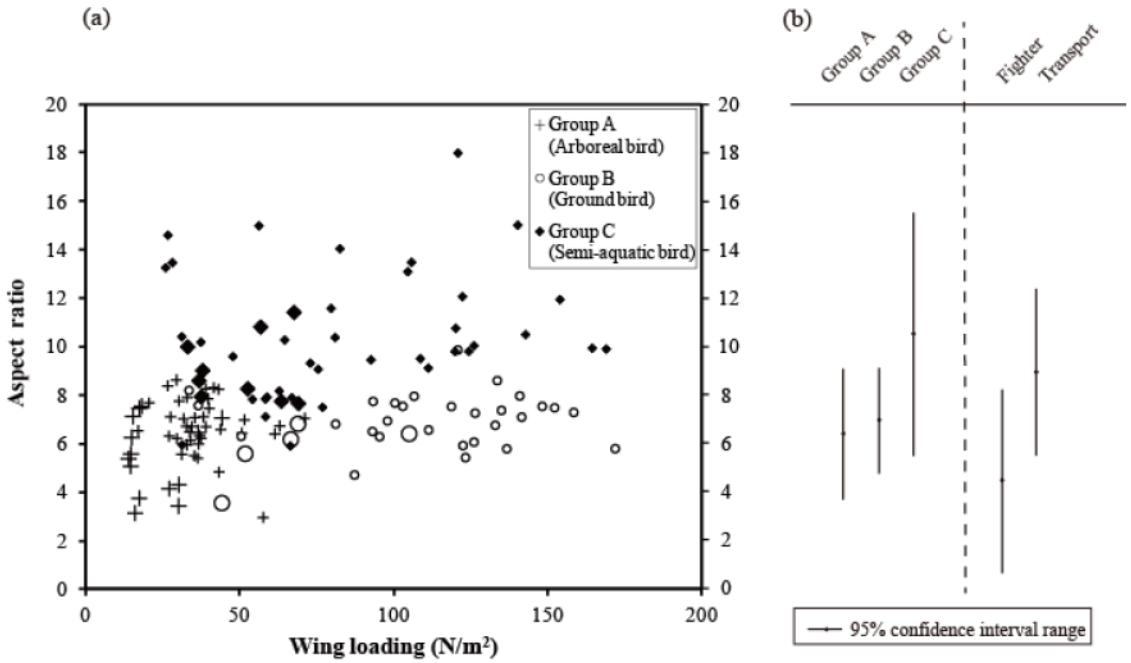

Fig. 3. Wing loading versus wing aspect ratio for 132 avian species. Groups A (crosses), B (open circles) and C (solid diamonds) are defined by track shape, as shown in Fig. 1. The data are from Tables 1 and 2. Groups A/B/C correspond to arboreal/ground/semi-aquatic birds. The large symbols show those obtained in this study and are the same data as in Fig 2.

As already mentioned, groups A, B and C have been defined based on track shape and correspond to the habitat types of arboreal, ground and semi-aquatic, respectively (Tanaka 2015). Arboreal birds refer to those living mainly in trees and the air. Ground birds refer to those living mainly on the ground rather than in the air or water. Semi-aquatic birds refer to those living mainly on or around water, such as ponds, seas and rivers. It should be noted that the wing shape and size constrain the flight behaviour, while the track shape reflects bipedal walking. The link between wings and legs may be related to avian body design, which is adapted to the habitat.

3.4.2. Correlation between wing area/wingspan and track area

The relationships between wingspan and track area and between wing area and track area were examined using regression analysis. The allometries between wingspan (b) and track area (S) were evaluated. Figure 4 shows a plot of wingspan versus track area. The grey line represents the regression line given by:

$$\log b = 0.50 \log S + 1.45 , \qquad (4)$$

where $R^2 = 0.84$ and probability is < 0.01. The 95% confidence interval of the slope is 0.47–0.53.

The allometries between wing area (a) and track area (S) were evaluated. Figure 5 shows a plot of wing area versus track area. The grey line represents the regression line given by:

$$\log a = 0.95 \log S + 2.20\,, \qquad (5)$$

where $R^2 = 0.75$ and probability is < 0.01. The 95% confidence interval of the slope was 0.89–1.02. These two equations are concordant with an isometric relationship. The wingspans and wing areas of extinct birds were estimated (Table 4) using equations (4) and (5).

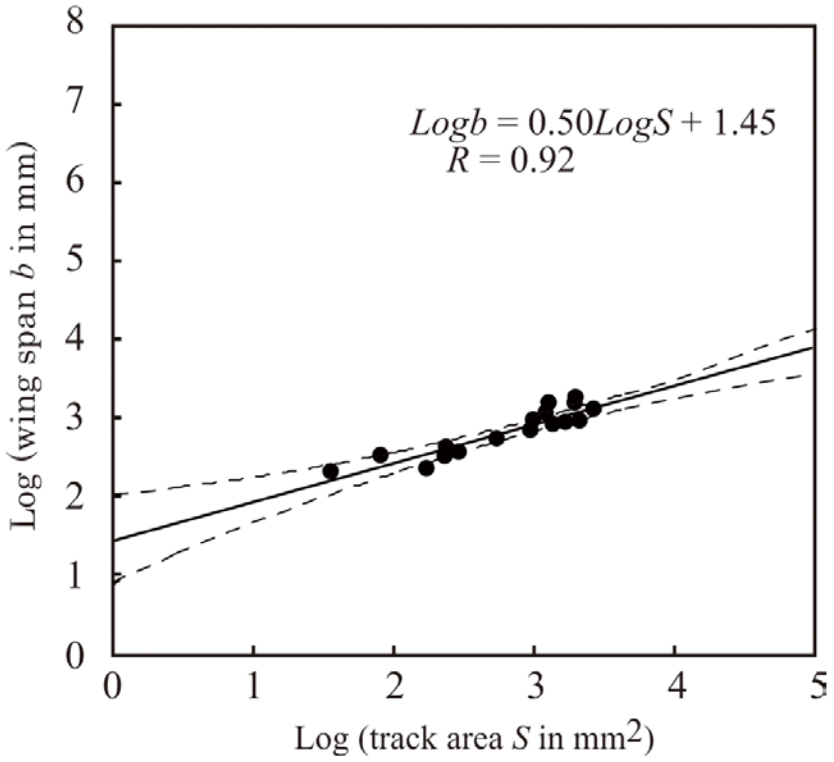

Fig. 4. Relationship between track area and wingspan.

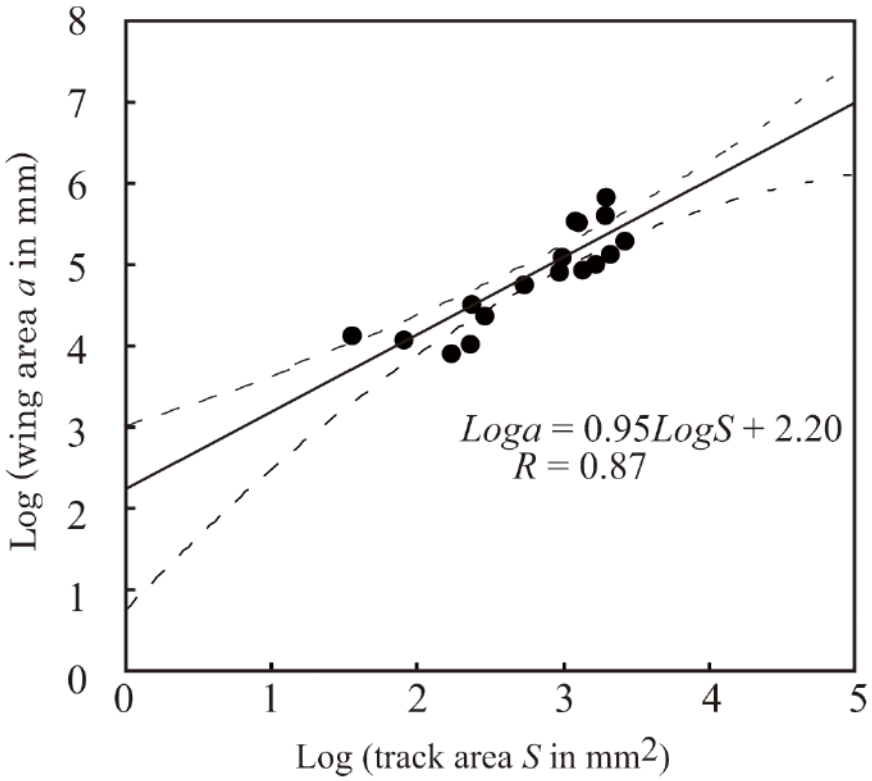

Fig. 5. Relationship between track area and wing area.

Table 4. The result of Cretaceous body estimation of extinct birds. Paper 1:Fuentes Vidarte, C.F. 1996. Paper 2:Lockley & Rainforth 2002 modified from Yang et al. 1995. Paper 3:Lockley et al. 2002 modified from Alonso & Marquillas 1986.

Species	Era	Region	Track area (cm2)	Wing area (cm2)	Wing span (cm)	Body weight (g) from Tanaka (2015) eqn(1)	Paper
	Cretacuous						
Archaeornithipus meijidei	Early	Spain	32.4	2388～5240	137～189	2110～2920	1
Hwangsanipes choughi	Late	Republic of Korea	12.1	869～2179	82～118	678～935	2
Yacoraitichnus avis	Late	Argentina	9.1	650～1694	70～103	489～674	3

3.5. Discussion

3.5.1. Interpretation based on flight dynamics

In previous studies, birds are morphologically divided into various groups based on flight. Wing morphology and flight characteristics are constrained by the flight mechanism and, therefore, the flight ecology and flight behaviour can be described in terms of aerodynamic theory (Hazlehurst &Rayner 1992). This relationship has been used for the study of wing design of extant birds (Greenwalt 1962; Rayner 1988). The wings of all flying birds must be able to generate sufficient lift and thrust on take-off and during cruising flight (Rayner 1985; Rayner 1988). The trade-off between efficiency and manoeuvrability inherent in different aspect ratios is a well-recognized engineering principle.

The wing aspect ratio constrains flight behaviour, especially flight efficiency, for flying objects, including birds and aircraft (Rayner 1988; O'Keefe 2001). We compared avian groups with aircraft groups based on the aspect ratio. Aircraft were divided into two groups. One was a group of fighter and attack aircraft that requires high manoeuvrability, designated as the "attack aircraft group". The other was a group of

transport and bomber aircraft that requires high flight efficiency, designated as the "transport aircraft group". Their aspect ratios were calculated using an aircraft data catalogue (Table 5; Japan Airlines Company, Ltd. 2011; Society of Japanese Aerospace Companies 2014). The avian groups A and B had lower aspect ratios of 95% confidence intervals ranging from 3.7 to 9.2 (mean 6.4) for A and from 4.6 to 9.2 (6.9 in average) for B (Fig. 3b). These intervals are in close agreement with that for the attack aircraft group, ranging from 1.0 to 8.2 (mean 4.6). It should be noted that the upper limits of the intervals are fairly consistent. This result suggests that arboreal birds and ground birds have high manoeuvrability similar to attack aircraft. In contrast, avian group C has higher aspect ratios of 95% confidence intervals ranging from 5.2 to 15.6 (mean 10.4). The interval of the aspect ratios encompasses that of the transport aircraft group ranging from 5.2 to 12.2 (mean 8.6) and the lower limits of the ranges for both groups almost coincide, which suggests that semi-aquatic birds have high flight efficiency similar to transport aircraft.

Thus, selection in birds for their wing aspect ratios is consistent with the trade-off between efficiency and manoeuvrability, as in aircraft (Rayner 1988; O'Keefe 2001). Group C (semi-aquatic) includes sea birds and wading birds. Most of the birds in the semi-aquatic group have wings with high aspect ratios and can travel over extremely

long distances, similar to transport aircraft. On the other hand, groups A and B (arboreal and ground) include song birds, birds of prey and pheasants, and most of these birds have wings with low aspect ratios and need to be able to manoeuvre around obstacles on the ground to take off at higher angles at the expense of reduced efficiency, similar to fighter aircrafts.

With respect to wing loading, birds in group A had low values, with 95 % confidence intervals ranging from 7.3 to 61.4 (mean 34.3), those in group B had high values with 95 % confidence intervals ranging from 37.5 to 178.6 (mean 108.0) and those in group C had values covering a wide range with 95 % confidence intervals ranging from 0 to 157.3 (mean 78.3; Fig. 3). Birds in groups A and B had similar aspect ratios, but different ranges of wing loading. This difference may also be interpreted by aerodynamics. A bird may experience selection for either high or low flight speed (Rayner 1985; Rayner 1988). Low wing loading permits slow flight and a smaller turning radius at a given speed, with horizontal flight maintained by using weaker movement of air. In contrast, heavy wing loading permits rapid flight and a larger turning radius at a given speed, with horizontal flight maintained by using stronger movement of air (Pennycuick 1975; Pennycuick 1983). Therefore, the birds in group B (ground birds) have high wing loading, rapid flight and a larger turning radius at a given

speed, and their horizontal flight can be maintained by using stronger movement of air. In contrast, the birds in group A (arboreal birds) have low loading, slow flight and a smaller turning radius at a given speed, and their horizontal flight can be maintained by using weaker movement of air. These relationships are expressed by Equation (3) which shows that the birds with smaller/larger values of track shape parameter (RW1) have smaller/larger aspect ratios and wing loading. Namely, higher wing loading provides higher flight speed and higher aspect ratios result in efficient fuel consumption. Wing loading and aspect ratio are essentially independent; however, they are related through track shape parameter (RW1). These facts suggest that avian locomotion is related to the effects of size, which depends on habitat type.

Table 5. The main combat aircraft in the world (citation from The society of Japanese aerospace companies 2014 and Japan Airlines Co.,Ltd. 2011). 1: Transport. 2: Fighter.

Type	Country	Company	Model	Weight (kg)	Wing area (m^2)	Wing span (m)	Aspect ratio	Wing loading (N/m^2)	group
Transport	USA	Lockeed	C-130H	70310	162.1	40.4	10.1	4250.7	1
	USA	Lockeed	C-141B	144250	300.0	48.8	7.9	4712.2	1
	USA	Lockeed	C-5B	379660	576.0	67.9	8.0	6459.5	1
	USA	Boeing	C-17	263090	353.0	50.3	7.2	7303.9	1
	USSR	Ilyushin	Il-76M/T	157000	300.0	50.5	8.5	5128.7	1
	USSR	Antonov	An-124	405000	600.0	73.3	9.0	6615.0	1
	Italy	Aeritalia	G222	29000	82.0	28.7	10.0	3465.9	1
Passenger	Japan	Boeing	777-200	201800	427.8	60.9	8.7	4622.8	1
	Japan	Boeing	767-300	133800	283.3	47.6	8.0	4628.5	1
	Japan	Boeing	737-400	62800	105.4	28.9	7.9	5839.1	1
	Japan	Boeing	DHC8-Q400	28000	63.08	28.4	12.8	4350.0	1
Air tanker	USA	Boeing	KC-135R	134720	226.3	39.9	7.0	5834.1	1
	USA	Boeing	KC-10A	267620	367.7	50.4	6.9	7132.7	1
Patrol	USA	Lockeed	P-3C	61235	120.8	30.4	7.7	4967.7	1
	USA	Lockeed	S-3	19295	55.6	20.9	7.9	3400.9	1
	USSR	Ilyushin	Il-38	63500	140.0	37.4	10.0	4445.0	1
	UK	BAE Systems	Nimrod	87090	197.0	35.0	6.2	4332.4	1
	France	Dassault Bureguet	ALT2	25300	120.3	37.4	11.6	2061.0	1
Airborne warning	USA	Grumman	E-2C	23355	65.0	24.6	9.3	3521.2	1
	USA	Boeing	E-3A	148000	283.0	44.4	7.0	5125.1	1
	USSR	Tupolev	Tu-126	175000	311.1	51.2	8.4	5512.7	1
	UK	BAe	Nimrod AEW	87090	197.0	35.0	6.2	4332.4	1
Electronic warfare	USSR	Antonov	An-12	61000	121.7	38.0	11.9	4912.1	1
	USSR	Ilyushin	Il-20/22	64000	140.0	37.4	10.0	4480.0	1
Reconnaissance	USA	Lockeed	SR-71A	63500	166.8	16.9	1.7	3730.8	2
Bomber	USA	Boeing	B-52H	221360	371.6	56.4	8.6	5837.8	2
	USA	Northrop	B-2	136080	470.0	52.4	5.8	2837.4	2
	USSR	Tupoev	Tu-22	75000	188.0	23.7	3.0	3909.6	2
Trainer･Attack	USA	Northrop	T-38A	5470	15.8	7.7	3.8	3392.8	2
	USA	Beechcraft	T-34C-1	1940	16.7	10.2	6.2	1138.4	2
	USA	Beechcraft	T-1A	4817	22.4	13.2	7.8	2107.4	2
	USA	Beechcraft/Pilatus	T-6A	2400	16.3	10.1	6.3	1442.9	2
	UK	BAE Systems	Hawk	5700	16.7	9.4	5.3	3344.9	2
	France	Aerospatiale	TB-30	1200	9.0	7.4	6.1	1306.7	2
	Japan	Fuji Heavy Industries	T-1	4355	22.2	10.5	5.0	1922.5	2
	Japan	Mitsubishi Heavy Industries	T-2	9637	21.1	7.9	3.0	4476.0	2
	Japan	Kawasaki Heavy Industries	T-4	7500	21.0	9.9	4.7	3500.0	2
	Japan	Fuji Heavy Industries	T-5	1585	16.5	10.0	6.1	941.4	2
	Japan	Fuji Heavy Industries	T-7	1585	16.5	10.0	6.1	941.4	2
	Switzerland	Pilatus	PC-7	1900	16.0	10.4	6.8	1163.8	2
	Switzerland	Pilatus	PC-9	2350	16.3	10.1	6.3	1412.9	2
	Italy	Aermacchi	MB339A	5895	19.3	10.9	6.2	2993.3	2
	ROK	KAI	KT-1	3205	16.0	10.6	7.0	1963.1	2
	Conjunction	Dassault Bureguet/Dornier	Alpha Jet	5000	17.5	9.1	4.7	2800.0	2
	Conjunction	Boeing/BAE Systems	T-45	5783	17.7	9.4	5.0	3201.9	2
	Czech Republic	Aero	L-39	4300	18.8	9.5	4.8	2241.5	2
	Spain	CASA	C-101	4850	20.0	10.6	5.6	2376.5	2
	Brazil	Embraer	EMB312	2550	19.4	11.1	6.4	1288.1	2
	Yugoslavia	Soko	G4	6300	19.5	9.9	5.0	3166.2	2
	Romania	ICA	IAR-825TP	1700	15.0	10.1	6.8	1110.7	2
	France	Dassault	Mirage2000	17500	41	9.13	2.0	4182.9	2
	France	Dassault	RafaleD	24500	45.7	10.8	2.6	5253.8	2
	Conjunction	Panavia	TornadoIDS	28000	26.6	13.91	7.3	10315.8	2
	Conjunction	Eurofighter	Typhoon	23500	50	10.95	2.4	4606.0	2
	Conjunction	Lockheed Martin	JSF(F-35)	29700	42.74	10.67	2.7	6810.0	2
	Italy	Aeritalia	AMX/A-1	13000	21	9.97	4.7	6066.7	2
	China	Shenyang	J-8	18900	42.2	9.35	2.1	4389.1	2
	China	Xi'an	JH-7	28500	52.3	12.71	3.1	5340.3	2
	China	Chengdu	J-10	18500	33.1	8.78	2.3	5477.3	2
	China	Chengdu	FC-1	12700	24.62	9	3.3	5055.2	2
	Russia	Mikoyan	MiG-31	46200	61.6	13.47	2.9	7350.0	2
	Russia	Mikoyan	MiG-29	19700	38	11.36	3.4	5080.5	2
	Russia	Sukhoi	Su-25	17600	33.7	14.36	6.1	5118.1	2
	Russia	Sukhoi	Su-27	33000	63	14.7	3.4	5133.3	2
	Russia	Sukhoi	Su-32	44400	63	14.7	3.4	6906.7	2
	Sweden	Saab	JAS-39 Gripen	14000	30	8.4	2.4	4573.3	2
	UK	BAE	Sea Harrier	11900	20.1	8.31	3.4	5802.0	2
	UK	Panavia	TornadoF3	28000	26.6	13.91	7.3	10315.8	2
	USA	Boeing	F-15	36700	56.49	13.05	3.0	6366.8	2
	USA	Lockheed Martin	F-16	21800	27.87	10	3.6	7665.6	2
	USA	Boeing	AV-8B	14100	21.37	9.25	4.0	6466.1	2
	USA	Lockheed Martin	F-22	27200	78	13.56	2.4	3417.4	2
	USA	Boeing	F-18E	29900	46.45	13.62	4.0	6308.3	2

3.5.2. Estimation of wingspan and area from track area

In general, it is difficult to estimate wingspan and area from fragmentary bones, except in rare cases (Ksepka 2014) because wing area is not preserved in fossils. Even if complete wing bones are excavated, it is difficult to estimate wingspan and area, because wing feathers do not contain bones, unlike bats and flying squirrels whose wing areas are easily estimated from bones. In comparison to avian body fossils, there are numerous avian track fossils. The relationship between wings and tracks determined in this study provides a method by which the size and shape of wings can be estimated from track data.

Equations (4) and (5) show the relationships between wingspan and wing area with respect to track area, respectively. The equations allow us to estimate the wingspan and wing area from the track area. According to the logarithmic error estimation (Smith 1984), the accuracy of predictive equations is assessed based on the percentage prediction error (PE) and percentage standard error (SEE) of the estimate. The values of PE and SEE for wingspan (Equation (4)) are 3.8 and 18.3 and those for wing area (Equation (5)) are 25.7 and 14.7, respectively. The prediction error is smaller for

wingspan than wing area. Thus, the errors can be estimated for the estimate from tracks, which is more accurate than the estimate from fragmental skeletal specimens.

Applying this method, we estimated the wingspan and area from the track of a Cretaceous bird (Table 4). *Archaeornithipus meijidei*, the largest Cretaceous avian track fossil (Lockley & Rainforth 2002), is the only Mesozoic avian ichnotaxon and exhibits parallel trackways suggestive of gregarious avian behaviour (Lockley & Rainforth 2002). Its height is estimated to have been at least 1.20 m from an average step length of 29.5 cm, based on the relationship between the step length of modern aquatic birds to acetabulum height (Fuentes Vidarte 1996). *A.meijidei* was previously classed as a semi-aquatic bird with a bodyweight ranging from 2.11 to 2.92 kg based on its track shape and area (Tanaka 2015). Using Equations (4) and (5), we estimate the ranges as 0.24 to 0.52 m^2 for wing area and 1.37 to 1.89 m for wingspan. Referring to the data in Table 2, these estimates suggest that the *A. meijidei* trackmaker was a semi-aquatic bird similar to a large heron or grus. It would have had relatively low wing loading, which indicates low flight speed, and a moderate aspect ratio, indicating moderate aerodynamic efficiency. *Hwangsanipes choughi*, a Cretaceous webbed avian track fossil (Yang et al. 1995), is assigned as a shore bird based on the tracks. The bodyweight was previously estimated to range from 0.68 to 0.94 kg from the track area and the habitat

was classed as semi-aquatic from the track shape (Tanaka 2015). Using Equations (4) and (5), we estimate the ranges as 0.087 to 0.218 m^2 for wing area and 0.82 to 1.18 m for wingspan. Referring to the data in Table 2, these estimates suggest that the *H. choughi* trackmaker was a semi-aquatic bird similar to a large sandpiper or small sea bird. This is consistent with the conclusion of Yang et al. (1995), who suggested that the *H. choughi* trackmaker was a shorebird, although they did not estimate its size. The Cretaceous avian track fossil *Yacoraitichnus avis* (Alonso & Marquillas 1986), was classed as a semi-aquatic bird with a bodyweight ranging from 0.49 to 0.67 kg based on track shape and area (Tanaka 2015). Using Equations (4) and (5), we estimate the ranges as 0.065 to 0.17 m^2 for wing area and 0.70 to 1.03 m for wingspan. Referring to the data in Table 2, these estimates suggest that the *Y.avis* trackmaker was a semi-aquatic bird similar to a medium-sized gull.

3.6. Conclusion

We used avian wing data to calculate the wing aspect ratio and loading, which are important parameters in aerodynamics. Discriminant analyses and multiple regression analyses yielded the following results: (1) avian wings can be divided into three groups,

similar to tracks, which are morphologically divided into three groups corresponding to the arboreal, ground and semi-aquatic habitat types; (2) avian wing loading and aspect ratio are closely related to track shape parameters; (3) wingspan and wing area are related to track area and the relationship provides a method for estimating the wingspan and area from the fossil track area; (4) the wingspan and area of Cretaceous extinct avian taxa estimated using this method, and their previously-estimated bodyweights, suggest that the *Archaeornithipus meijidei* trackmaker was a semi-aquatic bird similar to a large heron or grus, the *Hwangsanipes choughi* trackmaker was a shorebird, and the *Yacoraitichnus avis* trackmaker was a medium-sized gull; (5) the ecology of avian flight based on aerodynamics suggests that birds are divided by their wing aspect ratios into the two groups: “transport aircraft” and “fighter aircraft”.

Chapter 4

Variability of *Ciconia boyciana*'s footprints on the homogenious sediment

4.1. Introduction

Tetrapod track fossils can be preserved in great abundance and in different environments better than tetrapod body fossils. They are useful to elucidate the evolution (Klein & Lucas 2015) as well as locomotion and behaviors (Castanera et al. 2013), because of their containing anatomical information. For example, Wilson (2005) proposed a method to estimate taxa for trackmakers, by using limb's synapomorphies that were considered remained in track fossils. Ichnofossils identified by synapomorphies can act as an independent source of distributional data that can modify spatial, temporal, and character distributions, which in turn may influence hypotheses of locomotor evolution. Based on the conservative synapomorphy-based approach analysis of footprints, the origin of the dinosaur stem lineage was estimated to be approximately 5-9 Myr older than the time indicated by body fossils (Brusatte et al. 2011).

The first step of a track research is identification of taxa. It is followed by observations of detailed track's features, and further by classification of tracks based on the features. We finally find common features of taxa. The last step is essential for the study of tracks. It is most important for correct identification to decode pes anatomical features of a trackmaker. Tetrapod track morphology mainly consists of components of

pes anatomy, substrate, and pes-substrate interaction. Therefore, many studies have been conducted using modern tetrapods, to reveal relationships between track morphology and sediment of physical feature (Milàn 2006; Milàn & Bromley 2006; Milàn & Bromley 2008), and between track morphology and limb anatomy (Milàn & Bromley 2006; Falkingham & Gatesy 2014).

Recent technical innovations develop the experimental ichnology. Three dimentional documentation techniques such as laser scanning have been adopted for analyses of living animals' track morphology (e.g. Falkingham & Gatesy 2014). The method enables to read more detailed information of living animal's track anatomical morphology such as phalangeal pads and skin impressions. It also enables to reconstruct foot movements and read anatomical information of trackmakers even from poorly preserved specimens, e.g. those with obscure outlines. Some studies develop methods to estimate trackmaker's ecology and physiology from track data, focused on track morphology. For example, walking speeds (Alexsander 1976; 1992), rotations of limb posture (Kubo & Ozaki 2009), bodyweights (Kubo 2011; Tanaka 2015) and habitat types (Tanaka 2015) are estimated. The results of neoichnological experiments can contribute to paleoichnology, and further to paleobiology.

Large wading bird's track fossils are easily left on sediments have been reported from not only geological studies but also archeological ones. Although there are many reports of large wading bird's track fossils, they deal with only descriptions of fossils and none analyzes and mentions the track morphology. These large wading birds are phylogenically close to living birds. Therefore, investigations of living bird tracks can contribute to reveal behaviors and ecology of large wading bird track fossils. Moreover, the phylogenic position of large wading birds is between Mesozoic theropods and living

birds. Therefore, large wading birds are the best target of study to reveal evolution of birds.

In this study, we conduct an ichnological experiment using *Ciconia boyciana* to obtain track data on a sediment. The purposes are (1) to reveal features that enable to distinguish *Ciconia boyciana* from other wading birds leaving abundant fossil tracks, (2) to examine how correctly pes anatomy is reflected in the morphology of tracks, and (3) to reveal the relationship between track morhpology and walking behavior. We first use in ichnology a new track theoretical analysis, in which existent morphology and non-existent morphology are co-analyzed.

4.2. Material and method

Ciconia boyciana, a nationally protected species of Japan, is breeded in the Hyogo Park of the Oriental White Stork. We used individuals of male (Figure 1) and female kept in the park.

In order to accustom *Ciconia boyciana* to foreign substances, we spread a brown colored joint mat in the cage for ten days. After *Ciconia boyciana* became acclimatized with the joint mat, we replaced it with unconsolidated potter clay board of 70 cm × 120 cm× 2.5 cm in size. The board was made with 0.47-liter water and 1.0-liter potter clay, within the range that a clear-cut outline of a track is remained (e.g. Milàn & Bromley 2006). We have waited for 20 days until *Ciconia boyciana* walked on the board, after that we have taken data.

For individual tracks, lengths between digits I and III and widths between digits II and IV were measured. Regarding trackways, paces, strides and trackway widths were

measured following the method of Xing et al. (2015).

Horizontal shape of the footprint was observed by taking digital photos with resolution of 72 dpi, from which track areas were measured by the method of Ubukata (2003). The volume of a track was measured, pouring water into a mold of track after the potter clay became desiccated and impermeable.

Digit I is shorter and broader than other three digits. A track is identified as a right one for those whose tip of digit I points to the left, and vice versa. We analyze track data using the applied theoretical morphospace, that co-analyzes existence morphology and non-existence morphology. Avians have four digits, and thus they have 12 types of theoretical track morphology (Figure 2).

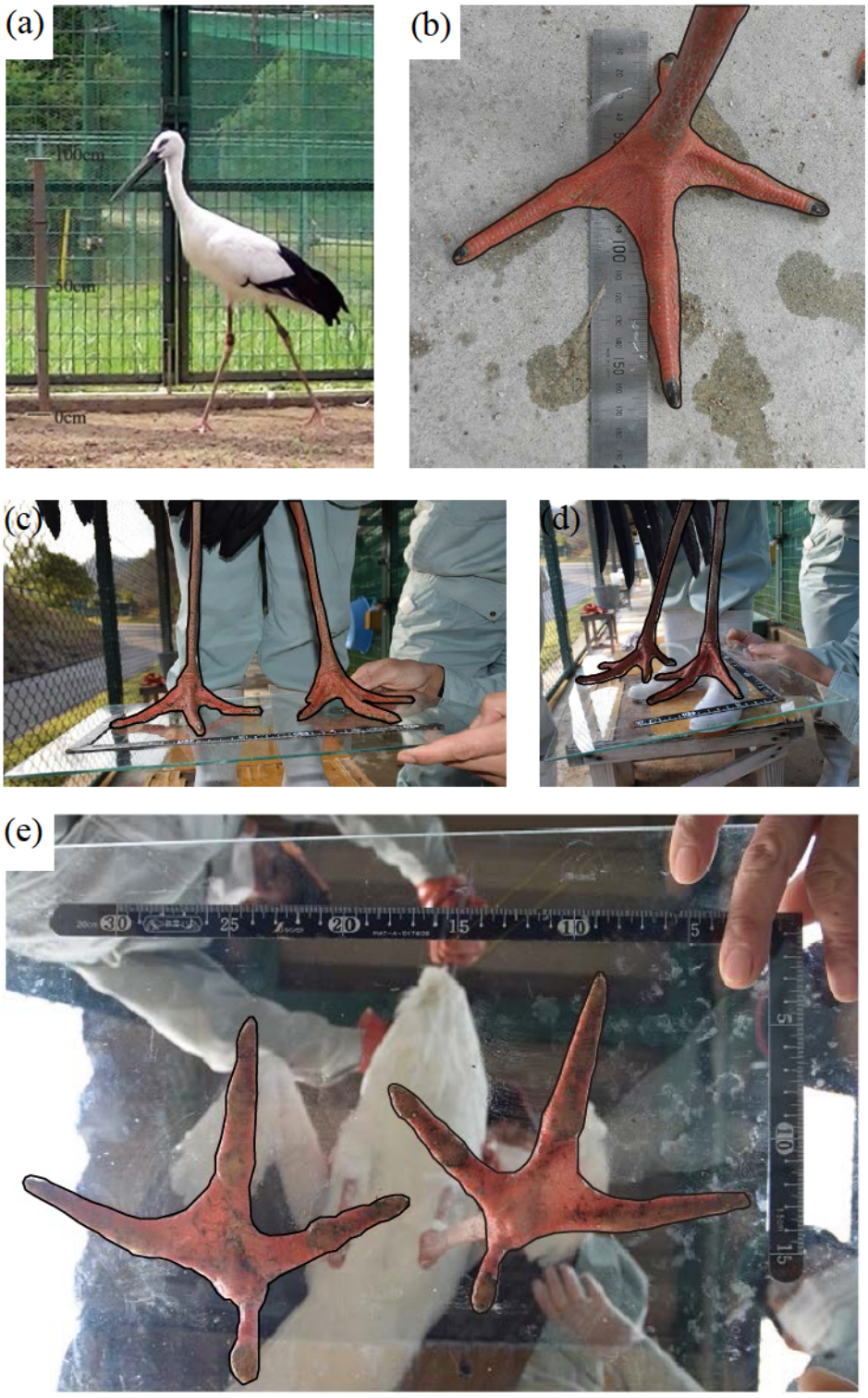

Fig. 1. Photographs of *Ciconia boyciana* used for experiment. (a) *Ciconia boyciana* walking in the cage. The vertically leant stick in front of *Ciconia boyciana* is 1m high. (b) *Ciconia boyciana*'s toy. (c) *Ciconia boyciana*'s feet from the front direction. (d) *Ciconia boyciana*'s foot from the side direction. (e) *Ciconia boyciana*'s foot soles.

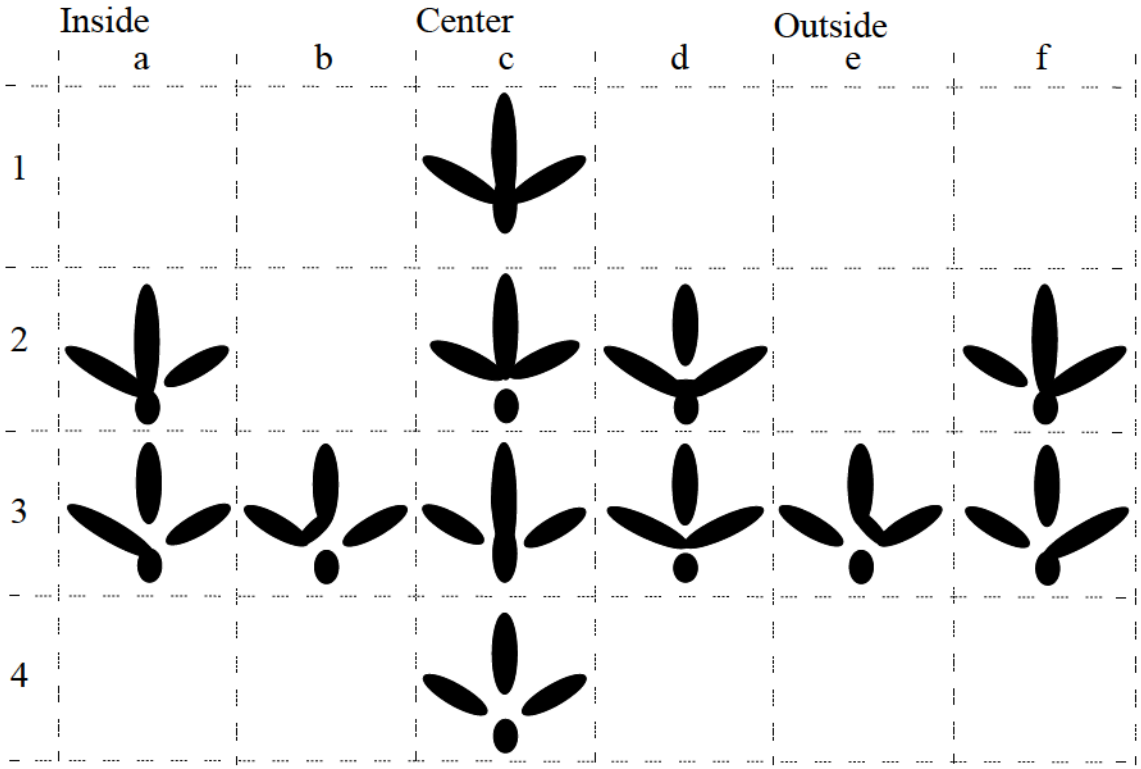

Fig. 2. Theoretical track morphospace for avians with four digits.

4.3. Result

Typical footprints left by *Ciconia boyciana* are shown in Figure 3. The data of measurements are summarized in Table 1.

Table 1. The track lengths, widths, areas and volumes, depths for *Ciconia boyciana's* footprints, and estimated body weights from track areas. (a) is male data and (b) is female data.

Track number	Right or Left	Length (mm)	Width (mm)	Area (mm2)	Volume (ml)	Depth (mm)	Devarication
1	Right	166	135	4278	16	4	111
2	Left	176	154	5013	21	4	112
3	Left	172	166	5529	27	5	121
4	Right	165	131	5495	25	5	125
5	Right	180	162	5605	22	4	115
6	Left	160	135	4476	24	5	130
7	Left	156	159	4387	20	5	112
8	Right	188	180	7245	23	3	127
9	Right	171	162	3821	22	6	122
10	Left	169	144	3717	26	7	116
11	Left	166	142	4052	20	5	118
12	Right	172	150	4182	20	5	116
13	Left	182	162	5190	25	5	128
14	Right	177	153	4946	22	4	117
15	Left	182	170	6292	25	4	118
16	Right	180	161	5200	18	3	111
17	Left	180	163	5561	17	3	114
18	Right	176	160	5142	19	4	119
19	Left	180	163	5142	19	4	115
20	Right	182	164	5429	19	4	121
21	Right	178	161	5431	22	4	105
22	Left	177	159	4931	20	4	112
23	Left	179	162	5021	25	5	123
24	Right	177	144	4230	21	5	110
25	Left	163	154	5262	19	4	114
26	Right	174	152	5001	20	4	120
27	Left	172	160	5421	23	4	110
28	Right	169	151	4721	22	5	116
Average		174	156	5026	21	4	117

Track number	Right or Left	Length (mm)	Width (mm)	Area (mm2)	Volume (ml)	Depth (mm)	Devarication
1	Left	146	147	3805	16	4	127
2	Right	159	144	4030	21	5	128
3	Right	144	134	3308	20	6	139
4	Right	157	138	4123	19	5	123
5	Left	162	148	4640	18	4	135
6	Right	150	158	4465	23	5	137
7	Left	155	156	4333	22	5	138
8	Right	162	146	4490	21	5	120
9	Right	168	162	5228	20	4	123
10	Left	160	153	4276	22	5	129
11	Left	153	149	4316	18	4	119
12	Right	162	129	4075	21	5	132
13	Left	144	125	4003	18	4	118
14	Left	156	139	3819	18	5	140
15	Right	145	141	3577	19	5	126
16	Right	143	148	4025	20	5	122
17	Left	164	143	4292	19	4	121
18	Right	167	156	4850	23	5	134
19	Right	146	140	4349	22	5	122
20	Left	156	124	4365	21	5	119
21	Right	144	123	4214	20	5	118
22	Left	164	134	4515	19	4	123
23	Right	143	137	3845	19	5	122
24	Left	140	115	3226	21	7	132
25	Right	141	122	3482	20	6	127
26	Left	155	147	3930	21	5	118
	Average	153	141	4138	20	5	127

Fig. 3. Photograph of the *Ciconia boyciana* footprints.

4.3.1. Track geometry

The male *Ciconia boyciana* remained 28 tracks, 14 of which are left, and the remaining are right. Averages of track lengths (between digits I and III) and widths (between digits II and IV), and total divarications are 174 mm ± 8 mm (k=2; the same hereinafter), 156 mm ± 11 mm, and 117±6°, respectively (Table 1(a)). On the other hand, the female *Ciconia boyciana* remained 26 tracks, 12 of which are left, and the remaining are right. Averages of track lengths and widths, and total divarications are 153 mm±9 mm (k=2), 140 mm±12 mm, and 127±7° , respectively (Table 1(b)).

For male *Ciconia boyciana*, averages of track areas and depths are 5.03×10^3 mm^2 ± 0.75×10^3 mm^2 and 4 mm ± 1mm, respectively. F-test shows there is no significant difference (5%) between left and right for track lengths, widths, areas, valumes and depths. On the other hand, for female *Ciconia boyciana*, averages of track areas and depths are 4.14×10^3 mm^2 ± 0.46×10^3 mm^2 and 5 mm ± 1mm, respectively. There is no significant difference (5%) between left and right tracks, the same above.

4.3.2. Description of footprints

Digits II, III and IV are slender, with thin nail traces, whose tips are inclined more deeply than the root of digits. Both of male and female usually left the 4-c type track (Figure 4). Almost all tracks have no metatarsal impression, except two male tracks and one female track (Figure 4(a)1-c,2-f ; Figure 4(b)1-c). Theoretical morhphospace analysis has 12 types of track. *Ciconia boyciana* left only four to five types out of them (male left 5 types, female left 4 types).

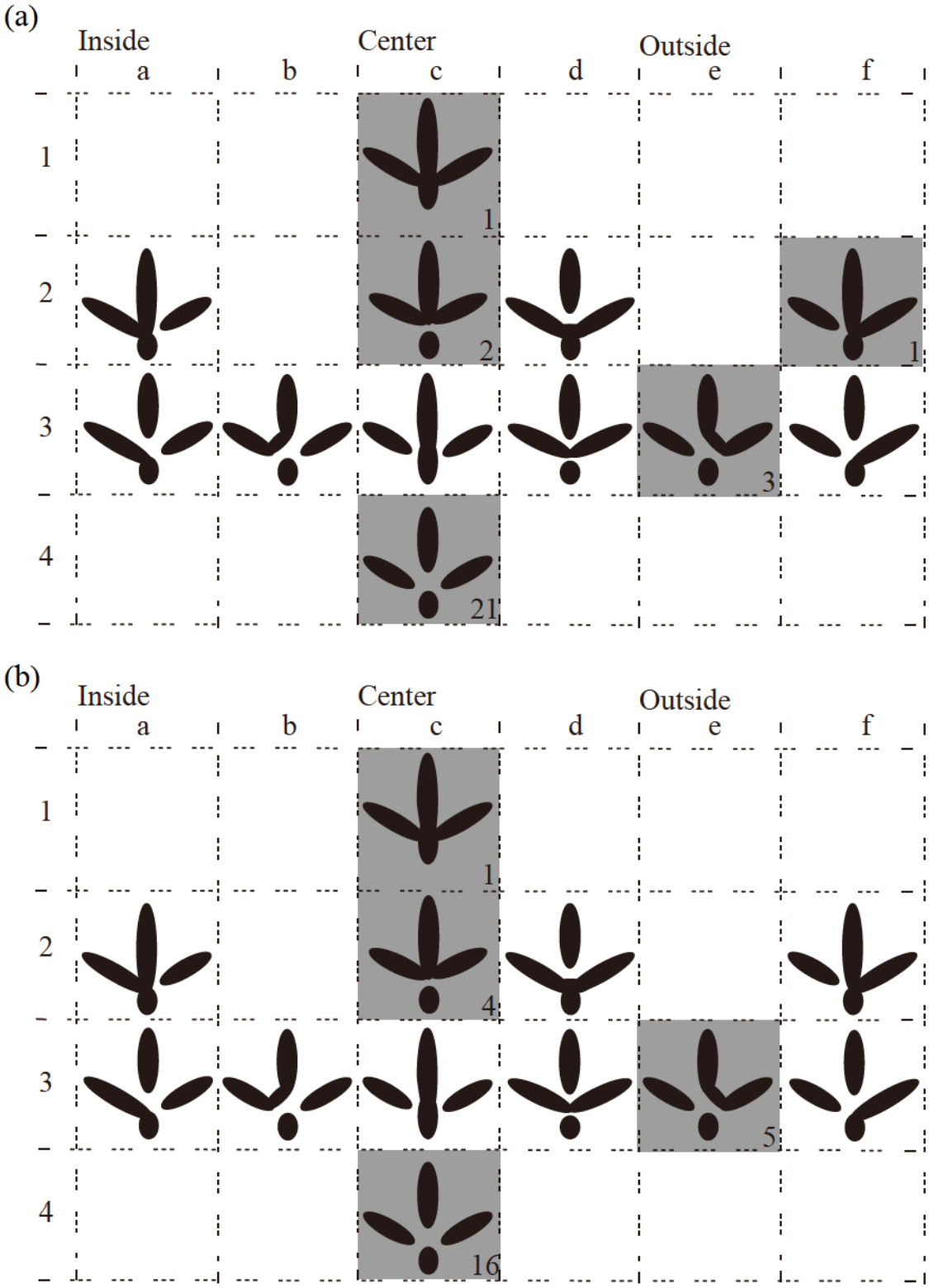

Fig. 4. Real track morhpospace. The upper and lower diagrams are for left and right tracks, respectively. The shaded areas represent *Ciconia boyciana* track morphology. The number in the shaded portion shows the counts of tracks. (a) is male data and (b) is female data.

4.3.3. Trackway

Figure 5 shows five typical trackways. Male *Ciconia boyciana* has an average pace length of 31.0 cm, average stride of 60.9 cm, and average trackway width of 8.6 cm. Female *Ciconia boyciana* has average pace length of 42.8 cm, average stride of 84.0 cm, and average trackway width of 2.7 cm.

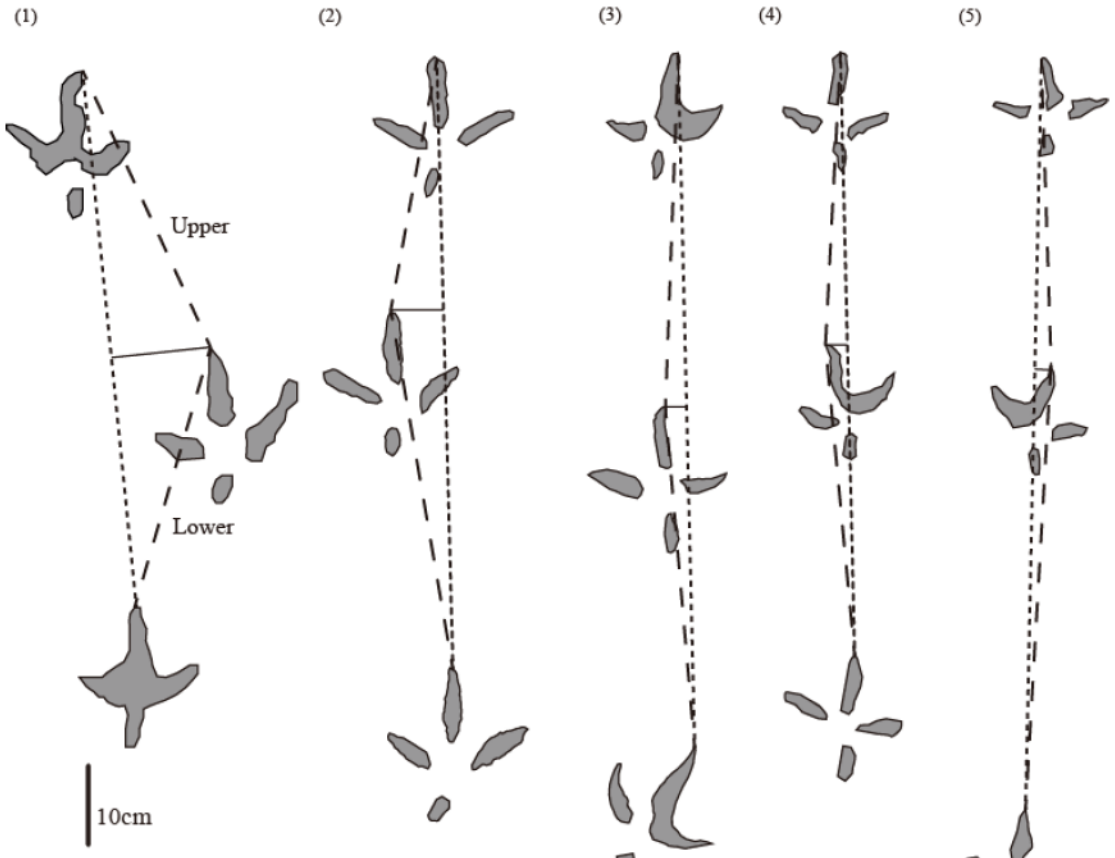

	Pace Length		Stride Length	Track Width (cm)
	Upper	Lower		
(1)	31.3	27.2	56.4	11.0
(2)	27.4	38.2	65.3	6.2
(3)	45.0	42.4	86.9	3.1
(4)	36.1	39.1	74.9	2.9
(5)	38.5	55.4	93.0	2.0

Fig. 5. *Ciconia boyciana*'s trackways. Trackway measurements: PL, pace length; SL, stride length; TW, trackway width. Measurements are followed by Xing et al. (2015).

4.4. Discussion

4.4.1. Track geometry

For male *Ciconia boyciana*, the median of track areas is 5.05×10^3 mm^2, being close to the average track area 5.03×10^3 mm^2 ± 0.75×10^3 mm^2. For female *Ciconia boyciana*, the median of track areas is 4.17×10^3 mm^2, being close to the average track area 4.14×10^3 mm^2 ± 0.46×10^3 mm^2. Thus, the average and median of track areas are quite close, and standard deviations are small. These results show the track areas are concentrated to a median value.

For male *Ciconia boyciana*, average track areas are $5.00\times10^3\pm0.67\times10^3$ mm^2 for left and $5.05\times10^3\pm0.85\times10^3$ mm^2 for right. F-test confirms there is no difference between left and right with P=0.20 (5%). For female *Ciconia boyciana*, average track areas are $4.13\times10^3\pm0.39\times10^3$ mm^2 for left and $4.15\times10^3\pm0.52\times10^3$ mm^2 for right. F-test confirms there is no difference between left and right with P=0. 17 (5%).

Table 2. Correlation coefficient matrix between track measurements for male (a) and female (b) *Ciconia boycianas*.

(a)

Length	0.68	0.60	0.03	-0.43
	Width	0.64	0.08	-0.43
		Area	0.19	-0.67
			Volume	0.58
				Depth

(b)

Length	0.50	0.74	0.17	-0.54
	Width	0.61	0.20	-0.43
		Area	0.24	-0.73
			Volume	0.46
				Depth

Table 2 shows the result of correlation analyses between track lengths, widths, areas, volumes and depths. The track lengths show positive correlations with widths and areas, and a negative correlation with depths. The track widths show a positive correlation with areas, a negative correlation with track depths. The track areas show a negative correlation with depths. The track capacities show a positive correlation with depths.

Both of male and female *Ciconia boycianas* have the wide range of track widths with a maximum difference of about 40%. In addition, there is no correlation between track lengths and widths. To reveal causes of the wide range, we examined the relationship between track lengths and aspect ratios. As shown in Figure 6, the track lengths vary within a narrow range, whereas rack aspect ratios vary in a wide range (0.9~1.3). Figure 6 shows examples of track morphology for large and small aspect ratios. The difference depends on the stretch of digits II and IV, which would variable during walking.

The wide range of track widths can be related to limb anatomy especially foot muscles. Foot has two muscles to move digits; flexor digitorum longus muscle to bend digits II, III and IV, and flexor pollicis longus to bending digit I. For Avians, these muscles are connected for some taxa, but not for others. With respect to *Ciconia boyciana*, these muscles are connected and co-moved (Hudson 1937; Raikow 1985). These muscles basically control limb's bending and stretching in the moving direction. *Ciconia boyciana* has no muscle to control the stretch of digits II and IV. This causes the wide range of track widths, or wide range of track aspect ratios.

The track volumes show no correlation with other track measurements (Table 2). The results of correlations show that the deeper the track depths, the smaller the track areas, and in addition the larger the track areas, the larger the track lengths and track widths. These relationships show the track width and depth have the trade-off relation under a condition of fixed track volume, and the track volume is proportional to trackmaker's body weight. Therefore, animals always would walk pressing foot to the ground with the same pressure. Although the pes-substrate interaction more or less changes morphology of tracks, nearly constant track volumes would be kept.

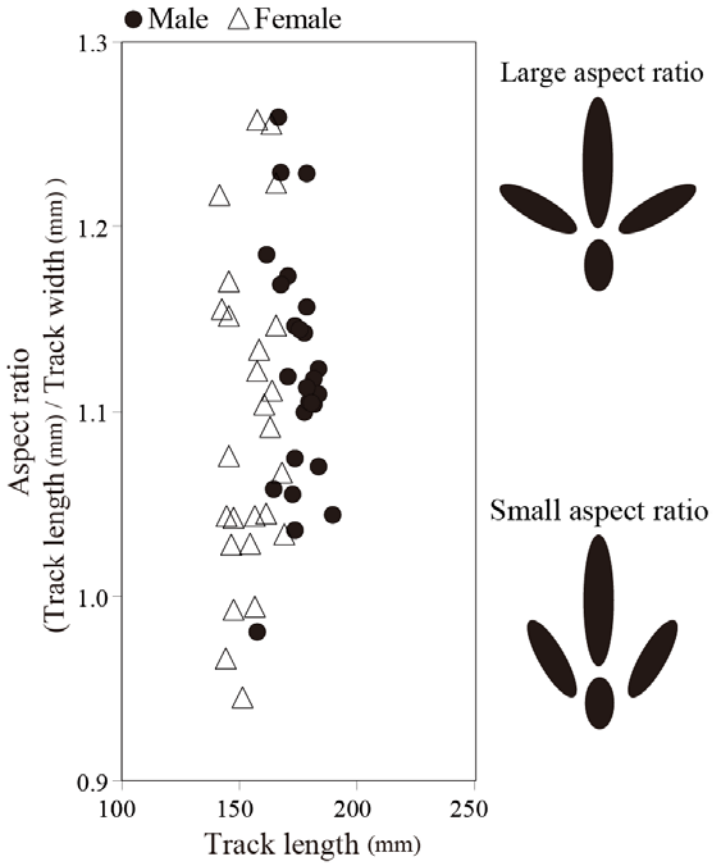

Fig. 6. The relationship between track length and track aspect ratio.

4.4.2. Description of tracks

Ciconia boycianas mostly left 4-c type tracks without metatarsal impression. Absence of metatarsal impression in the *Ciconia boyciana* tracks is caused by the standing on tiptoes as seen in the pictures in Figures 1(c) – (e). These pictures show no metatarsal touch on board. Because metatarsal impression is a unique and clear feature left on various kinds of sediments (Milàn 2006; Milàn & Bromley 2006), absence of it would be important in the ichnotaxonomic classification to distinguish *Ciconia* from others.

Large wading birds have left abundant track fossils on sediments, providing opportunities for ichnological studies. For more precise identifications, we compare the tracks of *Ciconia boyciana* with those of other large size wading birds, Crane and Ardeidae. Tracks of Crane have a large total divarication close to 180°, such as point impression for digit I, and a clear metatarsal impression. These features are useful to distinguish tracks of Crane from those of Ardeidae and *Ciconia* (e.g. Okamura et al, 2005 ; Fukushima 2008).

Previous studies show the total divarication for tracks of Ardeidae (Ardea cinerea, Ardea alba) is larger than that for tracks of *Ciconia boyciana*. This is supported by the present study. The average total divarication 122±8° for Ciconia is larger than the average total divarication 101±7° for Ardeidae (Fukushima 2008). Total divarication may be useful to distinguish tracks of *Ciconia boyciana* from tracks of Ardeidae. However, track morphology has large variability (e.g. Lockley et al. 2002; Martin et al. 2013), that makes identifications with total divarication difficult. Thus, total divarication cannot be a secure identification feature like metatarsal impression. Because such as crane and *Ciconia,* the animals live in similar habitats and have similar track sizes, do not distinguish each other, track size cannot determine which it shows the difference of species or the same species of same growth stage (Farlow & Pianka 2000). In ichnotaxonomic classification, size is a most important factor in all track morphological features (Bertling et al. 2006). However, the present study shows that metatarsal impression can be used to distinguish *Ciconia boyciana* from other large wading birds' tracks, although sizes cannot do it.

In the present experiment, male *Ciconia boyciana*'s tracks take only 5 types of track morphospace and 75 % of them are of type 4-c, and female *Ciconia boyciana* tracks

take only 4 types and 62 % of them are of type 4-c (Figure 4). This result suggests that *Ciconia boyciana* walks on the ground pressing its bodyweight on its outside of digits (pes). It also suggests that taking only four to five types of morphospace shows *Ciconia boyciana*'s controling its digits with a uniform fashion to keep balance. *Ciconia boyciana* often stands on a single leg during sleeping and taking a rest. This behavior may be related to the pressing the ground putting the center of gravity to the outside digits.

4.4.3. Track theoretical morphospace

We examine the track features within the central area surrounded by the four digits I to IV. Impressions are counted separing the central area into 9 parts, as in Figure 7. For example, one is counter for all parts for the fully impressed case like Figure 7(a), and zero is counted for all of nine parts for the case of no impression like left side of the Figure 7(b). The sum of counts for each part shown in Figure 8 represents frequency of impression. The frequency is higher in outside (tibia side) than inside (fibula side), indicating *Ciconia boyciana* tends to push track's outside during walking.

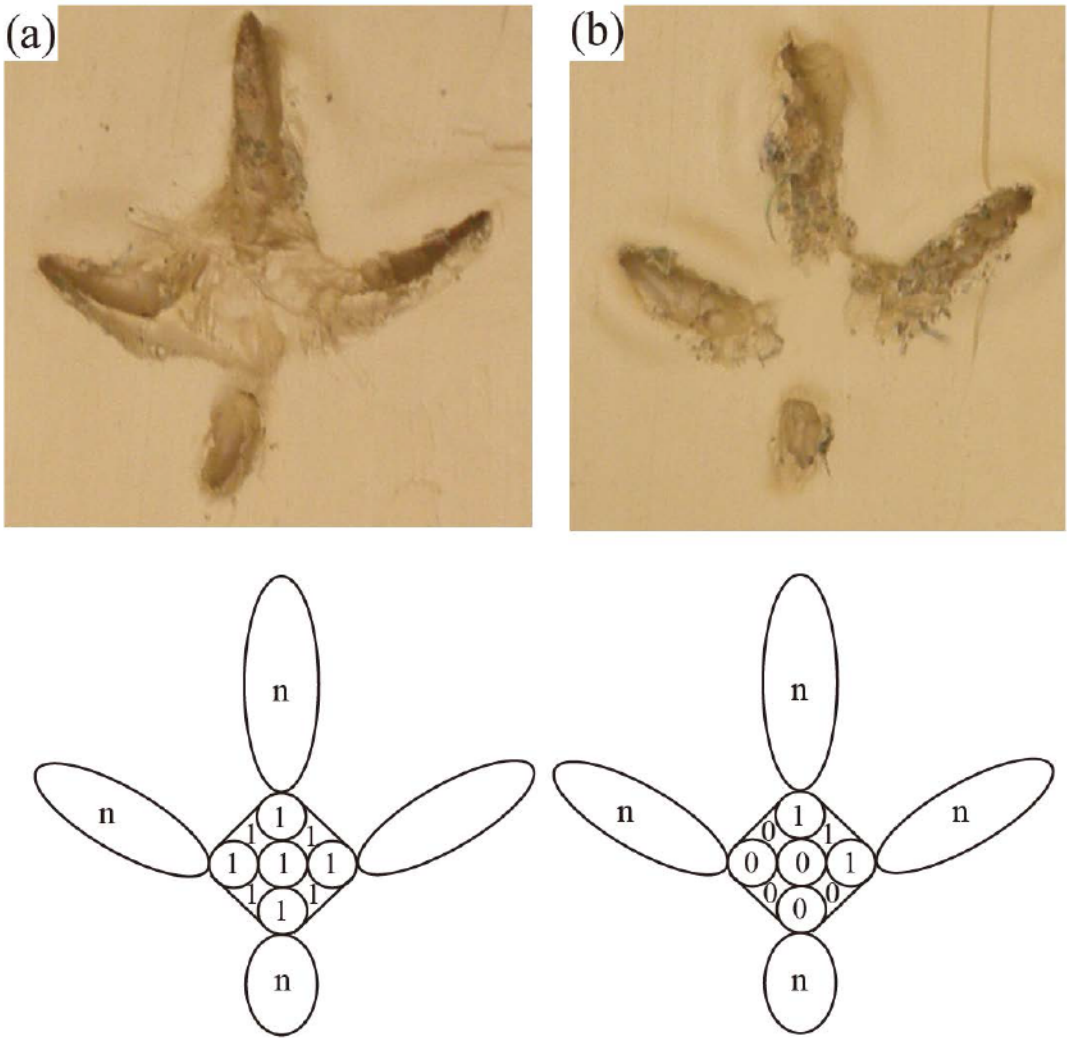

Fig. 7. The results of track morphospace analysis for *Ciconia boyciana*.

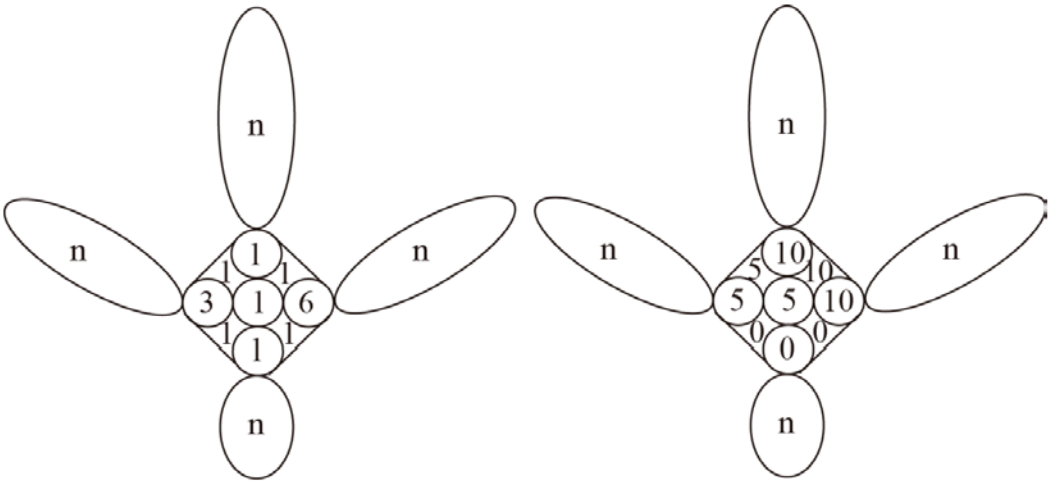

Fig. 8. The results of track morphospace analysis for male (left) and female (right) *Ciconia boyciana*. The number shows sum of counts of impression in each of nine parts. n is 28 for left and 26 for right.

We examined if the result of theoretical morphological analysis is consistent with the rules of biomechanics. The biomechanics rules show male *Ciconia boyciana*'s hip width is 32.4cm and its average trackway width is 9.6cm, and female *Ciconia boyciana*'s hip width is 28.5cm and average of trackway width is 2.7cm. These data show *Ciconia boyciana* walks shaking the hip and pressing the outside of digits. These results show *Ciconia boyciana* tend to push digit's outside during walking, although there are some variabilities in foot's touching on the ground.

The bipedal walking of birds is controlled by important factors of hip, foot muscles and bones. Because tracks are results of walking, the factors can be investigated through track morphology. This study suggests track morphology can refer to posture, and track morphology is related to hip width, foot muscles and bones. The combined method of theoretical morphology and biomechanics rules has a potential to clarify extinct bipedal animals walking style like theropod. Furthermore, we suggest that this method combined with 3D technique (e.g. Falkingham & Gatesy 2014) is useful to reveal trackmaker's limb motion more in detail.

4.5. Summary

The results of the neoichnological experiment with two *Ciconia boyciana*s and morphological analyses of the data are summarized as follows:

(1) *Ciconia boyciana*'s tracks have first been obtained; male *Ciconia boyciana* left 28 tracks, 14 of which are of left foot and the remaining are of right, and female *Ciconia boyciana* left 26 tracks, 12 of which are of left foot and the remaining are of right. The track areas have an average close to median and a small standard deviation. Therefore

track areas are concentrated to median. F-test reveals that the track areas have no difference of the left and right.

(2) *Ciconia boyciana* rarely left metatarsal impression. This character may be useful to ichnologically distinguish *Ciconia boyciana* from other wading birds.

(3) Theoretical track analysis reveals *Ciconia boyciana* generally left the same track type. Theoretical morphospace has 12 types, but *Ciconia boyciana* took only 4-5 types. This result is probably reflected by its controlling digits-substrate interaction to keep balance.

(4) The track widths have a wide range of variability with a maximum difference of about 40%. This feature may be related to feet muscles. Feet have two muscles to move digits; flexor digitorum longus muscle and flexor pollicis longus. These muscles are connected and co-moved as to control only limb's bending and stretching in the moving direction, and not control sideways motion. *Ciconia boyciana* has no muscle to control the stretch of digits II and IV. This causes the wide range of track width variability.

(5) The correlation analysis of track geometry reveals that there is a trade-off relation between track width and depth to keep a constant track volume. This trade-off relation suggests that the track volume is proportional to trackmaker's body weight, and during walking animals always give a same pressure to foot.

(6) The track data were analyzed by the methods of track theoretical morphology and biomechanics rules. We confirm the two methods provide the consistent result that *Ciconia boyciana* push their digit's outside during walking. The methods may be useful to analyze the extinct bipedal walking animals like theropods.

Chapter 5

Effects of Initial Symmetry on the Global Symmetry of One-Dimensional Legal Cellular Automata

5. 1. Introduction

Animals have many kinds of pattern formation. Leopards living in closed habitats, such as forests, have a frequency of stripes that is much higher, more irregular, and more complex than those living in open habitats (Allen et al. 2010). These body patterns reflect adaptations to the surrounding environment and, thus, pattern formation is substantially related to the conservation of species (Allen et al. 2010). When we observe pattern formation, we read "texture", which includes shape, among other factors. Texture is measured by terms including spectrum, entropy, and fractal dimension (Ubukata 2000; Nishiyama et al. 2008). The method of measurement combining entropy and symmetry, the two-dimensional discrete Walsh analysis, can be applied to analyses of two-dimensional surfaces (Nishiyama et al. 2008; Yamasaki et al. 2010, 2012). In previous studies, the two-dimensional discrete Walsh analysis has been used in theoretical studies with one-dimensional legal cellular automata. As a result, studies have revealed the theoretical process of pattern formation, which reduces entropy and increases specific symmetry (self-organization) (Yamasaki et al. 2012), and the real biological process of pattern formation, which reduces entropy and increases specific symmetry. They have also revealed that the real biological process has phase transitions, as seen in calculations with the two-dimensional Ising model (Yamasaki et al. 2010). However, the calculations in previous studies (Nishiyama et al. 2008; Yamasaki et al. 2010, 2012) always start with the condition of a random state. Pattern formation of a biological or animal surface does not necessarily start from such a random state, but rather from a regular state. Thus, clarifying the theoretical process of regular pattern

formation has the possibility of revealing general features and the real biological process of pattern formation.

The purpose of this study was to clarify the theoretical process of pattern formation, starting from a regular state. We applied a two-dimensional discrete Walsh analysis to one-dimensional legal cellular automata.

The structure of this paper is as follows. In Section 2, we explain the method of analysis and data on one-dimensional legal cellular automata (CAs). In Section 3, we explain the data of the regular initial conditions. In Section 4, we briefly review the discrete Walsh analysis for calculating the symmetry and symmetropy of CA patterns. In Section 5, we describe and discuss the results and consider the symmetry relationships between the initial conditions and final patterns. Section 6 provides our conclusions.

5. 2. Methods

5.2.1. The Discrete Walsh Analysis

We briefly outline the discrete Walsh analysis here (Figure 1). For details of the mathematical procedures, see previous studies (Yodogawa 1982; Allen et al. 2010; Yamasaki et al. 2012). The Walsh function $wal(r,x)$ of order r and argument x can be represented over the interval $0 \leq x < 1$ as follows:

$$wal(r,x) = \prod_{i=0}^{m-1} sgn\left[\left(cos 2^i \pi x\right)^{ri}\right] \quad (1)$$

where $r_i = 0$ or 1, $r = \sum_{i=0}^{m-1} r_i\, 2^i$, and m is the smallest positive integer such that $2^m > r$. Dyadic addition of non-negative integers r and s is defined as $r \oplus s = \sum_{i=0}^{f} |r_i - s_i|\, 2^i$, where $r = \sum_{i=0}^{f} r_i\, 2^i$ and $s = \sum_{i=0}^{f} s_i\, 2^i$. Consequently, the product of

the two Walsh functions is given by $wal(r,x)wal(s,x) = wal(r \oplus s,x)$. From this calculation, the Walsh function can be shown to form an orthonormal set. In this case, we can define a Walsh transform, similar to a Fourier transform.

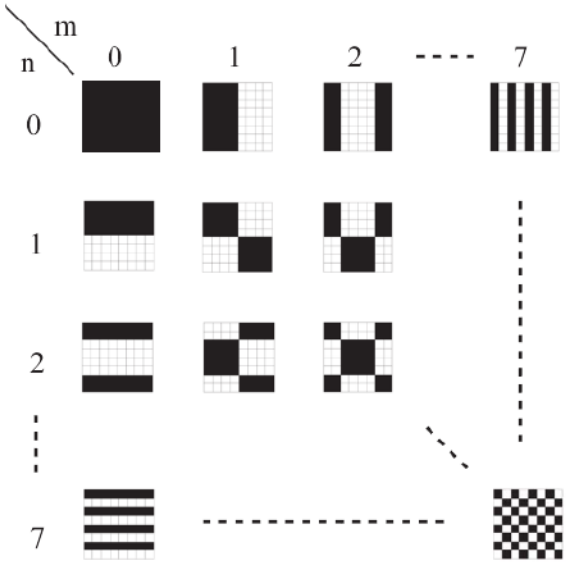

(**a**)

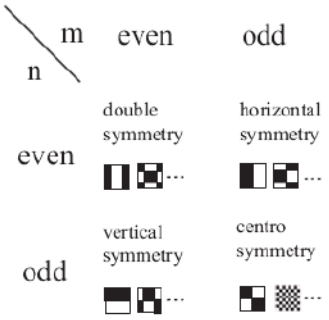

(**b**)

Fig. 1. (a) Examples of the two-dimensional discrete Walsh functions for $m = n = 8$. Black represents +1, and white represents –1; and (b) four types of symmetry in terms of the discrete Walsh function.

The two-dimensional discrete Walsh function can be represented in matrix form as $[W_{mn}(i,j)]$, where $W_{mn}(i,j)$ is the amount of the $(m,n)^{th}$-order Walsh function in the i^{th} row cell in the j^{th} column.

This pattern can be written as $[x_{ij}]$, where x_{ij} is the amount of the gray level in the i^{th} row cell in the j^{th} column and $i, j = 0,1, \ldots, N-1$. If just two gray levels exist, for example, "black" and "white", then x_{ij} is typically represented by 1 and 0, respectively (Figure 1a). The two-dimensional discrete Walsh transform of the pattern $[x_{ij}]$ is given by:

$$a_{mn} = \frac{1}{N^2} \sum_{i=0}^{N-1} \sum_{j=0}^{N-1} x_{ij} W_{mn}(i,j) \tag{2}$$

where $m, n = 0,1, \ldots, N-1$. The functions a_{mn} and $(a_{mn})^2$ are the two-dimensional Walsh spectrum and power spectrum, respectively.

The Walsh power spectrum can be normalized as follows:

$$P_{mn} = \frac{(a_{mn})^2}{K} \tag{3}$$

where $K = \sum_{m=0}^{N-1} \sum_{n=0}^{N-1} (a_{mn})^2 - (a_{00})^2$. In this case, we obtain:

$$\sum P_{mn} = 1 \tag{4}$$

where the sum is taken over all ordered pairs (m,n) for $0 \leq m, n \leq N-1$, except for $(m,n) = (0,0)$.

The spatial pattern is considered as an information source, consisting of dot patterns. The dot patterns emitted from the source are assumed to occur with the corresponding probabilities given by Equation (4).

Next, we consider the information entropy resulting from the symmetry of the pattern. Because the two-dimensional Walsh functions can be easily divided into four types of symmetry (Figure 1b), Equation (4) can be rewritten as:

$$\sum_{i=1}^{4} P_i = 1 \tag{5}$$

where vertical symmetric component:

$$P_1 = \sum_{m=\text{even}, n=\text{odd}} P_{mn} \tag{6}$$

horizontal symmetric component:

$$P_2 = \sum_{m=\text{odd},n=\text{even}} P_{mn} \tag{7}$$

centro symmetric component:

$$P_3 = \sum_{m=\text{odd},n=\text{odd}} P_{mn} \tag{8}$$

and double symmetric component:

$$P_4 = \sum_{m=\text{even},n=\text{even}} P_{mn} \tag{9}$$

When the spatial pattern is regarded as an information source consisting of four types of symmetry, the corresponding probabilities are given by Equations (6)–(9). Applying the entropy function from information theory to these four symmetric components, we obtain:

$$S = -\sum_{i=1}^{4} P_i log_2 P_i \tag{10}$$

As shown in Equations (5) and (10), S ranges from 0 to 2 bits. Since this entropy relates to the symmetry, it is called the "symmetropy" (Yodogama 1982). The symmetropy can be considered as a quantitative and objective measure of symmetry. If the amount of a certain component is larger than the amounts of the other three components, then the pattern is rich in symmetry related to the particular component. In this case, Equation (10) shows that S decreases. Conversely, if the amounts of the four components are almost equal to one another, then the pattern is poor in symmetry, and S increases. Previous studies have concentrated on symmetry (Yamasaki et al. 2012). Following this idea, in this study, we measured the symmetry of the initial condition and the final pattern to examine the effects on final patterns of the initial condition of symmetry in CA patterns.

5.3. Calculations

For simplicity, this paper uses only 'classical' CAs according to the Wolfram classification (Wolfram 1984); that is, the one-dimensional legal CA that obeys the 32 possible legal totalistic rules. The totalistic rules involve nearest and next nearest neighbors, and each cell has two possible colors: white (0) or black (1). In addition, because the total number of neighborhoods of five cells is equal to 2^5, we can obtain the 32 possible legal totalistic rules. Wolfram (1984, 2002) discovered that, although the patterns obtained with different rules differed in detail, they appeared to fall into four qualitative classes:

- Class I: fixed point (rules 0, 4, 16, 32, 36, 48, 54, 60, and 62) (Figure 2a).
- Class II: periodic (rules 8, 24, 40, 56, and 58) (Figure 2b).
- Class III: chaotic (rules 2, 6, 10, 12, 14, 18, 22, 26, 28, 30, 34, 38, 42, 44, 46, and 50) (Figure 2c).
- Class IV: complex (rules 20, 52) (Figure 2d).

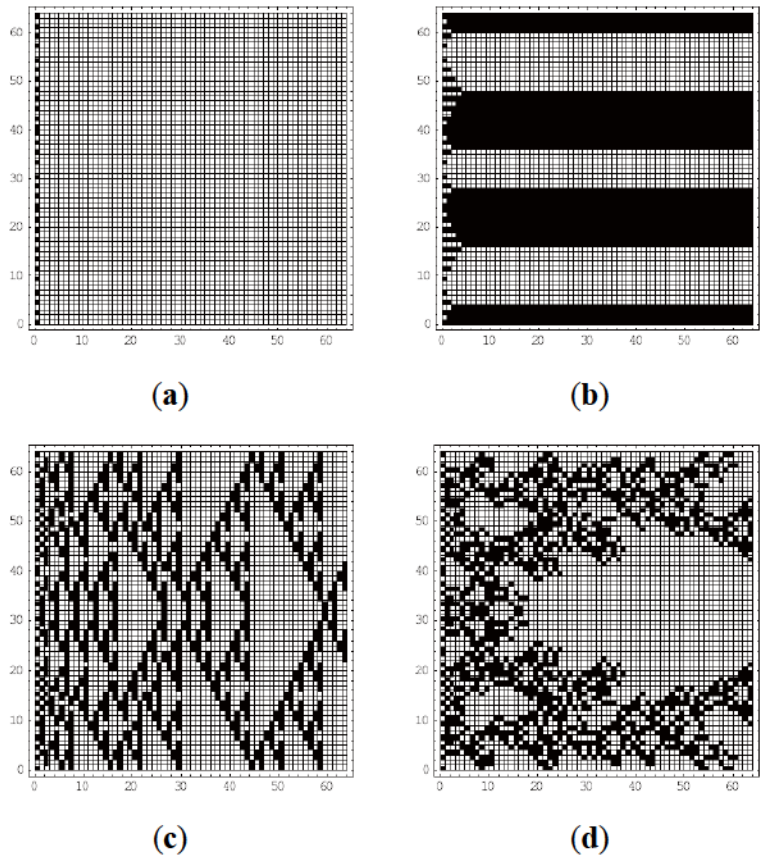

Fig. 2. Examples of final patterns in each class. (a) is an example of Class I, (b) of Class II, (c) Class III, and (d) is an example of Class IV.

In this paper, we do not use all codes in class I because the patterns are trivial. We measure the initial condition ($2^6 \times 1$) and the final pattern. The number of cells is $2^6 \times 2^6$ because, to measure the number of symmetries, this number of cells is the minimum needed (Yamasaki et al. 2012). In the present study, we can use only two kinds of initial condition, horizontal symmetry and double symmetry, because we consider $n = 2$ in the discrete Walsh function W_{mn} (as in Figure 3).

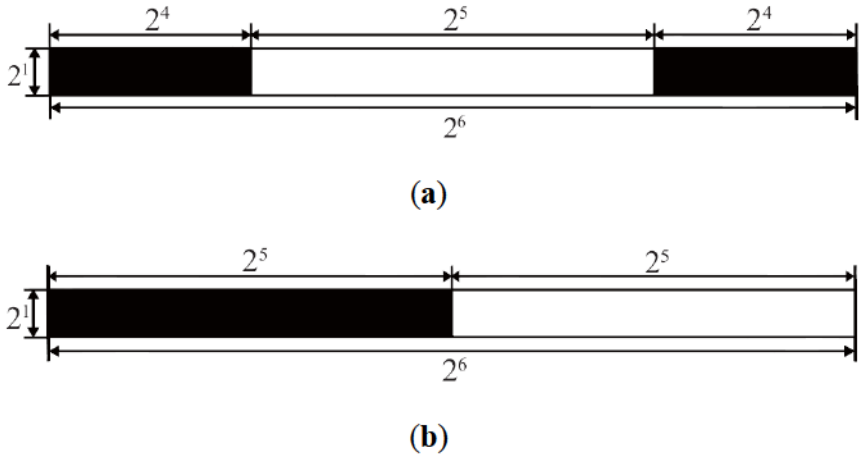

Fig. 3. An example of initial symmetry. (a) Double Symmetry is one example of DS_0, and (**b**) Horizontal Symmetry is one example of HS_0. In this study, the initial condition was limited to $n = 2$ because $2^1 = 2 = n$. Thus, (**a**) shows the case of $m = even$, and (**b**) shows the case of $m = odd$.

First, we run two types of regular initial conditions; the horizontal symmetry with 32 conditions, abbreviated as HS_0, and the double symmetry with 31 conditions, abbreviated as DS_0. Then, under each initial condition, the amounts of symmetry were averaged for each class. We compared this result with the random initial condition in [4], abbreviated as Ra_0. Then, for each initial condition, we compared the relationship between the amount of symmetry in the initial condition and that in the final pattern. The method can be extended to 2D cellular automata, but requires a large number of analysis.

5.4. Results

5.4.1. Class

Figure 4 shows the amount of symmetropy for the three initial conditions ($Ra_0, DS_0, and\ HS_0$) and the amount of symmetropy in each initial condition for the final patterns. The results show that under all initial conditions, the numbers of symmetries of the CA patterns correspond to three qualitative classes of CAs, identified as Classes II, III, and IV, according to Wolfram's original classification (Wolfram 1984; 2002). Additionally, the result of the measurement of symmetropy under regular and random initial conditions shows a relational expression: Class II < Class IV < Class III. In all classes, the amount of symmetropy under Ra_0 is larger than that under DS_0 and HS_0. In Ra_0, the amount of symmetropy of all classes decreased as time passed. In contrast, in DS_0 and HS_0, the amount of symmetropy of all classes increased as time passed. Thus, the final patterns of the regular initial condition (DS_0 and HS_0) are more regular than those of the random initial conditions (Ra_0).

5.4.2. Four Types of Symmetry

Figure 4 shows increases or decreases in the amount of symmetry for four kinds of symmetries in initial conditions and in final patterns. In HS_0, Classes II, III, and IV have all of the four kinds of symmetries: vertical symmetry, horizontal symmetry, centro symmetry, and double symmetry. However, in DS_0, Classes II, III, and IV have only two kinds of symmetries: vertical symmetry and double symmetry (Figure 4).

In DS_0, two kinds of symmetries, double symmetry and vertical symmetry, developed globally in the final formations. The design developed by DS_0 has a complicated pattern that lined up with a regular pattern (Figure 5a,b). Development was accompanied by a large increase in the amount of vertical symmetry. Thus, vertical symmetry contributed to the development of the spatial direction of the final patterns, whereas the double symmetry of DS_0 was preserved. In contrast, the design developed

by HS_0 has all four kinds of symmetry (Figure 4), and the horizontal symmetry of HS_0 was not preserved.

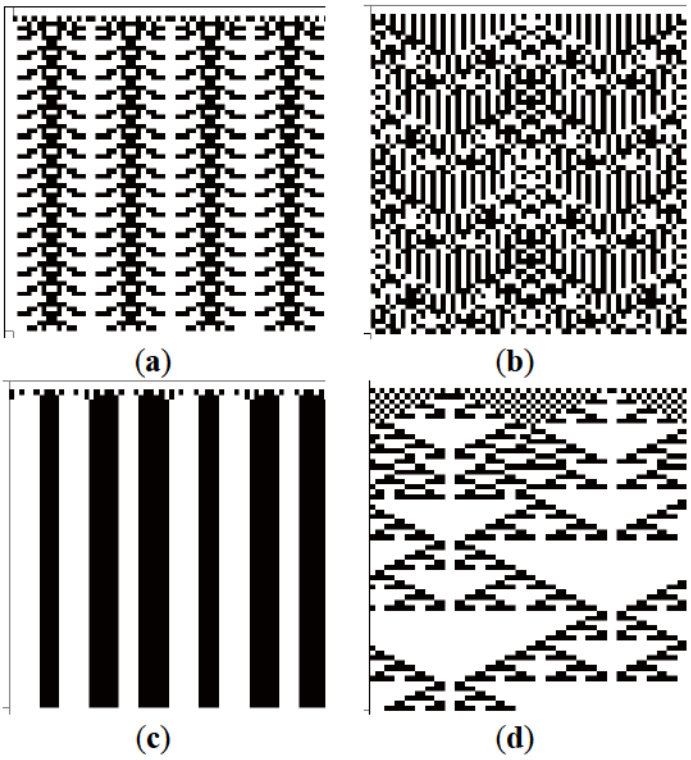

Fig. 5. Examples of final patterns with regular initial conditions. (a,b) belong to DS_0, and (c,d) belong to HS_0.

5.4.3. The Ratio of Final Formation

The ratios of developed final patterns in each Class for DS_0, Ra_0, and HS_0 are shown in Table 1. The ratio of developed of final patterns is calculated by dividing the number of final pattern formation for each class (periodic or chaotic or complex) by a product of the number of initial condition (if HS_0: 32 ,if DS_0: 31) and the total number of classes (the sum rules of periodic, chaotic and complex: 23)" For example, in the case of HS_0's periodic in Table 1, the ratio of periodic is 12 is calculated from 89, 32, and 23 for the numbers of final pattern formation, initial condition, and the sum rules of periodic, chaotic and complex, respectively. The ratio of 12 is obtained as: 89(final patterns) / 32rules / 23 (number of classes) × 100. According to Yamazaki *et al.*(2012), Ra_0 made

final patterns using every rule and class; the ratio of formation was 100%. In contrast, for DS_0 and HS_0, the ratio of formation is less than 50% for all classes, and the developing final pattern ratios are 12% for Class II, 43%–44% for Class III, and 6% for Class IV (Table 1).

Table 1. The rate of final patterns of DS_0 and HS_0.

Class	Horizontal Symmetry	Double Symmetry	Random
Periodic	12	12	100*
Chaotic	43	44	100*
Complex	6	6	100*

In all classes, the rate of the forming pattern of Ra_0 was larger than that of DS_0 and HS_0. Comparing DS_0 with HS_0, the rate of forming patterns of class III was larger than that of class II and class IV; also, in each class, the two types of DS_0 and HS_0 had the same rates. Data indicated by asterisks are from Yamasaki et al. (2012).

5.5. Discussion

5.5.1. Class

For all classes, the amount of symmetry for HS_0 is larger than that for DS_0, and the final pattern formations of DS_0 have a higher hierarchy than HS_0; in contrast, the final pattern formations of HS_0 had more broken regularity than HS_0 (Figure 5c,d). This result is interpreted as the double symmetry having a higher amount of symmetry than the horizontal symmetry, because DS_0 has an axis of symmetry with space and time, whereas HS_0 has an axis of symmetry with time alone.

From the measurement of symmetropy, developed pattern formations of HS_0 and DS_0 have many types of symmetries that predominate as time passes. This result corresponds to the viewpoint of the Curie Symmetry Principle (Yamasaki et al. 2012). In contrast, the developed pattern formations of Ra_0 show a situation in which one type of symmetry was predominant as time passed (Yamasaki et al. 2012); this result does not correspond to the viewpoint of the Curie Symmetry Principle (Yamasaki et al. 2012).

Here, it is shown that the theoretical process of pattern formation reduced entropy and increased specific symmetry (Yamasaki et al. 2010, 2012); however, this process has been examined only from Ra_0 (Yamasaki et al. 2010, 2012). In this study, the final pattern formations from regular initial conditions did not reduce entropy and increased specific symmetry. Thus, the Curie Symmetry Principle cannot be used to evaluate the proxy of pattern formation.

The final pattern formation of DS_0 is composed of the same scale forms, to stand in a line (Figure 5a,b). The pattern formations are supposed to be affected by "iteration" of the base rules of CAs, and this result is correlated with the previous studies, such as (Martin 2006) that shows that the Walsh transform allows one to compute the correlation between the inputs and the outputs of the iterations of a cellular automaton. Generally, as systems are put under greater stress, the observed states lose symmetry and gain in complexity (both spatial and temporal). However, as the systems are further stressed, states with more symmetries and more structures appear. Moreover, symmetries and chaos—patterns and disorder—can coexist naturally within the same simple mathematical framework (Stewart 1992). In this study, the natural coexistence of symmetry and chaos (iteration of CAs) is found in the final pattern formation of DS_0; this means a simple mathematical framework of a one-dimensional legal cellular automata. Complicated structure pattern formations are developed by a simple model; thus, the quantity of information needed to describe an object may be more than that needed to prescribe it. Thus, under an initial condition of strong regularity, theoretical phenomena revealed occurrences of iterations with regularity, and the concepts of the theoretical phenomena could be helpful to interpret the process and the circumstance of biological patterns with higher-complexity structures.

5.5.2. Four Types of Symmetry

For all classes, the amount of symmetropy for HS_0 is larger than that for DS_0 (Figure 4), because HS_0 has four types of symmetry, while DS_0 has only two types (Figure 4). This result coincides with that the final pattern of HS_0, which shows steady state decay, and that of DS_0, which shows switching of a steady state to a hierarchy.

HS_0 has four types of symmetry: vertical, double, horizontal, and centro symmetries. DS_0 has only two types: vertical and double symmetries. These results show that double and vertical symmetries are the basic ones for forming patterns, and whether they form random or regular patterns is affected by the amount of horizontal and centro symmetries. The direction of each symmetry shows that (1) vertical symmetry has an axis of symmetry with space, (2) horizontal symmetry has an axis of symmetry with time, (3) double symmetry has an axis of symmetry with space and time, and (4) centro symmetry has an axis of symmetry with space and time. Thus, combinations of double and vertical symmetries, which are the basic symmetries of pattern forming, have axes of symmetries with space and time. In contrast, the combination of horizontal and centro symmetries is a supplemental one, for pattern formation. Thus, the basic and supplemental symmetries have balance with space and time. Additionally, the initial condition constrains the combination of symmetries (the analysis decided the symmetry direction): vertical and double symmetries *versus* horizontal and centro symmetries.

We compared the amounts of the four types of symmetries among $DS_0, Ra_0,$ and HS_0. The amount of vertical symmetry and double symmetry increased in the order $HS_0 < Ra_0 < DS_0$, except for Class II's vertical symmetry. Additionally, the amount of horizontal symmetry and centro symmetry increased in the order $DS_0 < Ra_0 < HS_0$.

In regular and random initial conditions, Class III has equal amount of symmetries of the different types of symmetries, but Classes II and IV have different amounts. Here, we explain biological patterns from these results. The organisms' developed pattern formations can select the amounts of two types of symmetry (horizontal and centro) according to the circumstances, because both horizontal and centro symmetries have symmetry axes related to "time". Here, time is related to the future. Thus, the combination of symmetries with wide varieties, as in this study, may provide the opportunity for understanding how to develop pattern formation (heredity or circumstances), and may be able to manage pattern formation, and to predict the future.

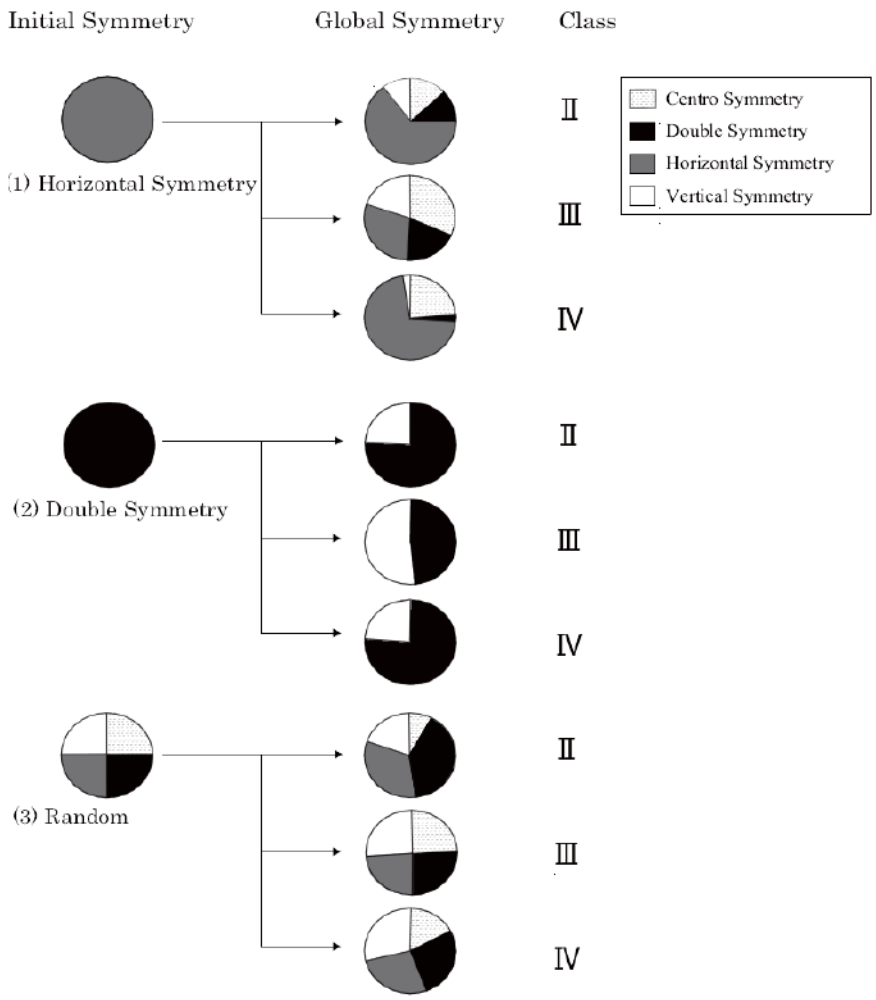

Fig. 4. Pie charts of the three types of initial condition (HS_0, DS_0, and Ra_0). For HS_0 and Ra_0, all classes have all four types of symmetry: vertical symmetry, horizontal symmetry, centro symmetry, and double symmetry. In contrast, DS_0 with all classes had two types of symmetry: vertical symmetry and double symmetry. Regarding vertical symmetry and double symmetry, the relational expression was $HS_0 < Ra_0 < DS_0$, and regarding horizontal symmetry and centro symmetry, it was $DS_0 < Ra_0 < HS_0$.

5.5.3. The Ratio of Final Formation

The growth design formations are limited in HS_0 and DS_0, but there is no limit in Ra_0 (Table 1). This means the variability of symmetries of Ra_0 is larger than that of HS_0 and DS_0. The numbers of developed final pattern rules for HS_0 and DS_0 are

almost equal in every class, because the numbers of initial conditions are almost the same; 32 for HS_0 and 31 for DS_0, and most of the HS_0 rules correspond to DS_0 ones.

The rules that did not develop final patterns under regular initial conditions need larger amounts and more symmetries. The ratio of rules developing final patterns to those with no developing final patterns was calculated for each Class (Table 1). The ratio of rules that developed final patterns under the regular initial condition decreased in the order of Class III, Class II, and Class IV. Thus, Class III does not need more of the amounts and types of symmetries, whereas Class IV requires much more in the way of amounts and many types of symmetries, and Class II requires moderate amounts and types of symmetry. We explain biological patterns from these theories. Class III is not influenced by circumstances, and allows easy development of final patterns, which means heredity. On the other hand, Class IV is influenced by circumstances, and Class II by circumstances and heredity. Animals having Class III biological patterns may select the circumstances by themselves, because their biological patterns are interpreted as genetic characteristics. The animals having Class IV biological patterns may adapt themselves to circumstances, because their biological patterns are interpreted as acquired characteristics. The animals having Class II biological patterns may be able to select a circumstance by themselves and may be able to adapt themselves to a circumstance, because their biological patterns are interpreted as random genetic characteristics and random circumstances. They may take an unplanned survival strategy.

Here, we discuss living animals. Although clams appear in Class III (Schiff 2008), their shell patterns are in heredity (Peignon et al. 1995). Additionally, the habitat of clams is decided by the height of ground level and drying time within 1 day, which has no relationship with pattern formation (Akiyama et al. 2011). This might be supported by the hypothesis "The animals having Class III biological pattern formation may select circumstance by themselves, because their biological patterns are interpreted as genetic characters." However, *Neritina*, a typical shellfish, appears in Classes II and IV (Schiff 2008); their shell design pattern formation has been found along the structure of the growth lines (Habe 1975). Thus, *Neritina* may be affected by the circumstances around them. In addition, their shell patterns have been found to be of color bands (Habe 1975); thus, *Neritina* may have been affected by circumstance and heredity.

5.6. Conclusions

We examined the structure of one-dimensional legal cellular automata from the viewpoint of symmetry to reveal the rules of animals' pattern generation. The following conclusions are derived. (1) Under all regular and random initial conditions, a relational expression, Class II < Class IV < Class III, was seen. In all classes, the pattern formation with regular initial conditions was more regular than that with random initial conditions. (2) We compared the pattern formation made with two types of regular initial conditions. The final pattern formations of HS_0, which have more broken regularity, have four types of symmetries, whereas that of DS_0 has only two types of symmetries, which are of a higher hierarchy. Both regular initial conditions show situations in which many types of symmetry predominated as time passed. We showed that when pattern formation develops, amounts of symmetries and types of symmetries do not always decrease. (3) We found that growth design formations have limited possibilities with regular initial conditions; the results of calculating the ratio of developing final patterns decreases in the order of Class III, Class II, and Class IV.

Chapter 6

Conclusion

The morphological analyses of avian body structures and tracks, and analysis of the structure of one-dimensional legal cellular automata were carried out. The following conclusions are drawn from the results.

The relationship between body weight and footprint area of modern avians was derived and used to estimate the body weights of extinct theropod ichnotaxa from the Triassic to Early Cretaceous periods and avian ichnotaxa from the latter period. Body weights estimated from track area are similar to body weights estimated from fragmentary bone fossils, so this approach is useful when the fossilized track record is richer than the fossilized skeletal record. Additionally, the data sets from avians were combined with those from other reptiles from Kubo (2011) and could derive the weight–area relation such as eqn (3). This generalized equation implies that the animals have a footprint area suitable for their weight and is applicable to a broader range of organisms, such as plantigrade-digitigrade quadrupeds and digitigrade bipeds. Finally, the relationship between habitat type and footprint shape of modern avians was assessed based on scatter plots. The principal component analysis revealed that the angle between digits II and IV and the length of digit I in the track record are related to habitat type: semi-aquatic, ground or arboreal bird. In addition to track area, foot shape thus contains important ecological information. The shape–habitat relation was applied to extinct avians and demonstrated that the pes of extinct animals living in a semi-aquatic environment is similar to that of the present semi-aquatic avians.

We used avian wing data to calculate the wing aspect ratio and loading, which are important parameters in aerodynamics. Discriminant analyses and multiple regression analyses yielded the following results: (1) avian wings can be divided into three groups, similar to tracks, which are morphologically divided into three groups corresponding to the arboreal, ground and semi-aquatic habitat types; (2) avian wing loading and aspect ratio are closely related to track shape parameters; (3) wingspan and wing area are related to track area and the relationship provides a method for estimating the wingspan and area from the fossil track area; (4) the wingspan and area of Cretaceous extinct avian taxa estimated using this method, and their previously-estimated bodyweights, suggest that the *Archaeornithipus meijidei* trackmaker was a semi-aquatic bird similar to a large heron or grus, the *Hwangsanipes choughi* trackmaker was a shorebird, and the *Yacoraitichnus avis* trackmaker was a medium-sized gull; (5) the ecology of avian flight based on aerodynamics suggests that birds are divided by their wing aspect ratios into the two groups: “transport aircraft” and “fighter aircraft”.

The results of the neoichnological experiment with two *Ciconia boyciana*s and morphological analyses of the data are summarized as follows: (1) *Ciconia boyciana*'s tracks have first been obtained; male *Ciconia boyciana* left 28 tracks, 14 of which are of left foot and the remaining are of right, and female *Ciconia boyciana* left 26 tracks, 12 of which are of left foot and the remaining are of right. The track areas have an average close to median and a small standard deviation. Therefore track areas are concentrated to median. F-test reveals that the track areas have no difference of the left and right. (2) *Ciconia boyciana* rarely left metatarsal impression. This character may be useful to ichnologically distinguish *Ciconia boyciana* from other wading birds. (3) Theoretical track analysis reveals *Ciconia boyciana* generally left the same track type. Theoretical

morphospace has 12 types, but *Ciconia boyciana* took only 4-5 types. This result is probably reflected by its controlling digits-substrate interaction to keep balance. (4) The track widths have a wide range of variability with a maximum difference of about 40%. This feature may be related to feet muscles. Feet have two muscles to move digits; flexor digitorum longus muscle and flexor pollicis longus. These muscles are connected and co-moved as to control only limb's bending and stretching in the moving direction, and not control sideways motion. *Ciconia boyciana* has no muscle to control the stretch of digits II and IV. This causes the wide range of track width variability. (5) The correlation analysis of track geometry reveals that there is a trade-off relation between track width and depth to keep a constant track volume. This trade-off relation suggests that the track volume is proportional to trackmaker's body weight, and during walking animals always give a same pressure to foot. (6) The track data were analyzed by the methods of track theoretical morphology and biomechanics rules. We confirm the two methods provide the consistent result that *Ciconia boyciana* push their digit's outside during walking. The methods may be useful to analyze the extinct bipedal walking animals like theropods.

We examined the structure of one-dimensional legal cellular automata from the viewpoint of symmetry to reveal the rules of animals' pattern generation. The following conclusions are derived. (1) Under all regular and random initial conditions, a relational expression, Class II < Class IV < Class III, was seen. In all classes, the pattern formation with regular initial conditions was more regular than that with random initial conditions. (2) We compared the pattern formation made with two types of regular initial conditions. The final pattern formations of *HSo*, which have more broken regularity, have four types of symmetries, whereas that of *DSo* has only two types of

symmetries, which are of a higher hierarchy. Both regular initial conditions show situations in which many types of symmetry predominated as time passed. We showed that when pattern formation develops, amounts of symmetries and types of symmetries do not always decrease. (3) We found that growth design formations have limited possibilities with regular initial conditions; the results of calculating the ratio of developing final patterns decreases in the order of Class III, Class II, and Class IV.

Reference

Akiyama, B.Y., Saito, H., Nanbu, R., Tanaka, Y., Kuwahara, H. 2011: The spatial distribution of Manila clam Ruditapes philippinarum associated with habitat environment in a sandy tidal flat on the coast of Matsunase, Mie Prefecture, Japan. *Ecology and Civil Engineering* 14, 21–34. (In Japanese)

Alexander, R. M. 1976: Estimates of speeds of dinosaurs. *Nature* 261, 129–130.

Alexander, R. M. 1992: *Exploring Biomechanic: Animals in Motion*. 248 pp. W. H. Freeman & company, New York, USA.

Alexander, R. McN. 2002: *Principles of Animal Locomotion.* 371 pp. Princeton University Press, New Jersey, USA.

Allen, W. L., Cuthill, I. C., Scott-Samuel, N. E., Baddeley, R. 2010: Why the leopard got its spots: Relating pattern development to ecology in felids. *Proceedings of the Royal Society of London B* 1373–1380.

Alonso, R. N. & Marquillas, R. A. 1986: Nueva localidad con huellas de dinosaurious y primer hallazgo de huellas de Aves en la Formacion Yacoraite (maastrichtiano) del Norte Argentino. *Actas 4°,Congreso Argentino de Paleontologia y Biostratigrafia* 2, 33–41.

Anderson, J. F. & Hall Martin, D. A. 1985: Long-born circumference and weight in mammals, bird and dinosaurs. *Journal of Zoology* 207, 53–61.

Avnimelech, M. A. 1966: Dinosaur track in the Judean Hills. Proceedings of the Israel Academy of Sciences and Humanities. *Section of Sciences* 1, 1–19.

Azuma, Y., Arakawa, Y., Tomida, Y., Currie, P.J. 2002: Early Cretaceous bird tracks from the Tetori Group. *Memoir-Fukui Prefectural Dinosaur Museum* 1, 1–6.

Baird, D. 1957: Triassic Reptile Footprint Faunas from Milford, New Jersey. *Bulletin of the Museum of Comparative Zoology* 117, 449–520.

Bertling, M., Braddy, S. J., Bromley, R.G., Demathieu, G.R., Genise, J., Mikuláš, R., Nielsen, J.K., Nielsen, S.S., Rindsberg, A.K., Schlirf, M., Uchman, A. 2006: *Names for trace fossils: a uniform approach. Lethaia* 39, 265–286.

Bookstein, F. L. 1996: *Combining the tools of geometric morphometrics*. In Marcus, L.F., Corti, M., Loy, A., Taylor, G.J.P. & Slice, D.E. (eds): Advances in Morphometrics, 131–151. Plenum, New York, USA.

Brown Jr., T. 1999: *The science and art of tracking*. 219 pp. The Berkley Publication, USA.

Brusatte, S. L., Niedźwiedzki, G., Butler, R. J. 2011: Footprints pull origin and

diversification of dinosaur stem lineage deep into Early Triassic. *Proceedings of the Royal Society B* 278, 1107–1113.

Castanera, D., Vila, B., Razzolini, N. L., Falkingham, P.L., Canudo, J.I., Manning, P. L., Galobart, À. 2013: Manus track preservation bias as a key factor for assessing trackmaker identity and quadrupedalism in basal ornithopods. *PLOS One* 8, e54177.

Council for Scientific and Industrial research, Pretoria. Ericson, M., Gregory, O.W., Rauhut, M., Zhoum, Z., Thrner, H.A., Inouye, B.D., Hu, D., Norell, M.A. 2009: Was Dinosaurian physiology inherited by birds? Reconciling slow growth in Archaeopteryx. *PLOS One* 4, 1–9.

Currie, P. J. 1981: Bird footprints from the Gething formation (Aptian, Lower Cretaceous) of northeastern British Columbia, Canada. *Journal of Vertebrate Paleontology* 1, 257–264.

Damuth, J. & MacFadden, B. J. 1990: *Body Size in Mammalian Paleobiology: Estimation and Biological Implications*, 397 pp. Cambridge University Press, New York.

Diffley, R. L. & Ekdale, A. A. 2002: Footprints of Utah's last dinosaurs: Track beds in the Upper Cretaceous (Maastrichtian) North Horn Formation of the Wasatch Plateau, Central Utah. *Palaios* 17, 327–346.

Ellenberger, P. 1970: Les Niveaux Paleontologiques De Premiere Apparition Des Mammiferes Primordiaux en Afrique du Sud et leur ichnologie: establissement de Zones stratigraphiques detaill_ees dans le Stormberg du Lesotho (Afrique du Sud) Trias Superieur A Jurassique). *International Union of Geological Sciences Commission on Stratigraphy, Second Gondwana Symposium South Africa Proceedings and Papers* 343–370.

Falkingham, P. L. 2014: Interpreting ecology and behaviour from the vertebrate fossil track record. *Journal of Zoology* 292, 222–228.

Falkingham, P. L. & Gatesy, S. M. 2014: The birth of a dinosaur footprint: Subsurface 3D motion reconstruction and discrete element simulation reveal track ontogeny. *Proceeding of National Academic Science* 111, 18279–18284.

Farlow, J. O. & Pianka, E. R. 2000: Body form and trackway pattern in Australian desert monitors (Squamata:Varanidae):Comparing zoological and ichnological diversity. *Palaios* 15, 235–247.

Feduccia, A. 1996: *The Origin and Evolution of Birds,* 432 pp. Yale University, New Haven, USA.

Fountaine, T.M.R., Benton, M.J., Dyke, G.J., Nudds, R.L. 2005: The quality of the fossil record of Mesozoic bird. *Proceedings of the Royal Society of London B*

272, 289–294.

Fuentes Vidarte, C.F. 1996: Primeras huellas de Aves en et Weald de Soria (Espana). Nuevo icnogenero, Archaeornithipus ynueva icnoespecie A. meijidei. *Estudios Geologicos* 52, 63–75.

Fukushima, T., Mukaiyama,T., Okamura,Y., Masubuchi,K., Momohara,A., Koizumi,A., Hatori, K. 2009: *Survey of the distribution of proboscidean and cloven-hoofed animalfootprint fossil groups in the lower Pleistocene series Kazusa level group seen in the bed of the Tama River.* 299 pp. The Tokyu foundation for better environment, Tokyo, Japan. (in Japanese)

Gatesy, S. M., K. M. Middleton., F. A. Jenkins jr & N. H. Shubin. 1999: Three-dimensionel preservation of foot movements in Triassic theropod dinosaurs. *Nature* 399, 141–144.

Gatesy, S.M., Shubin, N.H. and Jenkins, F.A. Jr. 2005: Anaglyph stereo imaging of dinosaur track morphology and microtopography. *Palaeontologia Electronica* 8, 1–12.

Gierliński, G.D. & Ahlberg, A. 1994: Late Triassic and Early Jurassic dinosaur footprints in the Höganäs Formation of southern Sweden. *Ichnos* 3, 99–105.

Gill, F. B. 2007: *Ornithology*, 3rd edition, 720 pp. W. H. Freeman, New York, USA.

Greenewalt, C.H. 1962: Dimensional relationships for flying animals. *Smithsonian Miscellaneous Collections* 144, 1–146.

Habe,T.1975: *Gakken Picture Book of Shellfish*, 294 pp. Gakken Holdings, Tokyo, Japan. (In Japanese)

Hackett, S. J., Kimball, R.T., Reddy, S., Bowie, R. C. K., Braun, E.L., Braun, M. J., Chojnowski, J. L., Cox, W. A., Han, K.-L., Harshman, J., Huddleston, C.J., Marks, B. D., Miglia, K. J., Moore, W. S., Sheldon, F. H., Steadman, D.W., Witt, C.C., Yuri, T. 2008: A phylogenomic study of birds reveals their evolutionary history. *Science* 320, 1763–1768.

Hazlehurst, G.A. & Rayner, J.M.V. 1992: Flight characteristics of Triassic and Jurassic Pterosauria: an appraisal based on aspect ratio. *Paleobiology* 18, 447 – 463.

Heckert, A.B. & Lucas, S.G. 1998: Global correlation of the Triassic theropod record. *Gaia* 15, 63–74.

Henderson, D. M. 1999: Estimating the mass and centers of mass of extinct animals by 3D mathematical slicing. *Paleobiology* 25, 88–106.

Henderson, D. M. 2010: Pterosaur body mass estimates from 3D mathematical slicing. *Journal of Vertebrate Paleontology* 30, 768–785.

Hone, D.W. E. & Benton, M. J. 2005: The evolution of large size: how does Cope's Rule work? *Trends in Ecology and Evolution* 20, 4–6.

Hone, D .W. E ., Dyke, G. J., Haden, M., Benton, M. J. 2008: Body size evolution in Mesozoic birds. *Journal of Evolutionary Biology* 21, 618–624.

Howard, H. 1957: A gigantic 'toothed' marine bird from the Miocene of California. *Santa Barbara Mus Nat Hist Depart Geol Bull* 1, 1–23.

Hudson, G. E. 1937: Studies on the Muscles of the Pelvic Appendage in Birds. *The American Midland Naturalist* 18, 1–108.

Ishigaki, S. 1986: Dinosaur footprints of the Atlas Mountains III. *Nature Study* 32, 6–9. (in Japanese)

Ishigaki, S. & Fujisaki, T. 1989: *Three dimensional representation of Eubrontes by the Method of Moiré topography.* In: Gillette, D.D. & Lockley. M.G. (eds.), *Dinosaur Tracks and Traces*, Cambridge University Press, Cambridge 421–425.

Japan Airlines Co., Ltd.. 2011: *Welcome to JAL*, 8pp. Japan Airlines Co., Ltd., public relations department ,Tokyo, Japan.

Klein, H. & Haubold, H. 2007: Archosaur footprints-potential for biochronology of

Triassic continental sequences. *New Mexico Museum of Natural History and Science Bulletin* 41, 120–130.

Klein, H. & Lucas, S.G. 2010: The Triassic footprint record of crocodylomorphs – a critical re-evaluation, in Milàn, J., Lucas, S.G., Lockley, M.G. and Spielmann, J.A., eds., Crocodyle Tracks and Traces. *Albuquerque, New Mexico Museum of Natural History and Science Bulletin* 51, 55–60.

Klein, K. & Lucas, S.G. 2015: Evolution of the Semi-aquatic Lifestyle in Archosaurs –Evidence from the Tetrapod Footprint Record. *Geological Association of Canada* 105–113.

Ksepka, D.T. 2014: Flight performance of the largest volant bird. *Proceedings of the National Academy of Sciences of the United States of America* 111, 29, 10624–10629.

Kubo, T. 2008: In quest of the *Pteraichnus* trackmaker: Comparisons to modern crocodilians. *Acta Palaeontologica Polonica* 53, 405–412.

Kubo, T. 2011: Estimating body weight from footprints: application to pterosaurs. *Palaeogeography, Palaeoclimatology, Palaeoecology* 299, 197–199.

Kubo, T. & Ozaki, M. 2009: Does pace angulation correlate with limb posture? *Palaeogeography, Palaeoclimatology, Palaeoecology* 275, 54–58.

Leonardi, G. 1994: *Annotated Atlas of South America Tetrapod Footprints (Devonian to Holocene)*, 248 pp. Companhia de Pesquisa de Recursos Minerals, Brasilia.

Lockley, M.G., Yang, S.Y., Matsukawa, M., Fleming, F., Lim, S.K. 1992: The track record of Mesozoic bird: evidence and implications. *Philosophical Transactions of the Royal Society of London B: Biological Sciences* 336, 113–134.

Lockley, M. G., T. J. Logue., J. J. Moratella., A. P. Hunt., R. J. Schultz & J. W. Robinson. 1995: The fossil trackway Pteraichnus is pterosaurian, not crocodillian: implications for the global distribution of pterosaur tracks. *Ichnos* 4, 7–20.

Lockley, M. G. & Rainforth, E. C. 2002: *The track record of Mesozoic birds and Pterosaurs: an ichnological and paleoecological perspective.* In Chiappe, L.M. & Witmer, L.M. (eds): *Mesozoic Birds: Above the Heads of Dinosaurs*, 405–418. University of California Press, Berkeley, USA.

Lockley, M. G. & Gierliński, G. D. 2009: A grallator-dominated tracksite from the Chinle Group (Late Triassic), Moab, Utah. *Geological Quarterly* 53, 433–440.

Lockwood, R., Swaddle, J. P & Rayner, J .M. V. 1998: Avian wingtip shape reconsidered: wingtip indices and morphological adaptations to migration. *Journal of Avian Biology 29*, 273 – 292.

Loope, D. B., 1986: Recognizing and utilizing vertebrate tracks in cross section: cenozoic hoofprints from Nebraska. *Palaios* 1, 141–151.

Lü, J.C., Chen, R., Azuma, Y., Zheng, W.J., Tanaka, I., Jin, X.S. 2010: New pterosaur tracks from the early Late Cretaceous of Dongyang City, Zhejiang Province, China. *Acta Geoscientica Sinica* 31(Suppl. 1), 46–48.

Martin, A., Rich, P.V., Rich, T., Hall, W.D.M. 2014: Oldest known avian footprints from Australia: Eumeralla Formation (Albian), Dinosaur Cove, Victoria. *Palaeontology* 57, 7–19

Martin, B. 2006: A Walsh exploration of Wolfram CA rules. In Proceedings of the 12th International Workshop on Cellular Automata, Hiroshima University, Higashi-Hiroshima, Japan, 12–15 September 2006, 25–30.

Martinez, R.N., Sereno, P.C., Alcober, O.A., Colombi, C.E., Renne, P.R., Montanez, I.P., Currie, B.S. 2011: A basal Dinosaur from the dawn of the Dinosaur Era in southwestern Pangaea. *Science* 331, 206–210.

Matthews, N. A., Noble, T. A., Breithaupt, B. H. 2006: The application of photogrammetry, remote sensing and geographic information systems (GIS) to fossil resource management. *New Mexico Museum of Natural History and Science Bulletin* 34, 119–131.

McKee, E. D. 1947: Experiments on the development of tracks in fine cross-bedded sand. *Journal of Sedimentary Petrology* 17, 23–28.

McKeewer, P. J. & Haubold, H. 1996: Reclassification of vertebrate trackways from the Permian of Scotland and related forms from Arizona and Germany. *Journal of Paleontology* 70, 1011–1022.

McMahon, T. A. & Bonner, J. T. 1983: *On Size and Life*, 255 pp. W. H. Freeman & Co., New York, USA.

Mehl, M.G. 1931: Additions to the vertebrate record of the Dakota Sandstone. *American Journal of Science* 21, 441–452.

Michilsens, F., Aerts, P., Van Damme, R., D'Août, K. 2009: Scaling of plantar pressures in mammals. *Journal of Zoology* 279, 236–242.

Milàn, J. 2006. Variations in the morphology of emu (Dromaius novaehollandiae) tracks, reflecting differences in walking pattern and substrate consistency: ichnotaxonomical implications. *Palaeontology* 49, 405–420.

Milàn, J. & Gierliński, G.D. 2004: A probable thyreophoran (Dinosauria, Ornithischia) footprint from the Upper Triassic of southern Sweden. *Bulletin of the Geological Society of Denmark* 51, 71–75.

Milàn, J. & Bromley, R.G. 2006: True tracks, undertracks and eroded tracks, experimental work with tetrapod tracks in laboratory and field. *Palaeogeography, Palaeoclimatology, Palaeoecology* 231, 253–264.

Milàn, J. & Bromley, R.G. 2008: The impact of sediment consistency on track and undertrack morphology: experiments with emu tracks in layered cement. *Ichnos* 15,18–24.

Nesbitt, S. J. 2011: The early evolution of Archosaurs: relationships and the origin of major clades. *Bulletin of the American Museum of Natural History* 352, 1–292.

Neuweiler, G. 2000: *The biology of Bads.* 320 pp. Oxford University Press, Oxford.

Nishiyama,Y., Nanjo, K.Z., Yamasaki, K. 2008: Geometrical minimum units of fracture patterns in two-dimensional space: Lattice and discrete Walsh functions. *Physica A* 387, 6252–6262.

Norberg, U.M.L. & Rayner, J. M. V. 1987: Ecological morphology and flight in bats (Mammalia; Chiroptera), wing adaptations, flight performance, foraging strategy and echolocation. *Philosophical Transactions of the Royal Society, London B* 316, 335 – 427.

Nudds, R. L. & Dyke, G. J. 2010: Narrow primary feature rachises in Confuciusornis

and Archaeopteryx suggest poor flight ability. *Science* 328, 887–889.

Okamura, Y., Takahashi, K., Saegusa, H. 2005: Track fossils in Kami town, the report of Kami town. *Fukui prefecture* 26–66 (in Japanese).

O'Keefe, F. R. 2001: Ecomorphology of plesiosaur flipper geometry. *Journal of Evolutionary Biology* 14, 987–991.

Padian, K. & P. E. Olsen. 1989: 454 pp. *Ratite Footprints and the Stance and Gait of Mesozoic theropods.* In Gillette, D. D. & M. G. Lockley (eds.). *Dinosaur Tracks and Traces*. pp 231–242. Cambridge University Press, UK.

Padian, K. 2003: Pterosaur stance and gait and the interpretation of trackways. *Ichnos* 10, 115–126.

Paul, G. S. 1988: *Predatory Dinosaurs of the World,* 464 pp. Simon and Schuster, New York.

Peignon, J. M., Gérard, A., Naciri, Y., Ledu, C., Phélipot, P. 1995: Analyse du déterminisme de la coloration et de l'ornementation chez la palourde japonaise Ruditapes Philippinarum. *Aquatic Living Resources* 8, 181–185. (In French)

Pennycuick, C. J. 1975: *Mechanics of flight*. Farner, D.S. & King, J.R.,(eds.). *Avian Biology 5*, 1–75. Academic press, New York, USA.

Pennycuick, C. J. 1983: Thermal soaring compared in three dissimilar tropical bird species, Fregata magnificens, Pelecanus occidentalis and Coragyps atratus. *The Journal of Experimantal Biology* 102, 307–325.

Raikow, J. R. 1985: *Locomotor system.* In A. S. King & J. McLelland, (eds.) *Form and Function in Birds*, 57–147, Academic Press, New York, USA.

Rayner, J. M. V. 1985: *Flight, speeds of.* In B. Campbell & E. Lack (eds.) *A Dictionary of Birds*, 224–226. T. & A. D. Poyser, Calton, UK.

Rayner, J .M. V. 1988: Form and function in avian flight. *Current Ornithology* 5, 1–66.

Schiff, J. L. 2008. *Cellular Automata: Discrete View of the World.*250 pp. John Wiley & Sons Inc.: City, NJ, USA.

Schmidt-Nielsen, K. 1984: *Scaling: Why is Animal Size So Important?*256 pp. Cambridge University Press, New York, USA.

Smith, R. J. 1984: Allometric scaling in comparative biology: problems of concept and method. *American Journal of Physiology* 246, 152–160.

Sollas, W. J. 1879: On some Three-toed Footprints from the Triassic Conglomerate of Southern Wales. *Quarterly Journal of the Geological Society of London* 35, 511–517.

Stewart, I. & Golubitsky, M. 1992: *Fearful Symmetry: Is God a Geometer?* 1st ed. 346 pp. Blackwell Pub: Oxford, UK.

Tanaka, I. 2015: Estimating body weight and habitat type from extinct avian and avian-like theropod footprints. *Lethaia* 48, 188–195.

The society of Japanese aerospace companies. 2014: *The database of aerospace industries*, 91 pp. The society of Japanese aerospace companies, Tokyo.

Thulborn, T. 1990: *Dinosaur Tracks*. 424 pp. Chapman and Hall, London, UK.

Ubukata, T. 2000: Theoretical morphology of composite prismatic, fibrous prismatic and foliated microstructures in bivalves. *Venus* 59, 297–305.

Ubukata, T. 2003: A morphometric study on morphological plasticity of shell form in crevice-dwelling Pterioida (Bivalvia). *Biological Journal of the Linnean Society* 79, 285–297.

Ubukata, T. 2004: A three-dimensional digitizing system based on triangulation using multiple viewing images. *Geoscience reports* of *Shizuoka University* 31, 65–72.

Wilson, J. A. 2005: Integrating ichnofossil and body fossil records to estimate locomotor posture and spatiotemporal distribution of early sauropod dinosaurs: a stratocladistic approach. *Paleobiology* 31, 400–423.

Witton, M. P. 2008: A new approach to determining pterosaur body weight and its implications for pterosaur flight. *Zitteliana* B28, 143–158.

Witton, M. P. & Habib, M. B. 2010: On the size and flight diversity of giant pterosaurs, the use of birds as pterosaur analogues and comments on pterosaur flightlessness. *PLOS One* 5, e13982.

Wolfram, S. 1984: Universality and complexity, in cellular automata. *Physica D* 10, 1–35.

Wolfram, S. 2002: *A New Kind of Science*.1197 pp. Champaign; IL Wolfram Media, Inc.: City, IL, USA.

Xing, L., Buckley, G. L., McCrea, R. T., Lockley, G. M., Zhang, J., Piñuela, L., Klein, H., Wang, F. 2015: Reanalysis of Wupus agilis (Early Cretaceous) of Chongqing, China as a Large Avian Trace: Differentiating between Large Bird and Small Non-Avian Theropod Tracks. *PLOS One* 10, e0124039.

Xing, L., Klein, H., Lockley, M. G., Wang, S., Chen, W., Ye, Y., Matsukawa, M.,

Zhang, J. 2013: Earliest records of theropod and mammal-like tetrapod footprints in the Upper Triassic of Sichuan Basin, China. *Vertebrata Pal Asiatica* 51, 184–198.

Yalden, D.W. 2008: The flying ability of Archaeopteryx. *Ibis* 113, 349–356.

Yamasaki, K., Nanjo, K. Z., Chiba, S. 2010: Symmetry and entropy of biological patterns: Discrete Walsh functions for 2D image analysis. *BioSystems* 103, 105–112.

Yamasaki, K., Nanjo, K.Z., Chiba, S. 2012: Symmetry and entropy of one-dimensional legal cellular automata. *Complex Systems* 20, 352–361.

Yang, S.Y., Lockley, M.G., Greben, P., Erickson, B.R., Lim, S.Y. 1995: Flamingo and ducklike bird tracks from the Late Cretaceous and Early Tertiary: evidence and implications. *Ichnos* 4, 221–234.

Yodogawa, E. 1982: Symmetropy, an entropy-like measure of visual symmetry. *Perception & Psychophysics* 32, 230–240.

Zelditch, M., Swiderski, D., Sheet, D., Fink, W. 2004: *Geometric Morphometrics for Biologists. A Primer*, 443 pp. Elsevier, New York, USA.

Zhen, S., Li, J., Chen, W.Z.S. 1994: Dinosaur and bird footprints from the Lower

Cretaceous of Emei County, Sichuan, China. *Memoirs of the Beijing Natural History Museum* 54, 108–120.

Appendix

Appendix A:

Tanaka, I. 2015: Estimating body weight and habitat type from extinct avian and avian-like theropod footprints, *Lethaia* 48,188-195.

Appendix B:

Tanaka, I. 2015: Effects of initial symmetry on the global symmetry of one-dimensional legal cellular automata, *Symmetry* 7,1768-1779.

Symmetry **2015**, *7*, 1768-1779; doi:10.3390/sym7041768

OPEN ACCESS

symmetry

ISSN 2073-8994

www.mdpi.com/journal/symmetry

Article

Effects of Initial Symmetry on the Global Symmetry of One-Dimensional Legal Cellular Automata

Ikuko Tanaka

Department of Earth and Planetary Sciences, Kobe University, Nada, 657-8501 Kobe, Japan;
E-Mail: itanaka@stu.kobe-u.ac.jp

External editor: Albert K. Harris

Received: 10 July 2015 / Accepted: 25 September 2015 / Published: 29 September 2015

Abstract: To examine the development of pattern formation from the viewpoint of symmetry, we applied a two-dimensional discrete Walsh analysis to a one-dimensional cellular automata model under two types of regular initial conditions. The amount of symmetropy of cellular automata (CA) models under regular and random initial conditions corresponds to three Wolfram's classes of CAs, identified as Classes II, III, and IV. Regular initial conditions occur in two groups. One group that makes a broken, regular pattern formation has four types of symmetry, whereas the other group that makes a higher hierarchy pattern formation has only two types. Additionally, both final pattern formations show an increased amount of symmetropy as time passes. Moreover, the final pattern formations are affected by iterations of base rules of CA models of chaos dynamical systems. The growth design formations limit possibilities: the ratio of developing final pattern formations under a regular initial condition decreases in the order of Classes III, II, and IV. This might be related to the difference in degree in reference to surrounding conditions. These findings suggest that calculations of symmetries of the structures of one-dimensional cellular automata models are useful for revealing rules of pattern generation for animal bodies.

Keywords: cellular automata; pattern formation; symmetry; discrete Walsh analysis; complex system

---

1. Introduction

Animals have many kinds of pattern formation. Leopards living in closed habitats, such as forests, have a frequency of stripes that is much higher, more irregular, and more complex than those living in open habitats [1]. These body patterns reflect adaptations to the surrounding environment and, thus, pattern formation is substantially related to the conservation of species [1]. When we observe pattern formation, we read "texture", which includes shape, among other factors. Texture is measured by terms including spectrum, entropy, and fractal dimension [2,3]. The method of measurement combining entropy and symmetry, the two-dimensional discrete Walsh analysis, can be applied to analyses of two-dimensional surfaces [3–5]. In previous studies, the two-dimensional discrete Walsh analysis has been used in theoretical studies with one-dimensional legal cellular automata. As a result, studies have revealed the theoretical process of pattern formation, which reduces entropy and increases specific symmetry (self-organization) [4], and the real biological process of pattern formation, which reduces entropy and increases specific symmetry. They have also revealed that the real biological process has phase transitions, as seen in calculations with the two-dimensional Ising model [5]. However, the calculations in previous studies [3–5] always start with the condition of a random state. Pattern formation of a biological or animal surface does not necessarily start from such a random state, but rather from a regular state. Thus, clarifying the theoretical process of regular pattern formation has the possibility of revealing general features and the real biological process of pattern formation.

The purpose of this study was to clarify the theoretical process of pattern formation, starting from a regular state. We applied a two-dimensional discrete Walsh analysis to one-dimensional legal cellular automata.

The structure of this paper is as follows. In Section 2, we explain the method of analysis and data on one-dimensional legal cellular automata (CAs). In Section 3, we explain the data of the regular initial conditions. In Section 4, we briefly review the discrete Walsh analysis for calculating the symmetry and symmetropy of CA patterns. In Section 5, we describe and discuss the results and consider the symmetry relationships between the initial conditions and final patterns. Section 6 provides our conclusions.

2. Methods

The Discrete Walsh Analysis

We briefly outline the discrete Walsh analysis here (Figure 1). For details of the mathematical procedures, see previous studies [3,4,6]. The Walsh function $wal(r,x)$ of order r and argument x can be represented over the interval $0 \le x < 1$ as follows:

$$wal(r,x) = \prod_{i=0}^{m-1} \mathrm{sgn}\left[\left(\cos 2^i \pi x\right)^{ri}\right] \quad (1)$$

where $r_i = 0$ or 1, $r = \sum_{i=0}^{m-1} r_i\, 2^i$, and m is the smallest positive integer such that $2^m > r$. Dyadic addition of non-negative integers r and s is defined as $r \oplus s = \sum_{i=0}^{f} |r_i - s_i|\, 2^i$, where $r = \sum_{i=0}^{f} r_i\, 2^i$ and $s = \sum_{i=0}^{f} s_i\, 2^i$. Consequently, the product of the two Walsh functions is given by $wal(r,x)wal(s,x) = wal(r \oplus s, x)$. From this calculation, the Walsh function can be shown to form an orthonormal set. In this case, we can define a Walsh transform, similar to a Fourier transform.

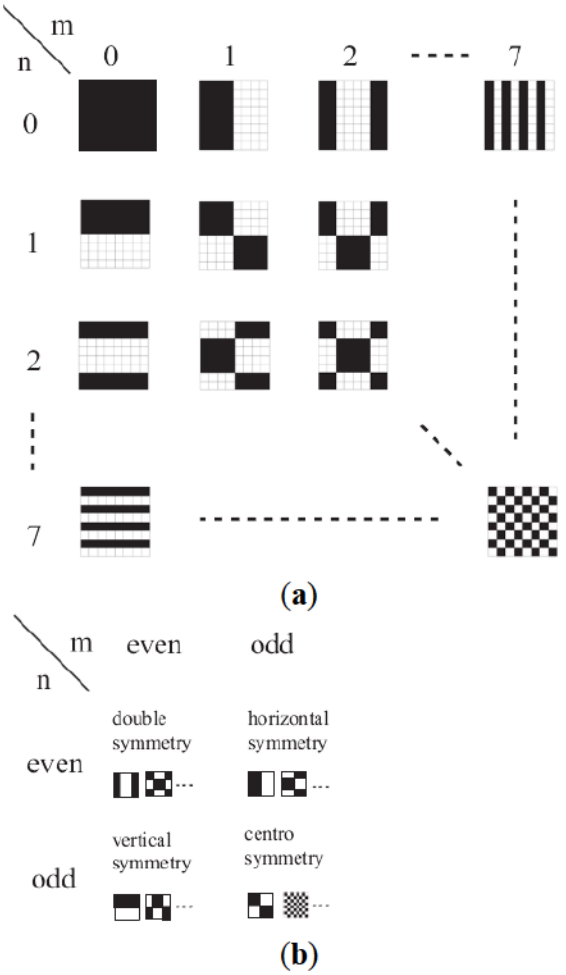

Figure 1. (**a**) Examples of the two-dimensional discrete Walsh functions for $m = n = 8$. Black represents +1, and white represents –1; and (**b**) four types of symmetry in terms of the discrete Walsh function.

The two-dimensional discrete Walsh function can be represented in matrix form as $[W_{mn}(i,j)]$, where $W_{mn}(i,j)$ is the amount of the (m,n)th -order Walsh function in the ith row cell in the jth column.

This pattern can be written as $[x_{ij}]$, where x_{ij} is the amount of the gray level in the i^{th} row cell in the jth column and $i,j = 0,1,\dots,N-1$. If just two gray levels exist, for example, "black" and "white", then x_{ij} is typically represented by 1 and 0, respectively (Figure 1a). The two-dimensional discrete Walsh transform of the pattern $[x_{ij}]$ is given by:

$$a_{mn} = \frac{1}{N^2}\sum_{i=0}^{N-1}\sum_{j=0}^{N-1} x_{ij}\, W_{mn}(i,j) \tag{2}$$

where $m,n = 0,1,\dots,N-1$. The functions a_{mn} and $(a_{mn})^2$ are the two-dimensional Walsh spectrum and power spectrum, respectively.

The Walsh power spectrum can be normalized as follows:

$$P_{mn} = \frac{(a_{mn})^2}{K} \tag{3}$$

where $K = \sum_{m=0}^{N-1}\sum_{n=0}^{N-1}(a_{mn})^2 - (a_{00})^2$. In this case, we obtain:

$$\sum P_{mn} = 1 \tag{4}$$

where the sum is taken over all ordered pairs (m,n) for $0 \le m,n \le N-1$, except for $(m,n) = (0,0)$.

The spatial pattern is considered as an information source, consisting of dot patterns. The dot patterns emitted from the source are assumed to occur with the corresponding probabilities given by Equation (4).

Next, we consider the information entropy resulting from the symmetry of the pattern. Because the two-dimensional Walsh functions can be easily divided into four types of symmetry (Figure 1b), Equation (4) can be rewritten as:

$$\sum_{i=1}^{4} P_i = 1 \tag{5}$$

where vertical symmetric component:

$$P_1 = \sum_{m=\text{even},n=\text{odd}} P_{mn} \tag{6}$$

horizontal symmetric component:

$$P_2 = \sum_{m=\text{odd},n=\text{even}} P_{mn} \tag{7}$$

centro symmetric component:

$$P_3 = \sum_{m=\text{odd},n=\text{odd}} P_{mn} \tag{8}$$

and double symmetric component:

$$P_4 = \sum_{m=\text{even},n=\text{even}} P_{mn} \tag{9}$$

When the spatial pattern is regarded as an information source consisting of four types of symmetry, the corresponding probabilities are given by Equations (6)–(9). Applying the entropy function from information theory to these four symmetric components, we obtain:

$$S = -\sum_{i=1}^{4} P_i \log_2 P_i \tag{10}$$

As shown in Equations (5) and (10), S ranges from 0 to 2 bits. Since this entropy relates to the symmetry, it is called the "symmetropy" [6]. The symmetropy can be considered as a quantitative and objective measure of symmetry. If the amount of a certain component is larger than the amounts of the other three components, then the pattern is rich in symmetry related to the particular component. In this

case, Equation (10) shows that S decreases. Conversely, if the amounts of the four components are almost equal to one another, then the pattern is poor in symmetry, and S increases. Previous studies have concentrated on symmetry [4]. Following this idea, in this study, we measured the symmetry of the initial condition and the final pattern to examine the effects on final patterns of the initial condition of symmetry in CA patterns.

3. Calculations

For simplicity, this paper uses only "classical" CAs according to the Wolfram classification [7]; that is, the one-dimensional legal CA that obeys the 32 possible legal totalistic rules. The totalistic rules involve nearest and next nearest neighbors, and each cell has two possible colors: white (0) or black (1). In addition, because the total number of neighborhoods of five cells is equal to 2^5, we can obtain the 32 possible legal totalistic rules. Wolfram [7,8] discovered that, although the patterns obtained with different rules differed in detail, they appeared to fall into four qualitative classes:

- Class I: fixed point (rules 0, 4, 16, 32, 36, 48, 54, 60, and 62) (Figure 2a).
- Class II: periodic (rules 8, 24, 40, 56, and 58) (Figure 2b).
- Class III: chaotic (rules 2, 6, 10, 12, 14, 18, 22, 26, 28, 30, 34, 38, 42, 44, 46, and 50) (Figure 2c).
- Class IV: complex (rules 20, 52) (Figure 2d).

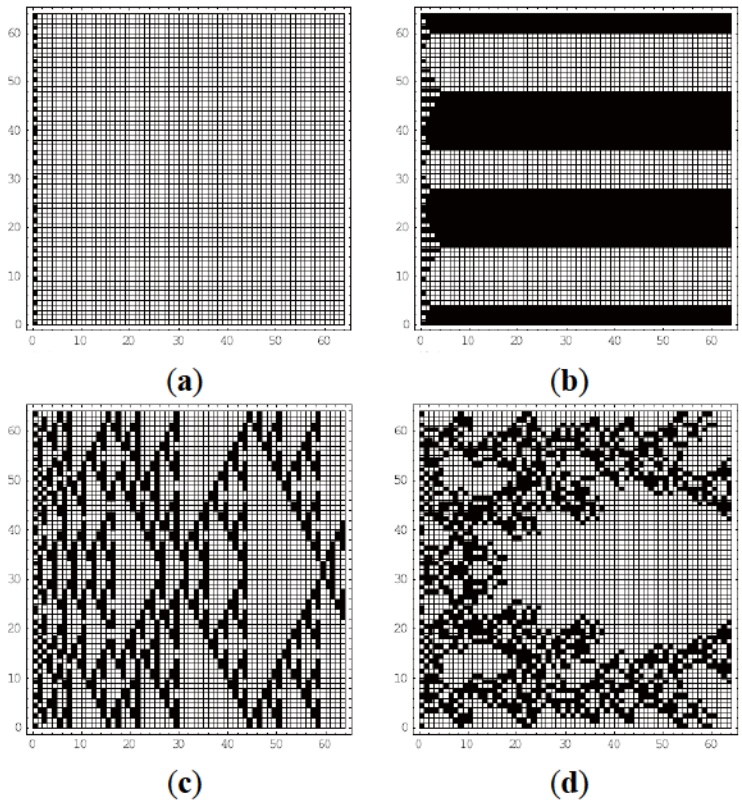

Figure 2. Examples of final patterns in each class. (**a**) is an example of Class I, (**b**) of Class II, (**c**) Class III, and (**d**) is an example of Class IV.

In this paper, we do not use all codes in class I because the patterns are trivial. We measure the initial condition ($2^6 \times 1$) and the final pattern. The number of cells is $2^6 \times 2^6$ because, to measure the number

of symmetries, this number of cells is the minimum needed [4]. In the present study, we can use only two kinds of initial condition, horizontal symmetry and double symmetry, because we consider $n = 2$ in the discrete Walsh function W_{mn} (as in Figure 3).

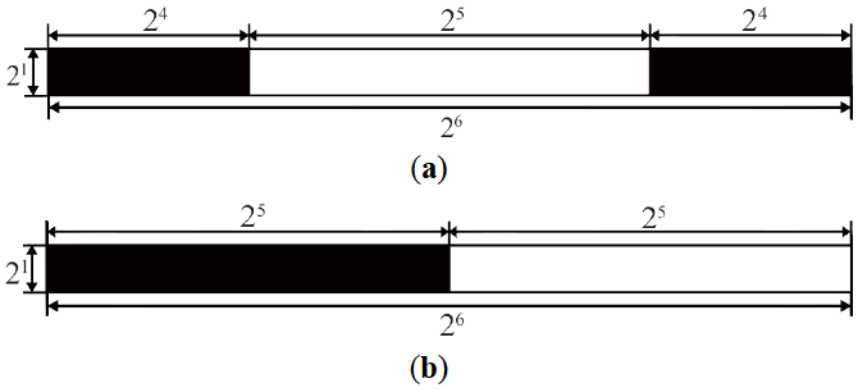

Figure 3. An example of initial symmetry. (**a**) Double Symmetry is one example of DS_0, and (**b**) Horizontal Symmetry is one example of HS_0. In this study, the initial condition was limited to $n = 2$ because $2^1 = 2 = n$. Thus, (**a**) shows the case of $m = even$, and (**b**) shows the case of $m = odd$.

First, we run two types of regular initial conditions; the horizontal symmetry with 32 conditions, abbreviated as HS_0, and the double symmetry with 31 conditions, abbreviated as DS_0. Then, under each initial condition, the amounts of symmetry were averaged for each class. We compared this result with the random initial condition in [4], abbreviated as Ra_0. Then, for each initial condition, we compared the relationship between the amount of symmetry in the initial condition and that in the final pattern. The method can be extended to 2D cellular automata, but requires a large number of analysis.

4. Results

4.1. Class

Figure 4 shows the amount of symmetropy for the three initial conditions (Ra_0, DS_0, $and\ HS_0$) and the amount of symmetropy in each initial condition for the final patterns. The results show that under all initial conditions, the numbers of symmetries of the CA patterns correspond to three qualitative classes of CAs, identified as Classes II, III, and IV, according to Wolfram's original classification [7,8]. Additionally, the result of the measurement of symmetropy under regular and random initial conditions shows a relational expression: Class II < Class IV < Class III. In all classes, the amount of symmetropy under Ra_0 is larger than that under DS_0 and HS_0. In Ra_0, the amount of symmetropy of all classes decreased as time passed. In contrast, in DS_0 and HS_0, the amount of symmetropy of all classes increased as time passed. Thus, the final patterns of the regular initial condition (DS_0 and HS_0) are more regular than those of the random initial conditions (Ra_0).

4.2. Four Types of Symmetry

Figure 4 shows increases or decreases in the amount of symmetry for four kinds of symmetries in initial conditions and in final patterns. In HS_0, Classes II, III, and IV have all of the four kinds of symmetries: vertical symmetry, horizontal symmetry, centro symmetry, and double symmetry. However, in DS_0, Classes II, III, and IV have only two kinds of symmetries: vertical symmetry and double symmetry (Figure 4).

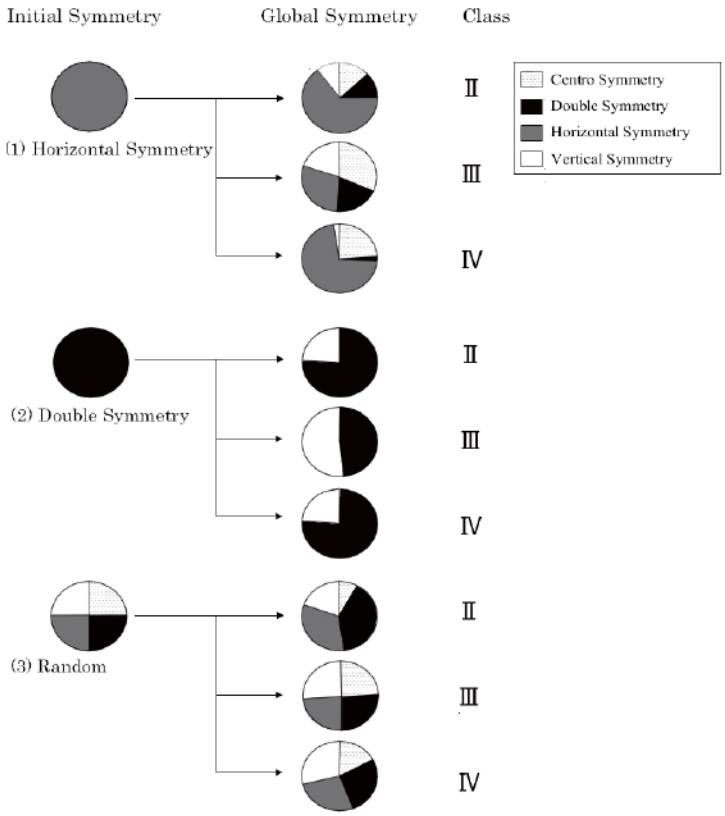

Figure 4. Pie charts of the three types of initial condition ($HS_0, DS_0,$ and Ra_0). For HS_0 and Ra_0, all classes have all four types of symmetry: vertical symmetry, horizontal symmetry, centro symmetry, and double symmetry. In contrast, DS_0 with all classes had two types of symmetry: vertical symmetry and double symmetry. Regarding vertical symmetry and double symmetry, the relational expression was $HS_0 < Ra_0 < DS_0$, and regarding horizontal symmetry and centro symmetry, it was $DS_0 < Ra_0 < HS_0$.

In DS_0, two kinds of symmetries, double symmetry and vertical symmetry, developed globally in the final formations. The design developed by DS_0 has a complicated pattern that lined up with a regular pattern (Figure 5a,b). Development was accompanied by a large increase in the amount of vertical symmetry. Thus, vertical symmetry contributed to the development of the spatial direction of the final patterns, whereas the double symmetry of DS_0 was preserved. In contrast, the design developed by HS_0 has all four kinds of symmetry (Figure 4), and the horizontal symmetry of HS_0 was not preserved.

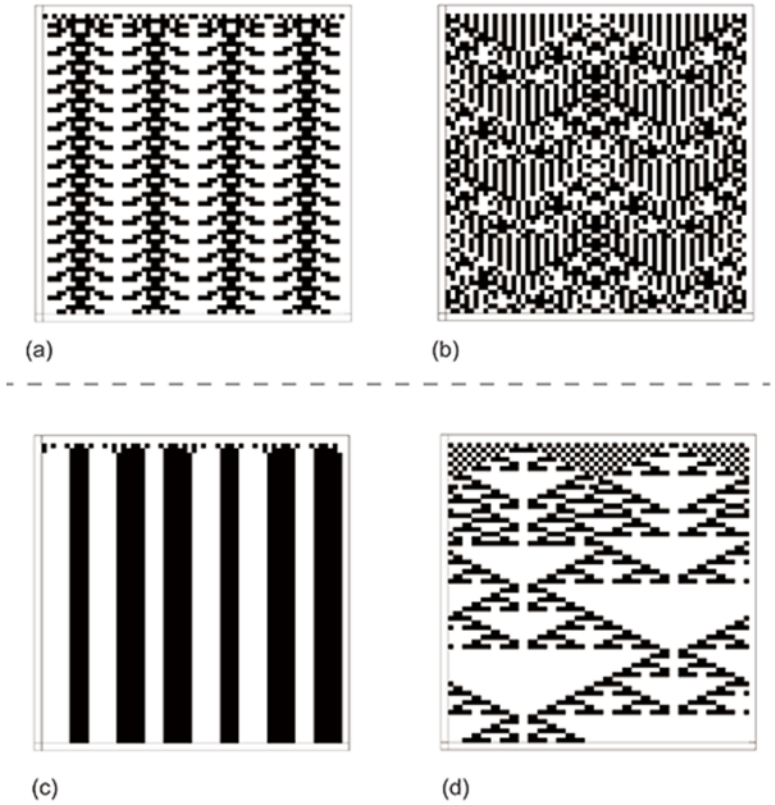

Figure 5. Examples of final patterns with regular initial conditions. (**a**,**b**) belong to DS_0, and (**c**,**d**) belong to HS_0.

4.3. The Ratio of Final Formation

The ratios of developed final patterns in each Class for DS_0, Ra_0, and HS_0 are shown in Table 1. The ratio of developed of final patterns is calculated by dividing the number of final pattern formation for each class (periodic or chaotic or complex) by a product of the number of initial condition (if HS_0: 32, if DS_0: 31) and the total number of classes (the sum rules of periodic, chaotic and complex: 23). For example, in the case of HS_0's periodic in Table 1, the ratio of periodic is 12 is calculated from 89, 32, and 23 for the numbers of final pattern formation, initial condition, and the sum rules of periodic, chaotic and complex, respectively. The ratio of 12 is obtained as: 89(final patterns)/32rules/23(number of classes) × 100. According to Yamazaki *et al.* [4], Ra_0 made final patterns using every rule and class; the ratio of formation was 100%. In contrast, for DS_0 and HS_0, the ratio of formation is less than 50% for all classes, and the developing final pattern ratios are 12% for Class II, 43%–44% for Class III, and 6% for Class IV (Table 1).

Table 1. The rate of final patterns of DS_0 and HS_0.

Class	Horizontal Symmetry	Double Symmetry	Random
Periodic	12	12	100×
Chaotic	43	44	100×
Complex	6	6	100×

In all classes, the rate of the forming pattern of Ra_0 was larger than that of DS_0 and HS_0. Comparing DS_0 with HS_0, the rate of forming patterns of class III was larger than that of class II and class IV; also, in each class, the two types of DS_0 and HS_0 had the same rates. Data indicated by asterisks are from [4].

5. Discussion

5.1. Class

For all classes, the amount of symmetry for HS_0 is larger than that for DS_0, and the final pattern formations of DS_0 have a higher hierarchy than HS_0; in contrast, the final pattern formations of HS_0 had more broken regularity than HS_0 (Figure 5c,d). This result is interpreted as the double symmetry having a higher amount of symmetry than the horizontal symmetry, because DS_0 has an axis of symmetry with space and time, whereas HS_0 has an axis of symmetry with time alone.

From the measurement of symmetropy, developed pattern formations of HS_0 and DS_0 have many types of symmetries that predominate as time passes. This result corresponds to the viewpoint of the Curie Symmetry Principle [4]. In contrast, the developed pattern formations of Ra_0 show a situation in which one type of symmetry was predominant as time passed [4]; this result does not correspond to the viewpoint of the Curie Symmetry Principle [4]. Here, it is shown that the theoretical process of pattern formation reduced entropy and increased specific symmetry [4,5]; however, this process has been examined only from Ra_0 [4,5]. In this study, the final pattern formations from regular initial conditions did not reduce entropy and increased specific symmetry. Thus, the Curie Symmetry Principle cannot be used to evaluate the proxy of pattern formation.

The final pattern formation of DS_0 is composed of the same scale forms, to stand in a line (Figure 5a,b). The pattern formations are supposed to be affected by "iteration" of the base rules of CAs, and this result is correlated with the previous studies, such as [9] that shows that the Walsh transform allows one to compute the correlation between the inputs and the outputs of the iterations of a cellular automaton. Generally, as systems are put under greater stress, the observed states lose symmetry and gain in complexity (both spatial and temporal). However, as the systems are further stressed, states with more symmetries and more structures appear. Moreover, symmetries and chaos—patterns and disorder—can coexist naturally within the same simple mathematical framework [10]. In this study, the natural coexistence of symmetry and chaos (iteration of CAs) is found in the final pattern formation of DS_0; this means a simple mathematical framework of a one-dimensional legal cellular automata. Complicated structure pattern formations are developed by a simple model; thus, the quantity of information needed to describe an object may be more than that needed to prescribe it. Thus, under an initial condition of strong regularity, theoretical phenomena revealed occurrences of iterations with regularity, and the concepts of the theoretical phenomena could be helpful to interpret the process and the circumstance of biological patterns with higher-complexity structures.

5.2. Four Types of Symmetry

For all classes, the amount of symmetropy for HS_0 is larger than that for DS_0 (Figure 4), because HS_0 has four types of symmetry, while DS_0 has only two types (Figure 4). This result coincides with

that the final pattern of HS_0, which shows steady state decay, and that of DS_0, which shows switching of a steady state to a hierarchy.

HS_0 has four types of symmetry: vertical, double, horizontal, and centro symmetries. DS_0 has only two types: vertical and double symmetries. These results show that double and vertical symmetries are the basic ones for forming patterns, and whether they form random or regular patterns is affected by the amount of horizontal and centro symmetries. The direction of each symmetry shows that (1) vertical symmetry has an axis of symmetry with space, (2) horizontal symmetry has an axis of symmetry with time, (3) double symmetry has an axis of symmetry with space and time, and (4) centro symmetry has an axis of symmetry with space and time. Thus, combinations of double and vertical symmetries, which are the basic symmetries of pattern forming, have axes of symmetries with space and time. In contrast, the combination of horizontal and centro symmetries is a supplemental one, for pattern formation. Thus, the basic and supplemental symmetries have balance with space and time. Additionally, the initial condition constrains the combination of symmetries (the analysis decided the symmetry direction): vertical and double symmetries *versus* horizontal and centro symmetries.

We compared the amounts of the four types of symmetries among $DS_0, Ra_0,$ and HS_0. The amount of vertical symmetry and double symmetry increased in the order $HS_0 < Ra_0 < DS_0$, except for Class II's vertical symmetry. Additionally, the amount of horizontal symmetry and centro symmetry increased in the order $DS_0 < Ra_0 < HS_0$.

In regular and random initial conditions, Class III has equal amount of symmetries of the different types of symmetries, but Classes II and IV have different amounts. Here, we explain biological patterns from these results. The organisms' developed pattern formations can select the amounts of two types of symmetry (horizontal and centro) according to the circumstances, because both horizontal and centro symmetries have symmetry axes related to "time". Here, time is related to the future. Thus, the combination of symmetries with wide varieties, as in this study, may provide the opportunity for understanding how to develop pattern formation (heredity or circumstances), and may be able to manage pattern formation, and to predict the future.

5.3. The Ratio of Final Formation

The growth design formations are limited in HS_0 and DS_0, but there is no limit in Ra_0 (Table 1). This means the variability of symmetries of Ra_0 is larger than that of HS_0 and DS_0. The numbers of developed final pattern rules for HS_0 and DS_0 are almost equal in every class, because the numbers of initial conditions are almost the same; 32 for HS_0 and 31 for DS_0, and most of the HS_0 rules correspond to DS_0 ones.

The rules that did not develop final patterns under regular initial conditions need larger amounts and more symmetries. The ratio of rules developing final patterns to those with no developing final patterns was calculated for each Class (Table 1). The ratio of rules that developed final patterns under the regular initial condition decreased in the order of Class III, Class II, and Class IV. Thus, Class III does not need more of the amounts and types of symmetries, whereas Class IV requires much more in the way of amounts and many types of symmetries, and Class II requires moderate amounts and types of symmetry. We explain biological patterns from these theories. Class III is not influenced by circumstances, and allows easy development of final patterns, which means heredity. On the other hand, Class IV is influenced by circumstances, and Class II by circumstances and heredity. Animals having Class III

biological patterns may select the circumstances by themselves, because their biological patterns are interpreted as genetic characteristics. The animals having Class IV biological patterns may adapt themselves to circumstances, because their biological patterns are interpreted as acquired characteristics. The animals having Class II biological patterns may be able to select a circumstance by themselves and may be able to adapt themselves to a circumstance, because their biological patterns are interpreted as random genetic characteristics and random circumstances. They may take an unplanned survival strategy.

Here, we discuss living animals. Although clams appear in Class III [11], their shell patterns are in heredity [12]. Additionally, the habitat of clams is decided by the height of ground level and drying time within 1 day, which has no relationship with pattern formation [13]. This might be supported by the hypothesis "The animals having Class III biological pattern formation may select circumstance by themselves, because their biological patterns are interpreted as genetic characters". However, *Neritina*, a typical shellfish, appears in Classes II and IV [11]; their shell design pattern formation has been found along the structure of the growth lines [14]. Thus, *Neritina* may be affected by the circumstances around them. In addition, their shell patterns have been found to be of color bands [14]; thus, *Neritina* may have been affected by circumstance and heredity.

6. Conclusions

We examined the structure of one-dimensional legal cellular automata from the viewpoint of symmetry to reveal the rules of animals' pattern generation. The following conclusions are derived. (1) Under all regular and random initial conditions, a relational expression, Class II < Class IV < Class III, was seen. In all classes, the pattern formation with regular initial conditions was more regular than that with random initial conditions. (2) We compared the pattern formation made with two types of regular initial conditions. The final pattern formations of HS_0, which have more broken regularity, have four types of symmetries, whereas that of DS_0 has only two types of symmetries, which are of a higher hierarchy. Both regular initial conditions show situations in which many types of symmetry predominated as time passed. We showed that when pattern formation develops, amounts of symmetries and types of symmetries do not always decrease. (3) We found that growth design formations have limited possibilities with regular initial conditions; the results of calculating the ratio of developing final patterns decreases in the order of Class III, Class II, and Class IV.

Acknowledgements

We would like to give thanks to Masayuki Hyodo, Kazuhito Yamasaki, Takao Ubukata, Sunao Mochizuki and Yusuke Seto for valuable discussions and advices on the manuscript. This work was financially supported by a grant from the Japan Society for the Promotion of Science awarded to IT (15J00351).

Conflicts of Interest

The authors declares no conflict of interest.

References

1. Allen, W.L.; Cuthill, I.C.; Scott-Samuel, N.E.; Baddeley, R. Why the leopard got its spots: Relating pattern development to ecology in felids. *Proc. R Soc. B.* **2010**, 1373–1380.
2. Ubukata, T. Theoretical morphology of composite prismatic, fibrous prismatic and foliated microstructures in bivalves. *Venus* **2000**, *59*, 297–305.
3. Nishiyama,Y.; Nanjo, K.Z.; Yamasaki, K. Geometrical minimum units of fracture patterns in two-dimensional space: Lattice and discrete Walsh functions. *Phys. A* **2008**, *387*, 6252–6262.
4. Yamasaki, K.; Nanjo, K.Z.; Chiba, S. Symmetry and entropy of one-dimensional legal cellular automata. *Complex Syst.* **2012**, *20*, 352–361.
5. Yamasaki, K.; Nanjo, K.Z.; Chiba, S. Symmetry and entropy of biological patterns: Discrete Walsh functions for 2D image analysis. *BioSystems* **2010**, *103*, 105–112.
6. Yodogawa, E. Symmetropy, an entropy-like measure of visual symmetry. *Percept. Psychophys.* **1982**, *32*, 230–240.
7. Wolfram, S. Universality and complexity, in cellular automata. *Phys. D* **1984**, *10*, 1–35.
8. Wolfram, S. *A New Kind of Science*; Wolfram Media, Inc.: Champaign, IL, USA, 2002.
9. Martin, B. A Walsh exploration of Wolfram CA rules. In Proceedings of the 12th International Workshop on Cellular Automata, Hiroshima University, Higashi-Hiroshima, Japan, 12–15 September 2006; pp. 25–30.
10. Stewart, I.; Golubitsky, M. *Fearful Symmetry: Is God a Geometer?* Blackwell Pub: Oxford, UK, 1992; p. 346.
11. Schiff, J.L. *Cellular Automata: Discrete View of the World*; John Wiley & Sons Inc.: Hoboken, NJ, USA, 2008; p. 250.
12. Peignon, J.M.; Gérard, A.; Naciri, Y.; Ledu, C.; Phélipot, P. Analyse du déterminisme de la coloration et de l'ornementation chez la palourde japonaise Ruditapes Philippinarum. *Aqua. Liv. Res.* **1995**, *8*, 181–185. (In French)
13. Akiyama, B.Y.; Saito, H.; Nanbu, R.; Tanaka, Y.; Kuwahara, H. The spatial distribution of Manila clam *Ruditapes philippinarum* associated with habitat environment in a sandy tidal flat on the coast of Matsunase, Mie Prefecture, Japan. *Ecol. Civil. Eng.* **2011**, *14*, 21–34. (In Japanese)
14. Habe, T. *Gakken Picture Book of Shellfish*; Gakken Holdings: Tokyo, Japan, 1975; p. 294. (In Japanese)

© 2015 by the authors; licensee MDPI, Basel, Switzerland. This article is an open access article distributed under the terms and conditions of the Creative Commons Attribution license (http://creativecommons.org/licenses/by/4.0/).